NOTICE

The quality of this microform is heavily dependent upon the quality of the original thesis submitted for microfilming. Every effort has been made to ensure the highest quality of reproduction possible.

If pages are missing, contact the university which granted the degree.

Some pages may have indistinct print especially if the original pages were typed with a poor typewriter ribbon or if the university sent us an inferior photocopy.

Previously copyrighted materials (journal articles, published tests, etc.) are not filmed.

Reproduction in full or in part of this microform is governed by the Canadian Copyright Act, R.S.C. 1970, c. C-30.

AVIS

La qualité de cette microforme dépend grandement de la qualité de la thèse soumise au microfilmage. Nous avons tout fait pour assurer une qualité supérieure de reproduction.

S'il manque des pages, veuillez communiquer avec l'université qui a conféré le grade.

La qualité d'impression de certaines pages peut laisser à désirer, surtout si les pages originales ont été dactylographiées à l'aide d'un ruban usé ou si l'université nous a fait parvenir une photocopie de qualité inférieure.

Les documents qui font déjà l'objet d'un droit d'auteur (articles de revue, tests publiés, etc.) ne sont pas microfilmés.

La reproduction, même partielle, de cette microforme est soumise à la Loi canadienne sur le droit d'auteur, SRC 1970, c. C-30.

Canada

Influence of Fluoride Ions, Stoichiometry, Reaction Temperature and Time on the Composition and Symmetry of Superionic $PbSnF_4$ Obtained by Aqueous Reactions between Lead (II) Nitrate and Stannous Fluoride.

Juanita Marcia Parris

A Thesis

in

The Department

of

Chemistry

Presented in Partial Fulfillment of the Requirements
for the Degree of Master of Science at
Concordia University
Montréal, Québec, Canada

March 1988

ISBN 0-315-41639-4

ABSTRACT

Influence of Fluoride Ions, Stoichiometry, Reaction Temperature and Time on the Composition and Symmetry of Superionic $PbSnF_4$ Obtained by Aqueous Reactions Between Lead (II) Nitrate and Stannous Fluoride.

Juanita Marcia Parris

Superionic $PbSnF_4$ is the best fluoride ion conductor known to date. A controversy on the symmetry of the cell and the sequence of phase transitions in $PbSnF_4$ casts serious doubts on the reproducibility of the electrical properties. The results presented here show that the disagreement originates in minute variations in the conditions of preparation from aqueous reactions between solutions of stannous fluoride and lead (II) nitrate. The influence of fluoride ions, $Pb(NO_3)_2/SnF_2$ molar ratio, reaction temperature and time were investigated and related to the composition of product obtained as well as the symmetry of the cell.

ACKNOWLEDGEMENTS

Many thanks to Dr. G. Dénès, my research thesis supervisor, for his supervision and motivation throughout my graduate studies.

Also, I would like to thank the members of my Research Committee, Drs. P.H. Bird and C. Langford, whose interest and advice were valuable towards the completion of this thesis.

Support from the Technical Staff at Concordia University and Mr. B. Patterson of S.I.R.U. was greatly appreciated, as well as the friendships and input from my fellow colleagues.

Finally, I would like to thank my husband, brothers, Wayne and Clark and sister, Lori for all their support and my parents, for their confidence and belief in me.

Dedicated to the memory of
Ucris Hamilton Parris

TABLE OF CONTENTS

LIST OF FIGURES

LIST OF TABLES

LIST OF APPENDICES

LIST OF SYMBOLS

α	Tetragonal phase of $PbSnF_4$.
o	Orthorhombic phase of $PbSnF_4$.
m	Monoclinic phase of $PbSnF_4$.
δ	Chemical isomer shift.
t	Time, minutes or hours.
T	Temperature, °C.
X	Molar ratio $Pb(NO_3)_2/SnF_2$ in the reaction mixture.
C	Concentration in moles/L.
$a_o/\sqrt{2}$	a parameter of the orthorhombic phase relative to the tetragonal phase $PbSnF_4$.
$b_o/\sqrt{2}$	b parameter of the orthorhombic phase relative to the tetragonal phase of $PbSnF_4$.
a/b	Orthorhombic distortion relative to the tetragonal structure.
V_o	Volume of the orthorhombic phase relative to the tetragonal phase of $PbSnF_4$.
c/2a	Tetragonal distortion relative to the cubic fluorite structure.
$c_o\sqrt{2}/(a_o+b_o)$	Tetragonal distortion relative to the cubic fluorite structure of the orthorhombic phase of $PbSnF_4$.

1.0 INTRODUCTION

1.1 SOLID ELECTROLYTES

1.1.1 DEFINITION

"Solid electrolytes", or "superionic conductors", is the term given to a class of solid materials that exhibit uncharacteristically high values of conductivity due to ionic motion at temperatures well below melting coupled with unusually low values of activation enthalpy. Solid electrolytes derive their interest from application devices. High conductivity solid electrolytes have revolutionized conventional concepts of ionic compounds and their uses range from high energy density batteries and fuel-cell electrolytes to chemical sensors.

1.1.2 FLUORINE ION CONDUCTORS

The thermodynamic properties of fluorides readily explains the interest in these compounds for energy storage batteries. The reaction of a fluorinating agent with a metal corresponds to a considerable change in the free energy of the system as a result of the high oxidizing power of the halogen. If such a couple is used in a galvanic cell utilizing the F- ion as the charge conductor, it is possible

to obtain a high voltage and a high power density. The F- ion is the smallest of the anions, and it possesses a single charge. As a consequence, fluorides are expected to be the best anionic conductors.

1.1.3 CRYSTAL STRUCTURES AND FAST ION CONDUCTION

Materials which exhibit fast ionic conduction do so because of special characteristics related to their structure.

The best fluoride ion conductors belong to the fluorite-type (CaF_2) family of closely related structures. This can be explained by the ability of this structure to accommodate a large number of structural defects of the Frenkel type on the fluoride sublattice, i.e. a significant number of fluoride ions leave their normal positions to go to interstitial positions (empty cubes) (fig. 1).

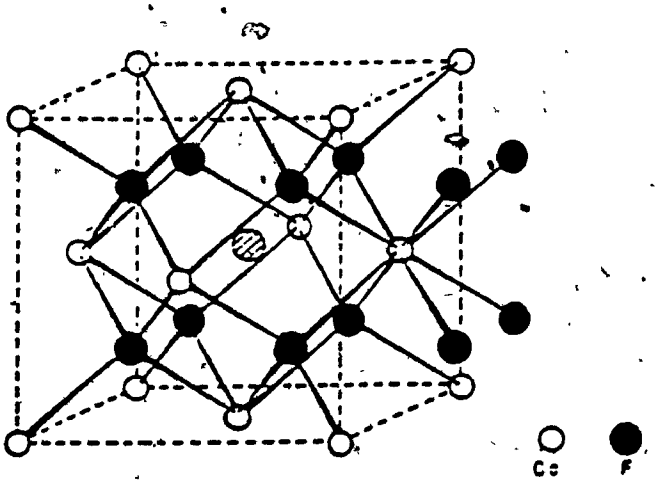

Fig. 1. Frenkel-type defects in fluorite (CaF_2) structure.

Defects up to a certain concentration, lead to a reduction of free energy (fig. 2).

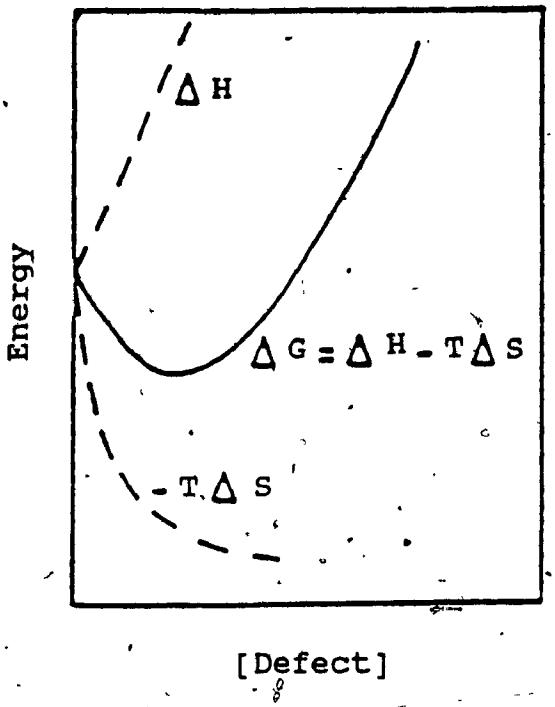

Fig. 2. Energy changes on introducing defects into a perfect crystal.

The effect on the free energy of a perfect crystal in creating a single defect, in the case of Frenkel defects the creation of a vacancy, requires a certain amount of energy, H. This in turn causes a considerable increase in entropy, S, of the crystal, because of the large number of positions this defect can occupy. As a result of this increase in S, the enthalpy required to form the defect initially is more than offset by the gain in entropy of the crystal and therefore the free energy, G decreases. Long distance ion

motion then occurs by a mechanism of ion hopping between normally occupied lattice sites, vacancies and interstitials.

1.2 $PbSnF_4$

1.2.1 INTEREST IN $PbSnF_4$

$PbSnF_4$ is far the best fluoride ionic conductor so far known (fig. 3) with negligible electronic conductivity and a low activation energy [$\sigma = 10^{-2}$ $(ohm.cm)^{-1}$ at 500K, > 0.99, E_a = 0.31 - 0.34 eV] (1).

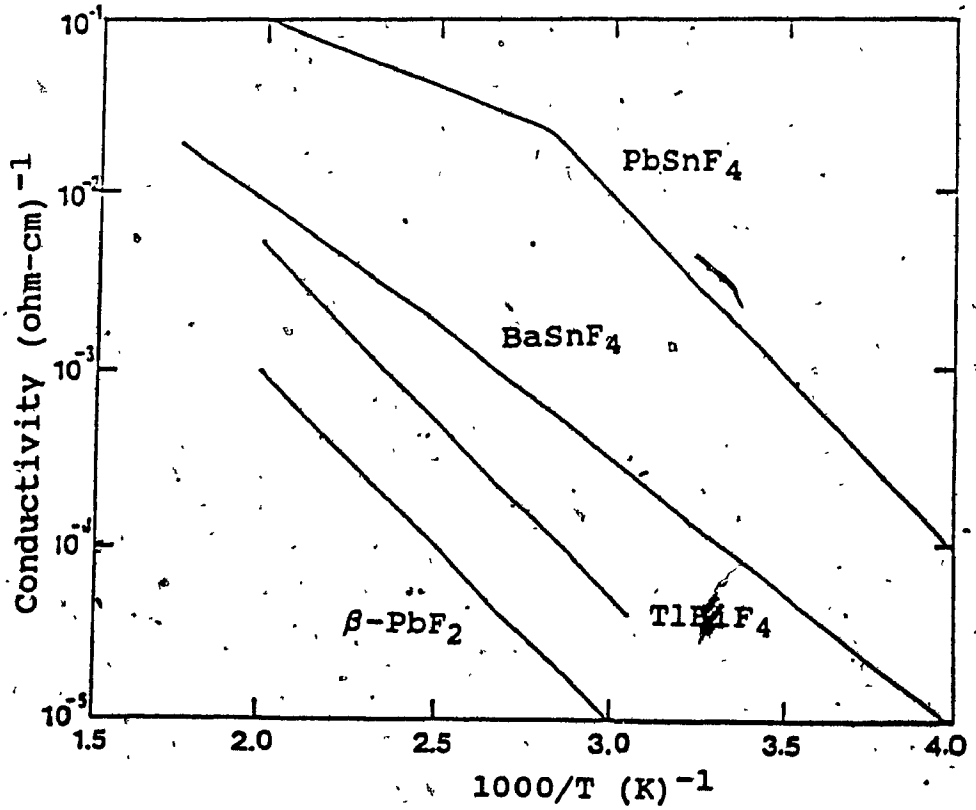

Fig. 3. Electrical conductivity of some fluoride ion conductors related to the fluorite structural type.

Replacing half of the lead (II) ions by tin (II) in β-PbF_2 to give $PbSnF_4$ results in a dramatic increase in the conductivity of close to three orders of magnitude.

The tetragonal $PbSnF_4$ structure is a distortion of the CaF_2 fluorite structural type, with long range order between tin and lead. The β-PbF_2 structure, undistorted CaF_2 type, is shown in fig. 4.

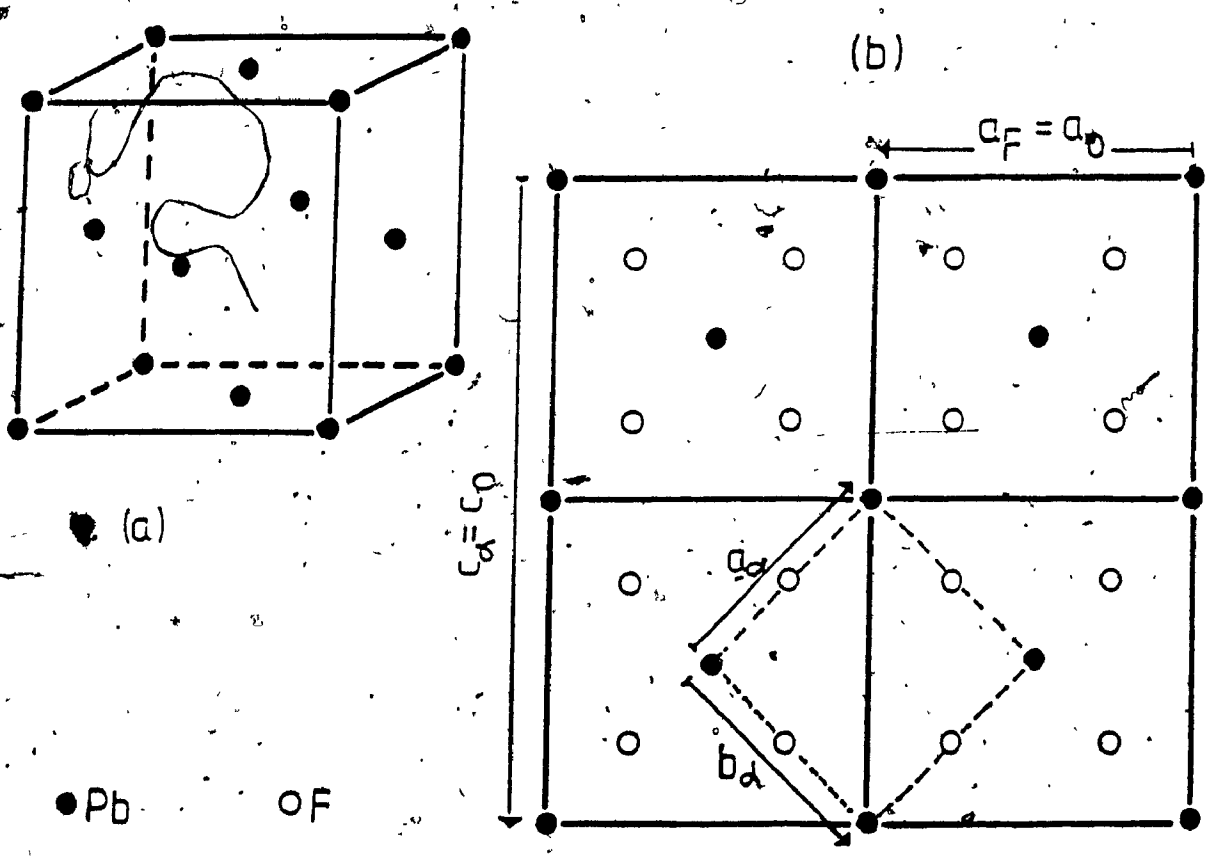

Fig. 4. β-PbF_2 Fluorite structural-type (a) fcc lattice of Pb(II) ions and (b) projection of four adjacent β-PbF_2 cells onto one face of the cube.

All lead atoms are in the plane of the figure while the fluorine atoms on the projection are located at the z

coordinates +1/4 and -1/4. As a result, they are located at the corners of fluorine cubes. These cubes of fluorine atoms form a three dimensional network of intersecting rows of cubes parallel to the axes of the cell. In each row, empty cubes alternate with cubes having a Pb in their center, giving a occupancy factor of 50%. As there are 8/8 = 1 fluorine per cube and 1/2 Pb per cube (i.e. one for every two), this description accounts for the PbF_2 formula, i.e. Pb/F = 1/2. The presence of vacant lead positions in the fluorite structure is thought to be responsible for the high ionic conductivity. Indeed, the center of the cubes of fluorine atoms not occupied by lead are likely to be the receiving sites for fluoride ions leaving their normal positions to form Frenkel-type defects. The availability of such vacant sites (one per two cubes, i.e. one per two fluorine atoms) can, in theory, allow up to half of the fluorine atoms to be at a given time in interstitial positions, having created as many vacancies. Although it is unlikely that such a large number of defects can be created without destabilizing the fluorite-type structure, it is undoubtedly the presence of a large number of vacancies which is at the origin of the high fluorine mobility. Fig. 4(b) also shows that the a and b parameters of tetragonal α-$PbSnF_4$ (a_α and b_α) are equal to half of the diagonal of a face of the cube, while c_α is twice the edge of the cube. The a and b parameters of orthorhombic o-$PbSnF_4$ (a_o and b_o)

are equal to a_α of the fluorite-type (a_F) while c (c_o) is also doubled. The relationship between the cells of the fluorite-type (F), tetragonal α-$PbSnF_4$ (α) and orthorhombic o-$PbSnF_4$ (o) can be written as follows:

Unit cell parameters:		
	$a_\alpha = b_\alpha \approx a_F/2$	$a_o \approx a_F$
		$b_o \approx a_F$ ($b_o < a_o$)
	$c_\alpha \approx 2c_F$	$c_o \approx 2c_F$
Volume:	$V_\alpha \approx V_F$	$V_o \approx 2V_F$
# molecules/unit cell:		
	$Z_\alpha = Z_F$	$Z_o \approx 2Z_F$

One should take $a_o < b_o$ unless there is a specific reason for not doing it. Réau et. al. (5) have taken $b_o < a_o$, which is unconventional.

The change in bonding pattern going from β-PbF_2 to α-$PbSnF_4$ is illustrated in fig. 5. Fig 5(a) shows the regular bonding in PbF_2, with lead being bonded to 8 fluorine atoms forming an exactly cubic environment, and each fluorine is tetrahedrally coordinated by four lead atoms. This arrangement gives a regular three-dimensional structure with isotropic properties. α-$PbSnF_4$ shown in fig. 5(b) has the same cationic sublattice, except that half of the lead (II) are replaced by tin (II) which are located in a five-fold coordination, with four equal equatorial bonds

and one short axial bond. Such a coordination for divalent tin is unique. It compares to the distorted five-fold coordination of Sn(II) in α-SnF_2 and to the square pyramidal coordination of SnO where the axial anion is missing. The position facing the axial F in the polyhedron of

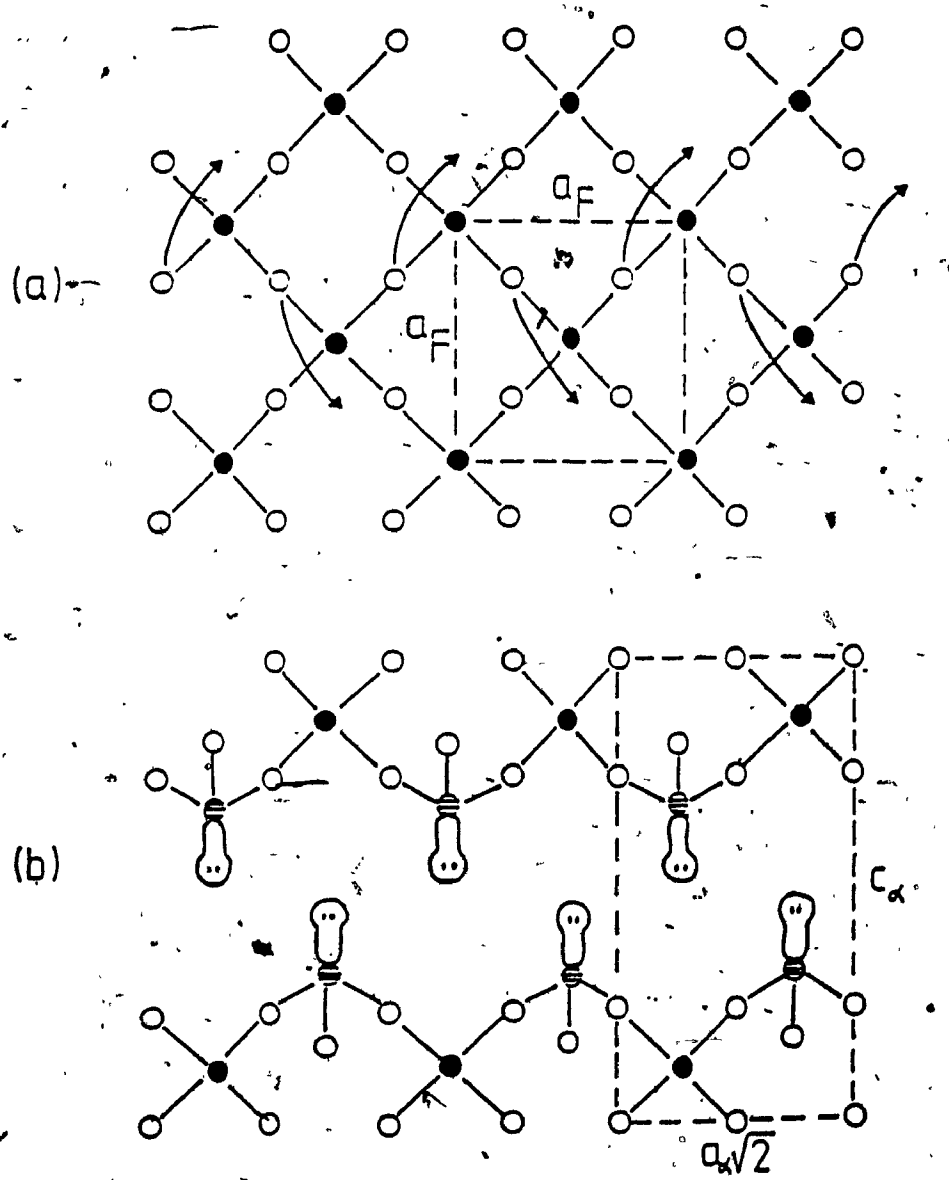

Fig. 5. Comparison of bonding in (a) three-dimensional β-PbF_2 structure and (b) layered α-$PbSnF_4$ structure.

coordination of tin is apparently vacant, however it is not, as it is occupied by the tin non-bonding electron pair which is stereoactive and therefore occupies the sixth corner of the polyhedron of coordination, which is better described as a pseudo-octahedron rather than a square pyramid, the tin (II) hybridization being a distorted sp^3d^2.

Two lead layers every four are replaced by tin, ordering occurring as follows:

. . . Pb Pb Pb Pb Pb . . . β-PbF_2

<——a_F——>

. . . Pb Pb Sn Sn Pb . . . α-$PbSnF_4$

<————c_α————>

resulting in the doubling of the c parameter.

Metal layers are separated by a fluorine layer, except in α-$PbSnF_4$ where the fluorine layer between the tin layers has migrated half above the upper tin layer ($F/_2$), half below the lower tin layer ($F/_2$) and is replaced by two half layers of lone pairs ($E/_2$). The layer sequence is as follows:

Pb F Pb F Pb F Pb β-PbF_2

<————a_F————>

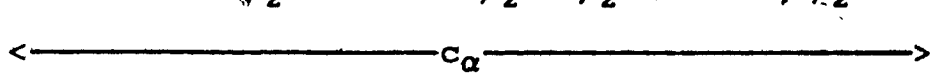

As there is no bonding fluorine between the two tin layers, but instead lone pairs repelling each other, α-$PbSnF_4$ is a layered structure and exhibits highly anisotropic properties (2) contrary to β-PbF_2 which has no discontinuity in the fluorine bridges and therefore is isotropic (cubic symmetry).

1.2.2 HISTORY OF $PbSnF_4$

In 1967, Donaldson and Senior (3) first prepared $PbSnF_4$ by the addition of a hot saturated solution of lead (II) nitrate to an aqueous solution of tin (II) fluoride (30% w/v) at 90°C under oxygen-free nitrogen until the precipitate just formed. The precipitate was redissolved by the addition of a minimum of 1.0N nitric acid and the resultant solution cooled. The product was filtered off, washed with a minimum of cold water, and recrystallized from 10% (w/v) aqueous solution of tin (II) fluoride. It is also mentioned that the same $PbSnF_4$ phase was obtained in cooled melts of a mixture of SnF_2 and PbF_2, but that no analogous $MSnF_4$ compound could be obtained for M = Mg, Ca, Sr, and Ba. In addition, it is reported that, under the identical conditions as those followed for $PbSnF_4$ prepared by aqueous

reaction, except that hot tin (II) fluoride solution was added to the lead (II) nitrate solution, a nitrate containing phase, $Pb_2SnNO_3F_5.2H_2O$, was obtained. The products obtained were characterized by I.R., Mössbauer spectroscopy and powder X-ray diffraction

In 1975, Dénès et al. (4) repeated the preparation of $PbSnF_4$ under the same conditions as Donaldson. They found that the same product was obtained. They also obtained the same compound by adding a cold solution of SnF_2 to a cold solution of lead (II) nitrate as well as by solid state reactions at 250°C. Also prepared were the isomorphous compounds $SrSnF_4$ and $BaSnF_4$ by solid state reaction at 550°C. The products were characterized by X-ray diffraction and found to be identical to Donaldson's. The space group was determined on a single crystal as being P4/nmm - D^4_h, No. 129, tetragonal. Although the crystal quality was too poor for a crystal structure determination, Dénès et. al. suggested that the $PbSnF_4$ structure was closely related to the fluorite-type structure, perhaps PbFCl type, with order between tin and lead along the c axis.

In 1978, Réau et al. (5) confirm the preparation of $PbSnF_4$ by addition of a solution of lead nitrate to a solution of SnF_2 in the molar ratio $1Pb(NO_3)_2/4SnF_2$; they also confirm the solid state synthesis of $PbSnF_4$ in gold containers as described in (4). However, it is claimed in (5) that the product obtained from aqueous solution has

orthorhombic symmetry, space group C222 or Cmma, in conflict with earlier findings (3,4). In addition, a sequence of phase transitions is given (Table I). They describe two new phases β and $PbSnF_4$.

In 1979, Pannetier et al. (6) confirm their earlier findings and Donaldson and Seniors' (3) as being correct and also report the existence of two new phases β and -$PbSnF_4$ that are however different from those reported be Réau (5) (Table I). They also showed that some of the low symmetry material reported by Réau could be interpreted as a mixture of phases. Furthermore, their results were further confirmed by detailed neutron diffraction (7).

However, in a new publication in 1980, Pérez and his coworkers (8) reported their previous findings as being incorrect and now claim that five phases of $PbSnF_4$ were observed, (Table I), with the phase obtained from solution being monoclinic instead of orthorhombic.

A summary from the literature of the conditions of the reactions in aqueous solutions and their results are given in Table II.

Table I

Phase Transitions in $PbSnF_4$ Reported in the Literature.

Réau (5) α-orthorhombic $\overset{80°C}{\rightleftharpoons}$ β-tetragonal $\overset{355°C}{\rightleftharpoons}$ γ-cubic $\overset{390°C}{\rightleftharpoons}$ liquid
Pannetier (6) and Birchall (7) α-tetragonal $\overset{260\text{-}290°C}{\longrightarrow}$ β-tetragonal $\overset{390°C}{\rightleftharpoons}$ γ-cubic γ-cubic $\overset{>420°C}{\longrightarrow}$ Decomposition with loss of SnF_2
Pérez (8) α-monoclinic $\overset{80°C}{\longrightarrow}$ β-tetragonal $\overset{350°C}{\rightleftharpoons}$ β'-tetragonal $\overset{380°C}{\rightleftharpoons}$ γ-cubic α'-monoclinic γ-cubic $\overset{390°C}{\rightleftharpoons}$ liquid

Table II

Preparative Conditions of $PbSnF_4$ from Aqueous Solutions Reported in the Literature.

conc. SnF_2	conc. $Pb(NO_3)_2$	$\frac{Pb(NO_3)_2}{SnF_2}$	HF	T(°C)	Product	Ref.
30%w/v	saturated	-	-	90	Tetragonal	3
30%w/v	saturated	-	No	90/RT	Tetragonal	4
-	-	1/4	-	-	Orthorhombic	5
30%w/v	saturated	-	No	90/RT	Tetragonal	6
-	-	1/2	Yes	20	Monoclinic	8
-	-	ca. 1	Yes	20	Monoclinic	8

Table II shows that the conditions of preparation, although similar, are not identical, and all authors do not clearly specify the conditions they use. For example, in (5) and (8) the concentrations of the solutions is not specified and in (5) the temperature is not given. In (8), the SnF_2 solution is acidified with HF when in all other reports, no use of HF is mentioned and we therefore presume it was not used. In (3) and (4), the molar ratio $Pb(NO_3)_2/SnF_2$ is not

given but the concentration of the solution is.

The above conflicting results induced us to suspect that poorly defined preparative conditions were at the origin of the conflict. The first goal of the present study was to use well defined reaction conditions in order to get reproducible results. In a second step, we hoped that careful modifications of these conditions could lead to different results and we would be able to establish precise reaction parameters, yielding different modifications of $PbSnF_4$, obtained under slightly different conditions. This, in turn, would allow one to get reproducible physical properties for this fast ion conductor.

2.0 EXPERIMENTAL

2.1 INSTRUMENTAL

2.1.1 POWDER X-RAY DIFFRACTION

2.1.1.1 PRINCIPLES

In the powder method utilizing X-rays, the sample to be examined is reduced to a fine powder and placed in a beam of monochromatic rays. Each tiny particle of the powder, called a crystallite, is a small single crystal oriented at random with respect to the incident beam and with respect to other crystallites. For each position of the detector, corresponding to a Bragg peak, there are some crystallites of the powder oriented such that the appropriate (hkl) plane are in diffraction positions. The mass of the powder is equivalent to a single crystal rotated, not about one axis, but about all positions.

The number of different (hkl) reflections obtained in a powder diffraction experiment depends, in part, on the relative magnitudes of the wavelength and the crystal-lattice parameters as well as the crystal lattice symmetry.

An X-ray powder pattern is a set of peaks, each of different intensity and position (d-spacing or Bragg angle, θ), on a length of chart paper. For a given crystalline

material the line positions are essentially fixed and are characteristic of that substance.

2.1.1.2 INSTRUMENTATION

Structural determination requires accurate information about position and intensity of Bragg peaks. The powder method was used for phase identification of the bulk product and for lattice parameter determination. The products were obtained as powders and usually no single crystal large enough for single crystal diffraction could be obtained. Also, the relative intensities of the Bragg peaks were strongly affected by the preferred orientation that the compound typically exhibits.

A Philips PW 1050-25 diffractometer, with a moveable counter was used. Monochromatic radiation with CuKα (Ni filter) (λ = 1.54178A) was the source of X-rays. The Philips system makes use of the parafocussing effect illustrated in fig. 6.(9). The line of focus of the X-ray tube, L, and the entrance slit (S_1) of the counter are constrained to lie on a circle, the focusing circle, so as to be equidistant from the sample (P), the surface of which is tangential to the circle. This ensures that the X-rays diffracted from the surface of the sample are focussed in the detector.

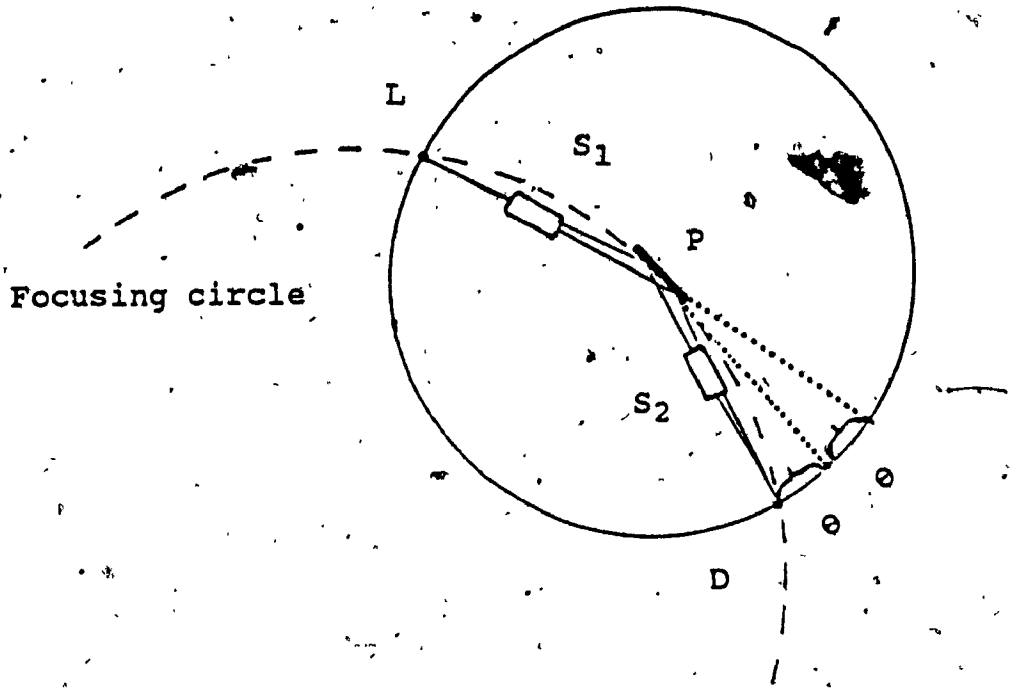

Fig. 6. Geometry of an X-ray powder diffractometer.

The X-rays are then effectively focused on the entrance slit (S_2) of the count (D).

The diffraction pattern is scanned by rotating the counter at a constant speed about the center of the surface of the sample. In order to maintain the geometry of the focusing circle, the sample is geared to rotate about the same axis at half the speed of the counter. Scanning speeds of 0.5°(θ) per minute was used. The detector, a Xe/CO_2 scintillation counter, outputs through amplification and

pulse height analyzer, to a pen recorder which plots count/second, as a measure of intensity, versus diffractometer θ, on a continuous paper chart. The chart moves at a steady speed so that the distance parallel to its length provide a measure of difference θ.

The diffraction pattern of the samples were obtained with a continuous motion of the sample and detector. The pattern was started at 3°(θ) and covered an range to 30°(θ). A chart paper recorder operating at a speed of 0.5° min/(2θ) so that the distance of 1" on the chart paper correspond to one degree θ.

2.1.1.3 PHASE IDENTIFICATION

Powder X-ray diffraction is the most powerful and the most commonly used technique to identify any crystalline phase, be it pure or in a mixture. Diffraction patterns are a function of the crystal periodicity and show minute changes in the size and shape of the lattice. An X-ray powder pattern is a one-dimensional projection of the three-dimensional reciprocal lattice. Fig. 7 shows typical X-ray powder patterns obtained at room temperature of β-PbF_2 and the tetragonal and orthorhombic phases of $PbSnF_4$. γ-$PbSnF_4$, stable only above 400°C, crystallizes in the fluorite-type like β-PbF_2, spacegroup Fm3m. Tetragonal distortion to α-$PbSnF_4$, (P4/nmm) is mainly characterized by:

i) the splitting of all (hkl) Bragg peaks with h = 1 followed by a transformation of the axes in the (a,b) plane such that $a_t = 1/2(a_c + b_c)$ and $b_t = 1/2(a_c - b_c)$ (fig. 4b). For example:

$$(200)_c \longrightarrow (\bar{1}10)_t \text{ and } (004)_t$$

ii) the presence of extra peaks at lower angles, such as (001), (002), (101) and (003); these are superstructure reflections which are due to the removal of some absence conditions when changing from cubic to tetragonal and from a F Bravais lattice to a P lattice, and to the doubling of the c parameter because of ordering between Pb and Sn along $\vec{c}$. The change of h and k indices for the peaks is due to the change of orientation of the $\vec{a}$ and $\vec{b}$ axis, which, in tetragonal are equal to half of the diagonal of the face of the cube. The subsequent distortion to orthorhombic symmetry, as described by Réau et al. (5), gives a less dramatic change of the powder pattern. The $\vec{a}$ and $\vec{b}$ axes of the cell are oriented as in the cubic phase. Then the peaks with $h = k \neq 0$ in tetragonal split and this splitting can be taken as a measure of the orthorhombic distortion. For example, as shown in fig. 7:

$$(110)_t \xrightarrow[\text{change}]{\text{axes}} (200) \xrightarrow[\text{distortion}]{\text{orthorhombic}} (200)_o \text{ and } (020)_o$$

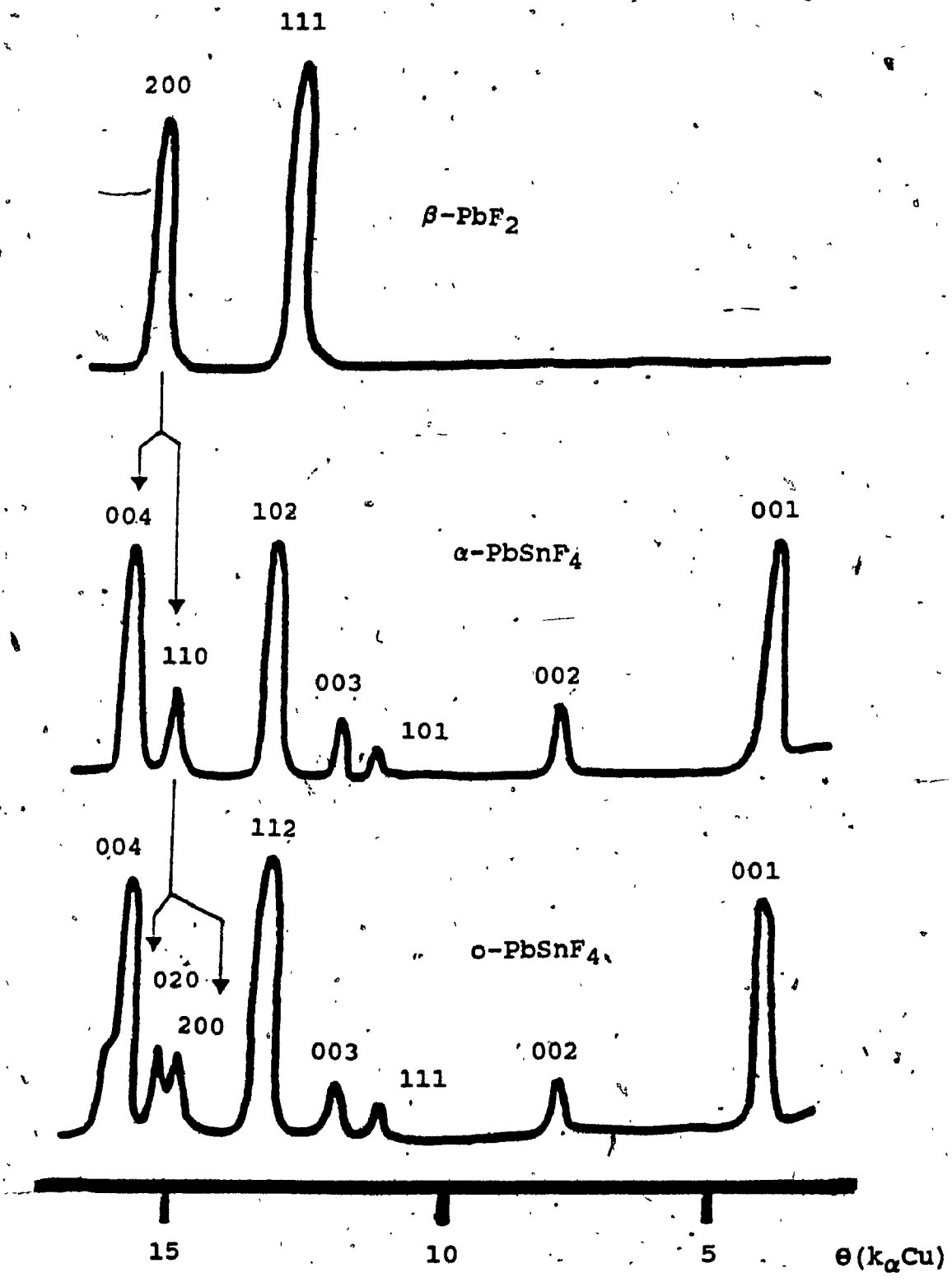

Fig. 7. Room temperature X-ray powder patterns of (a) β-PbF_2 (cubic), (b) α-$PbSnF_4$ (tetragonal) and (c) o-$PbSnF_4$ (orthorhombic).

It is noteworthy that the shoulder on the (004) peak of o-$PbSnF_4$, although clearly shown on fig. 8 of (5), is not accounted for. For clarity, we hereafter call the $PbSnF_4$ phase obtained from solution as follows:

tetragonal	α-$PbSnF_4$
orthorhombic	o-$PbSnF_4$
monoclinic	m-$PbSnF_4$

Therefore, any change in the lattice will be reflected by some changes in the powder pattern.

Since each crystalline substance has its own characteristic symmetry and lattice dimensions, powder diffraction may be used for its identification. Mixtures of substances may be identified provided, of course, that the patterns of the component phases are available for comparison. The powder X-ray method may be used as a check on purity provided the impurities are present as a separate crystalline phase(s).

2.1.1.4 TEXTURE EFFECTS

Texture effects are observed only in polycrystalline samples. In order to get meaningful peak intensities from polycrystalline samples the crystallites must be randomly oriented. Perfectly randomly oriented samples are hard to

get and quasi-impossible in the case where the crystal shape favors preferred orientation of the crystallites, such as for plate or needle shaped crystallites. In the case of plates, the crystallites tend to stack parallel to each other causing texture effects. In $PbSnF_4$, the c axis is perpendicular to the plates. More crystallites, oriented in the (001) direction, give enhanced Bragg peaks in that direction, while the (hK0) reflections are much weaker. After grinding, the (001) reflections are depressed while the (101) reflections are considerably enhanced with many other reflections. However, it is apparent that there is still not complete randomization of the crystallites.

2.1.1.5 DETERMINATION OF ACCURATE UNIT CELL PARAMETERS

The interplanar spacing d_{hkl} is a function both of the plane indices (hkl) and the unit cell parameters (a, b, c, α, β, γ). Unit cell lattice parameters are normally determined by single crystal on films (oscillation, Weissenburg and precession methods) are often accurate to only two or three significant figures. More accurate cell parameters may be obtained from the powder pattern, provided the various lines have been assigned Miller indices hkl and their positions have been measured accurately. Accurate unit cell parameters are particularly useful in enabling complex powder patterns to be indexed, for studying effects

of composition on cell parameters and for measuring thermal expansion coefficients.

The exact relation of the interplanar spacing and the unit cell parameters depends on the crystal system involved (Appendix I). The d_{hkl} spacing is determined from the θ positions by the relationship known as Bragg's Law, where $2d\sin\theta = n\lambda$.

2.1.1.6 SAMPLE PREPARATION

The most convenient way to prepare a sample for powder diffraction was to press the powder in the form of a flat plate, having been ground and pressed in a plexiglass holder with a glass slide. This often induced preferred orientation (i.e. unequal distribution of orientations of crystallites). Too much pressure can cause preferred orientation, but as it is sometimes difficult to control, preferred orientation was always be kept in mind when assessing relative peak intensities.

The product was hand-ground by a mortar and pestle to a fine powder. However, if the grain size of the crystallites was larger than 1000Å, broadening of the peaks did not occur. Surface roughness can also have a marked effect on relative peak intensities and position. If too rough, as in the case of a coarse powder compact, the intensity of low angle reflections will be abnormally low. The only way to

avoid this was to grind the specimen to a fine powder.

It should be noted that since the area of the sample irradiated by the incident beam varies with the Bragg angle, it was important that the sample should be homogeneous and large enough to catch the whole of the incident beam at the lowest and highest Bragg angles to be used. The dimensions of the surface used in all experiments was fixed by the sample holder whose area measured 2cm wide by 1cm high..

2.1.2 ATOMIC ABSORPTION SPECTROMETRY

2.1.2.1 PRINCIPLES

A solution is aspirated into a flame and the sample element is converted to atomic vapor. The flame then contains atoms of that element. Some are thermally excited by the flame, but most remain in the ground state (usually >99%). These ground state atoms can absorb radiation given off by a special source made from that element. The wavelengths given off by the source are the same as those absorbed by the atoms in the flame. The absorption follows Beer's Law. That is, the absorbance is directly proportional to the path length in the flame and to the concentration of atomic vapor in the flame. Although difficult to determine, by holding the path length constant the concentration of atomic vapor is directly proportional

to the concentration of the analyte in the solution being aspirated.

In spite of the small fraction of excited atoms available for emission, with high temperature flames a large number of elements can be determined. This occurs because we are in principle measuring the difference between zero and a small but finite signal so the sensitivity is limited by the sensitivity and stability of the detector and the stability (noise level) of the flame-aspiration system. Detection limits for this technique are typically in the ppm or ppb regions.

2.1.2.2 INSTRUMENTATION

All studies performed were done on a Perkin Elmer Atomic Absorption Spectrometer Model 503. The requirement for atomic absorption spectrometry are a light source, a cell (the flame), a monochromator, and a detector. The flame is placed between the source and the monochromator. A schematic diagram of an atomic absorption spectrometer is illustrated in fig. 8.(10) for a system with a single detector shared by both beams.

The source beam was alternately directed through the flame and around the flame by the chopper. After recombination, the two beams passed through a monochromator to a detector and readout system. The difference between

the two beams was integrated over 3 seconds and then displayed.

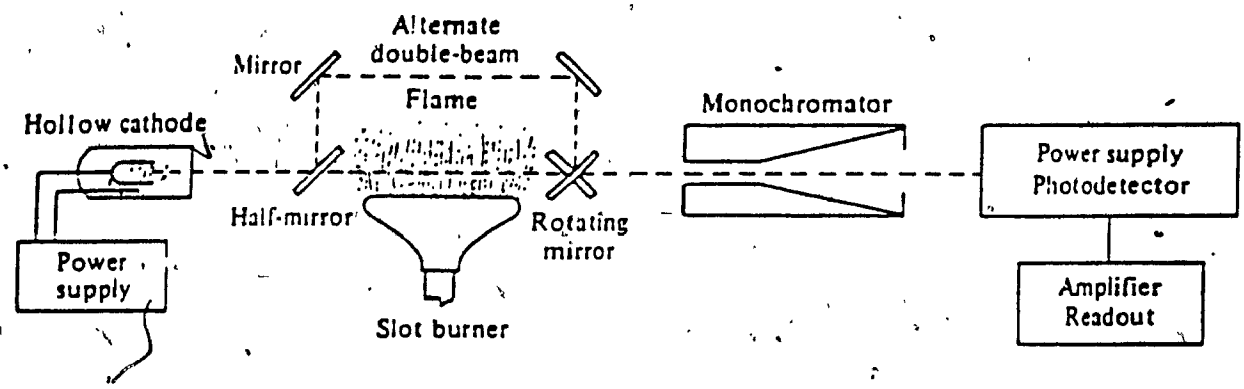

Fig. 8. Schematic diagram of the double beam optical atomic absorption spectrometer.

The source used is a hollow cathode lamp. It is a sharp line source that emits specific wavelengths. A premix chamber burner is used in which the fuel and support gas are mixed before entering the burner head where they combust. The sample solution is aspirated through a capillary by the "Venturi effect" using the support gas for aspiration. Large droplets of the sample condense and drain out of the chamber. The remaining fine droplets mix with the gases and

enter the flame.

2.1.2.3 INTERFERENCES

There are three broad categories into which interferences fall. They are chemical and physical and spectral.

Chemical interferences include ionization interference and the formation of refractory compounds. Ionization interference occurs when an appreciable amount of some elements become ionized by the flame resulting in a decrease in sensitivity. The formation of refractory compounds, characterized by their high melting points, results in slow, if any, conversion to the gaseous state.

Physical interferences are usually due to unevaporated droplets in the flame leading to a reduction in signal. This is particularly true with viscous and dense solutions. Frequent aspiration with pure solvent helps remove encrusted sample from burner orifices and the detection limit is often set by the matrix concentration that can be tolerated.

Spectral interferences are closely associated with the resolving power of the optical system employed. This is particularly serious when the test substance and interferant have nearly the same wavelength and fail to be resolved by the monochromator. This difficulty is overcome by selecting other spectral line or by prior separation.

2.1.2.4 SAMPLE PREPARATION

The sample was studied in solution as no difference in the chemical form is taken as it would be dissociated to the free elemental vapor in the flame. In the preparation of standards, the matrix of the analyte was always matched with that of the sample.

In the case of $PbSnF_4$, two main factors affect the method of sample preparation. First, $PbSnF_4$ is insoluble in neutral solution and must be acidified. Also, loss of tin from aqueous solution occurs during storage (8): such losses have been reported for dilute solutions. In dilute solutions, loss of up to 80% of tin is observed overnight when glass vessels are used. Acidifying the solutions greatly reduces these losses. No explanation is given in (8) either for the mechanism of tin loss or for why acidifying prevents it.

All samples were prepared by dissolving $PbSnF_4$ in a minimum of 10% (v/v) solution of HCl and then diluting with 1.0M HCl stock solution. The sample size of $PbSnF_4$ was taken between 100 to 200mg and the appropriate dilutions made with 1.0M HCl to bring the sample into the linear range.

Standard solutions were prepared using purchased 1000ppm stock solutions of Sn and Pb. To each solution the appropriate amount of SnF_2 or PbF_2 was added in the ratio

Pb/Sn = 1, in order to have the same matrix in the sample as well as standard.

For analysis of Sn, a wavelength of 284.0nm giving an absorption of 0.075 for a 100ppm solution was used. A Cathodeon Ltd., Type C hollow cathode lamp was used as the source. The flame was nitrous oxide-acetylene, reducing. For Pb, the wavelength was 180.5nm giving an absorption of 0.165 for a 20ppm solution. A Perkin Elmer Intensitron hollow cathode lamp was used and the flame was air-acetylene, oxidizing. Subsequent standard solutions for tin of 75, 50 and 25ppm and 15, 10 and 5 for lead were run. Linear least squares was performed on the results from the standards, correlation coefficient calculated and an equation best fitting the data obtained. Then, by interpolation, the concentration in ppm is obtained from the absorption results. Error for standard curves for Pb and Sn were 0.99908 and 0.99978 respectively.

2.1.3 MÖSSBAUER SPECTROSCOPY

2.1.3.1 PRINCIPLES

The phenomenon of the emission or absorption of a γ-ray photon without loss of energy due to recoil of the

nucleus and without thermal broadening is know as the a Mössbauer effect. Its unique feature is in the production of monochromatic γ-radiation with a very narrowly defined energy spectrum, so that it can be used to resolve minute energy differences. The direct application of the Mössbauer effect to chemistry arises from its ability to detect the slight variations in the energy of interaction between the nucleus and the extra-nuclear electrons, variations which had previously been considered negligible.

2.1.3.2 - INSTRUMENTATION

The measurement of a Mössbauer spectrum is almost exclusively carried out by repetitively scanning the whole velocity range required, thereby accumulating the whole spectrum simultaneously, and allowing continuous monitoring of the resolution. This can be achieved electromechanically by scanning the γ-ray energy range of interest by doppler effect. A schematic of a Mössbauer spectrometer is shown in fig. 9.

The major component is the multichannel analyzer (Tracor Northern TN7200) which can store an accumulated total γ-counts, using binary memory storage like a computer, in individual registers or channels. Each channel is held open in turn for a short time interval of fixed length, which is derived from a very stable constant frequency clock

device.

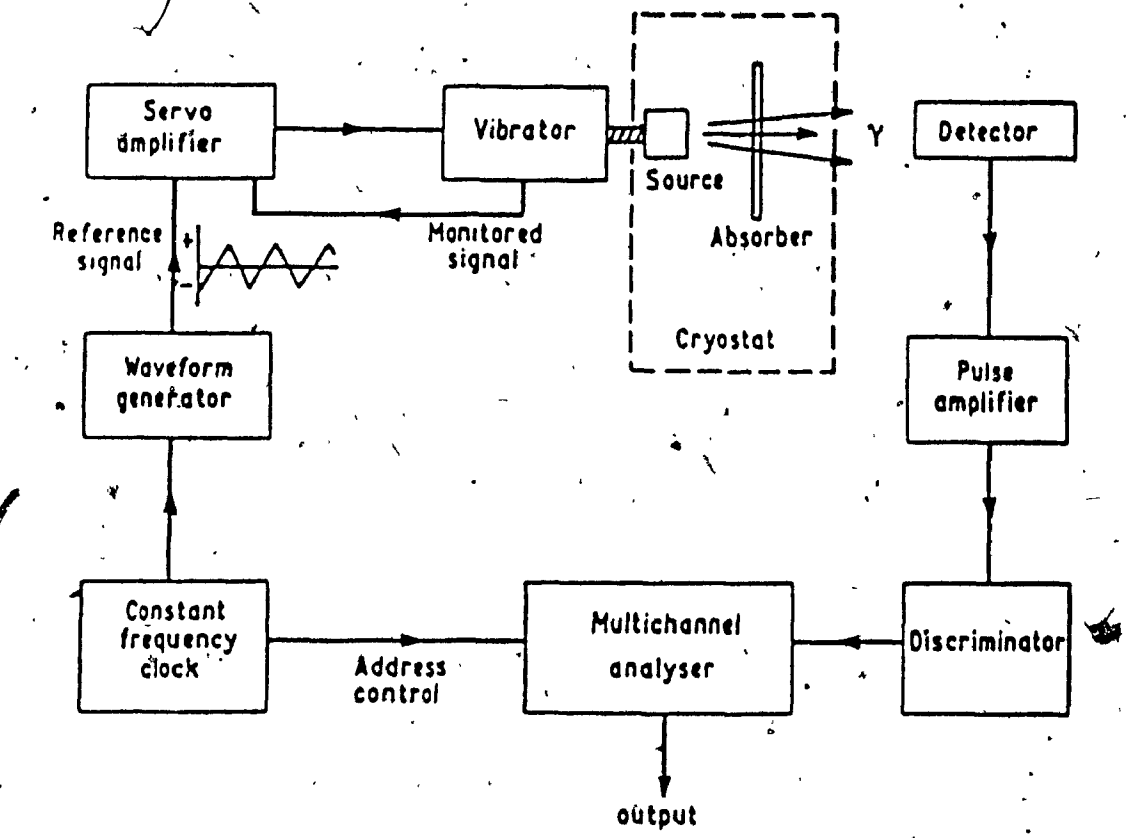

Fig. 9. Schematic Mössbauer spectrometer.

Any γ-counts registered by the detection system during that time interval are added to the accumulated total already stored in the channel.

The timing pulses from the clock are also used to synchronize a voltage waveform, which is used as a command signal to the servo-amplifier controlling an electromechanical vibrator (transducer). The latter moves the source relative to the absorber. A waveform, using the Elcint driving system, with a voltage increasing linearly with time, imparts a motion with a constant acceleration in

which the drive shaft and the source spend equal time intervals at each velocity increment. The multichannel analyzer and the drive are synchronized so that the velocity changes linearly from -v to +v with increasing channel numbers. In this way the source is always moving at the same velocity when a given channel is open.

For ^{119}Sn Mössbauer spectroscopy, a Harshaw Na(Tl)I scintillation detector was used. The pulses are passed through a discriminator which rejects most of the non-resonant background radiation, and finally fed to the open channel address.

The geometric arrangement of the source, absorber and detector are important due the angle θ that the emitted γ-ray makes with the axis of motion. The 'cosine-effect' causes a spread in the apparent Doppler energy thus causing line broadening. Adequate separation between source and detector reduces this effect.

The velocity range required to completely encompass the energy differences for all spectra acquired was fixed at ±8mm/sec.

2.1.3.3 CHEMICAL INFORMATION - HYPERFINE INTERACTIONS

A Mössbauer spectrum gives a picture of the nuclear energy levels. These are slightly modified by the electric

and magnetic environment of the atom. The total Hamiltonian of the interaction between the γ-ray and the nucleus can be described as follows:

$$H = H_o + E_o + M_1 + E_2 + \ldots$$

where: H is the total Hamiltonian.

H_o includes all terms except hyperfine interactions

E_o is the change in the electric monopole or Coulombic interactions between the electronic and nuclear charges, which is caused by a difference in the size of the nucleus in its ground and excited states. This causes a shift away from zero velocity, called chemical isomer shift, δ.

M_1 is the magnetic dipolar interaction between the magnetic moment of the nucleus and the magnetic field. The origin of the latter may be intrinsic or extrinsic to the atom. It results in multiplet line structure in the spectrum .

M_2 is the electric quadrupole interaction between the nuclear quadrupole and the local electric field gradient tensor at the nucleus. This also results in multiplet line structure in the spectrum.

The isomer shift gives information on the s valence electron density, the oxidation state, and electronegativity of the ligands. Appendix II gives typical Mössbauer data for different environments and oxidation states of tin.

2.1.3.4 SAMPLE PREPARATION

All spectra were taken at room temperature using a 15mCi $Ca^{119}SnO_3$ γ-ray source supplied by Amersham. The isomer shifts were referenced to a standard $CaSnO_3$ absorber at room temperature as zero isomer shift. The sample was ground and weighed to give 50mg Sn in sample. This usually required about 200mg of sample. This was then placed in a teflon base and pressed into a thin layer by the teflon cap which was screwed into the base. In the case where sample sizes were too small to ensure an even layer forming, charcoal was ground with the sample. The sample was then placed into the γ-ray beam, covered with a thin, 0.10mm, palladium foil and the data acquired.

2.2 SYNTHESIS

2.2.1 REAGENTS

SnF_2	Omnium Scientific Industrial
	Alfa
	Ozark-Mahoning
$Pb(NO_3)_2$	Sharpe
PbF_2	Pfaltz & Bauer, Inc.
HF, 48%	Mallinckrodt
Certified Atomic Absorption Standard, 1000ppm Sn and Pb	Fisher Scientific Co.

2.2.2 AMBIENT TEMPERATURE REACTIONS

All syntheses of $PbSnF_4$ were performed by precipitation reaction between SnF_2 and $Pb(NO_3)_2$. All chemicals were used without further purification and carried out in doubly distilled water. The beakers were made of pyrex or polytetrafluoroethylene (teflon) as specified in the results section

A saturated solution (1.7 M) of $Pb(NO_3)_2$ was always added to a solution of SnF_2 at a rate of 5 mL/min by burette. The solution of SnF_2 always had a final volume of 11.0 mL and its concentration was 1.5 M. The SnF_2 solvent was a variable mixture of H_2O and 48% aqueous HF. The molar ratio $Pb(NO_3)_2/SnF_2$ (X) was regulated by the addition of the appropriate amount of the $Pb(NO_3)_2$ solution to the SnF_2 solution. A time $t(SnF_2)$ = 0 to 100 hours separated the dissolution of SnF_2 to the beginning of addition of the

$Pb(NO_3)_2$ solution. For $t(SnF_2) > 0$, the beaker was covered with a paraffin sheet to prevent evaporation. For reactions where the product was left unfiltered for $t(PbSnF_4) = 0$ to 6 hours, the beaker was also covered with a paraffin sheet. The product was filtered immediately after the final addition of $Pb(NO_3)_2$ or after the time delay $t(PbSnF_4)$ indicated. It was then washed twice with distilled water and left to dry. The temperature under which these reactions was carried out was room temperature in air.

2.2.3 NON-AMBIENT TEMPERATURE REACTIONS

All reactions above room temperature were carried out in a closed system. A three necked, round bottomed flask was fitted with a condenser and thermometer. The appropriate amount of water was added to this closed system, stirring bar added and cold water circulated through the condenser to prevent evaporation. The round bottomed flask was set inside a heater and the entire apparatus mounted on a stirring plate. The system was allowed to equilibrate at the appropriate temperature.

For the reactions carried out below room temperature, the appropriate amount of water required was let to equilibrate in a paraffin covered beaker in an ice bath. Once the required temperature had been reached HF was added as indicated and followed immediately by the pre-weighed

SnF_2. As soon as the entire SnF_2 had dissolved $Pb(NO_3)_2$, at the same temperature as the SnF_2 system, was added dropwise with a funnel. As soon as the final addition of $Pb(NO_3)_2$ was complete, the product was filtered immediately, washed twice with distilled water at the same temperature as the reaction was carried out and left to dry.

3.0 RESULTS AND DISCUSSION

3.1 INTRODUCTION

Many parameters of the aqueous reaction between $Pb(NO_3)_2$ and SnF_2 may be responsible for determining the phase of $PbSnF_4$ obtained. Examination of the preparation conditions described in (3-7) shows that Donaldson and Senior (3) and Denes et al. (4,7) do not specify X, the $Pb(NO_3)_2/SnF_2$ molar ratio in the reaction mixture, but they give the concentration of the solutions used, saturated $Pb(NO_3)_2$ and 30% (w/v) SnF_2. On the other hand, Réau et al. (5) and Pérez et al. (6) do not specify the concentration of the solutions but they give X as being 1/4 in (5) and 1/2 or c.a. 1 in (6). This leads us to suspect that X and/or the concentration of the two solutions may be responsible for the observed discrepancies. The ideal molar ratio for the reaction is 1/2 in agreement with equation (I)

Equation I

$$Pb(NO_3)_2 + 2SnF_2 \xrightarrow{H_2O} \underline{PbSnF_4} + Sn^{2+} + 2NO_3^-$$

3.2 AMBIENT TEMPERATURE REACTIONS.

3.2.1 INFLUENCE OF $Pb(NO_3)_2/SnF_2$ MOLAR RATIO AT FIXED SOLUTION CONCENTRATIONS

In a first attempt to find the conditions of preparation for tetragonal α-$PbSnF_4$ and orthorhombic o-$PbSnF_4$ saturated solution (1.7 M) of $Pb(NO_3)_2$ was added to an 11 mL aqueous solution of SnF_2 (1.5 M) containing c.a. 1 mL of 48% aqueous HF. X was varied from 0.05 to 1.00 by adding the appropriate amount of $Pb(NO_3)_2$ solution. No preparations were done beyond X = 1.0 as beyond this ratio $Pb_2SnNO_3F_5.2H_2O$ was obtained in such amounts as to make interpretation of which phase of $PbSnF_4$ was obtained impossible. The orthorhombic distortion versus X is given on fig. 10. No trend is observed, the a/b ratio varying erratically from 1.00 (tetragonal) to 1.03 (orthorhombic). Even repeats of some preparations for given molar ratios gave highly irreproducible results.

Even though these results do not look encouraging, they lead to some conclusions:

(1) For the first time we obtained o-$PbSnF_4$. However, contrary to Réau et al. (5), we find a variable orthorhombic distortion.

(2) Some parameters, that we are not aware of, must be important, such that they are not monitored and may

from one preparation to another.

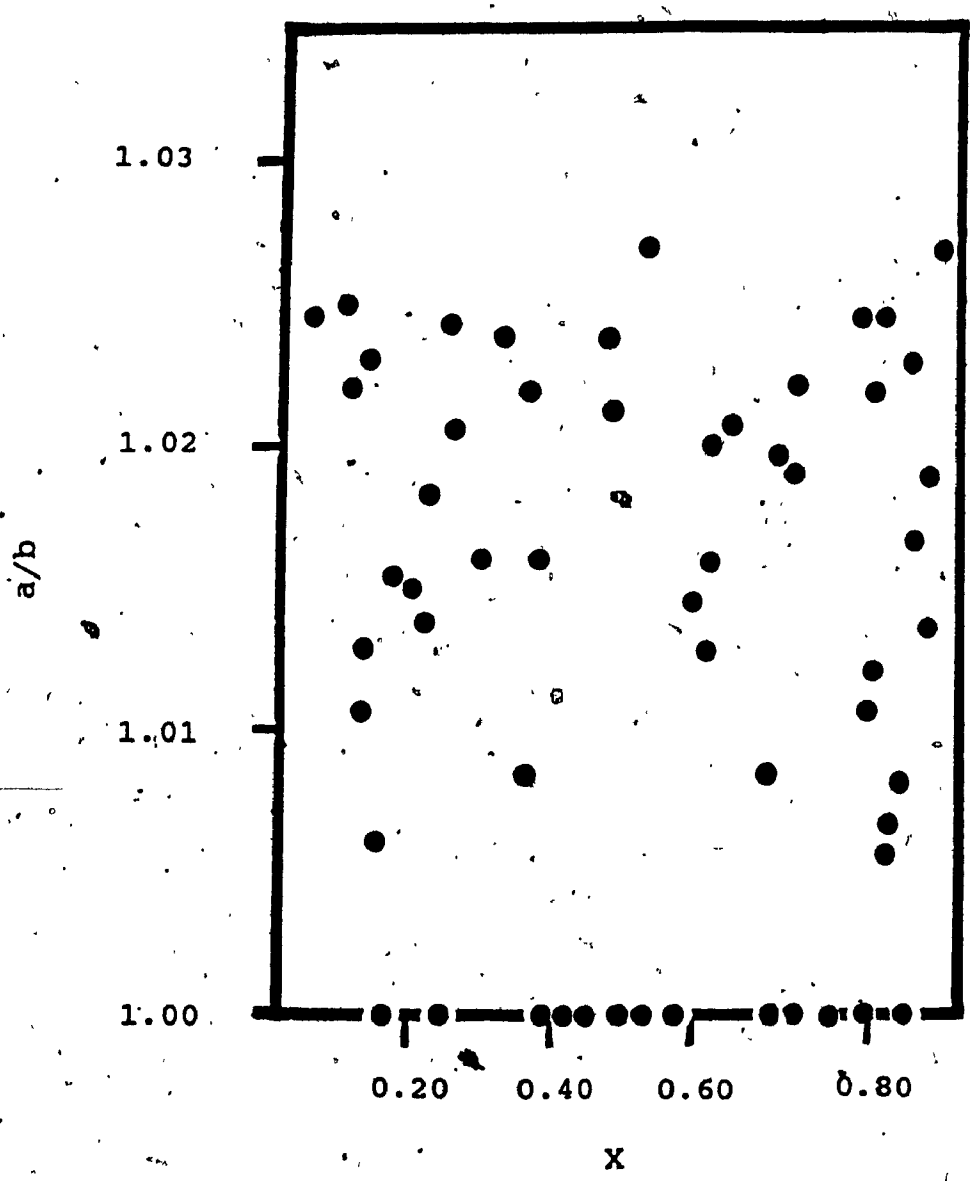

Fig. 10. Orthorhombic distortion of $PbSnF_4$ versus X at fixed solution concentrations

A summary of the conditions used are shown in Table III for those preparations performed at room temperature.

Table III

Important Parameters Controlling Symmetry of $PbSnF_4$ Obtained from Solution at Room Temperature.

Parameters	Description	Range
X	$Pb(NO_3)_2/SnF_2$ molar ratio in reaction mixture.	0.05 - 1.00
$t(SnF_2)$	Time between dissolution of SnF_2 in H_2O (and HF where indicated) and beginning of addition of first drop $Pb(NO_3)_2$.	0 - 100 hrs.
$t(PbSnF_4)$	Time between end of addition of $Pb(NO_3)_2$ and filtration of product.	0 - 6 hrs.
$C(SnF_2)$	Concentration of SnF_2 solution.	1.5M
$C(Pb(NO_3)_2$	Concentration of $Pb(NO_3)_2$ solution.	1.7M
HF/H_2O	Volume 48% aqueous HF/volume H_2O (V_{final} = 11.0mL).	0 - 0.55

Table III cont'd

Parameters	Description	Range
Beaker	Nature of the beaker used for reaction.	Glass or Teflon
Gas	Degassing the water solvent and gas blanket over reaction.	Air
Rate	Rate of addition of one solution into the other.	5.0mL/min.
Order	The $Pb(NO_3)_2$ solution is added to the SnF_2 solution.	Pb in Sn
T	Temperature of reaction	0, 25, 75, and 90°C

3.2.2 INFLUENCE OF HF/H_2O AND THE NATURE OF THE BEAKER

Acidifying the SnF_2 solution with some HF was reported in (7) only. This could be a key parameter and its influence on the nature of the product was investigated, while monitoring very carefully all other parameters that could be influential. HF/H_2O was varied from 0 to 0.55 and the influence of the nature of the beaker, namely whether glass (pyrex) or teflon (polytetrafluoroethylene) was used, was studied. X was fixed at 0.20 and $t(SnF_2)$ and $t(PbSnF_4)$ = 0. The results on fig. 11-15 show that no erratic behavior is obtained when the appropriate preparative conditions are carefully controlled. Fig. 11 shows that when no HF is used, a and b are equal, i.e. α-$PbSnF_4$ is obtained.

However as HF is added, a increases and b decreases until HF/H_2O = c.a. 0.10 at which point a constant difference of 0.095Å is obtained which does not change upon further addition of HF. The average value of $(a_o+b_o)/2$ falls slightly from 4.223 to 4.209Å, showing that the distortion taking place in the (a,b) plane occurs with a small lattice contraction in this plane.

Fig. 12 gives the orthorhombic distortion vs HF/H_2O. When HF/H_2O = 0, the a/b ratio distortion equals one as there is no orthorhombic distortion, and α-$PbSnF_4$ is obtained.

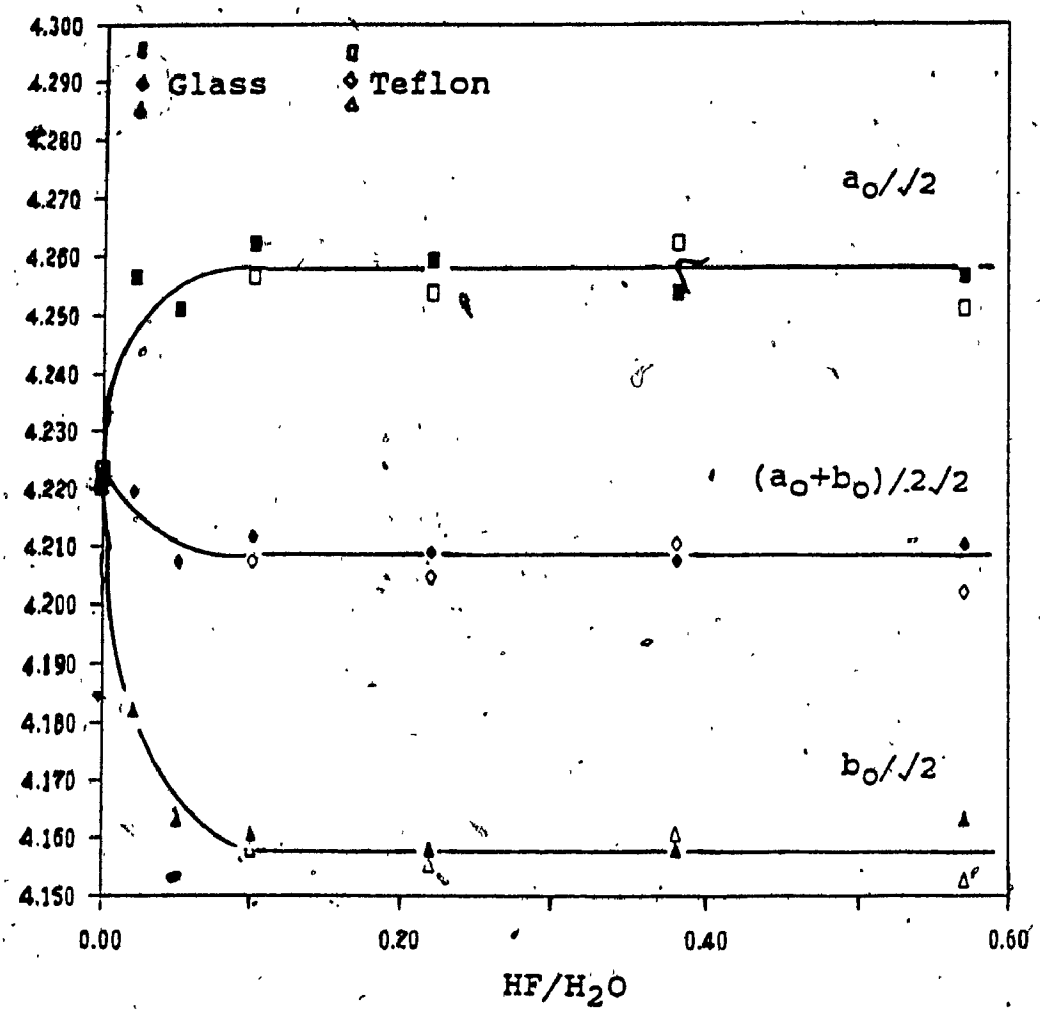

Fig. 11. Evolution of the a and b parameters of $PbSnF_4$ versus HF/H_2O and the nature of the beaker, X = 0.20, $t(SnF_2) = 0$ and $t(PbSnF_4) = 0$.

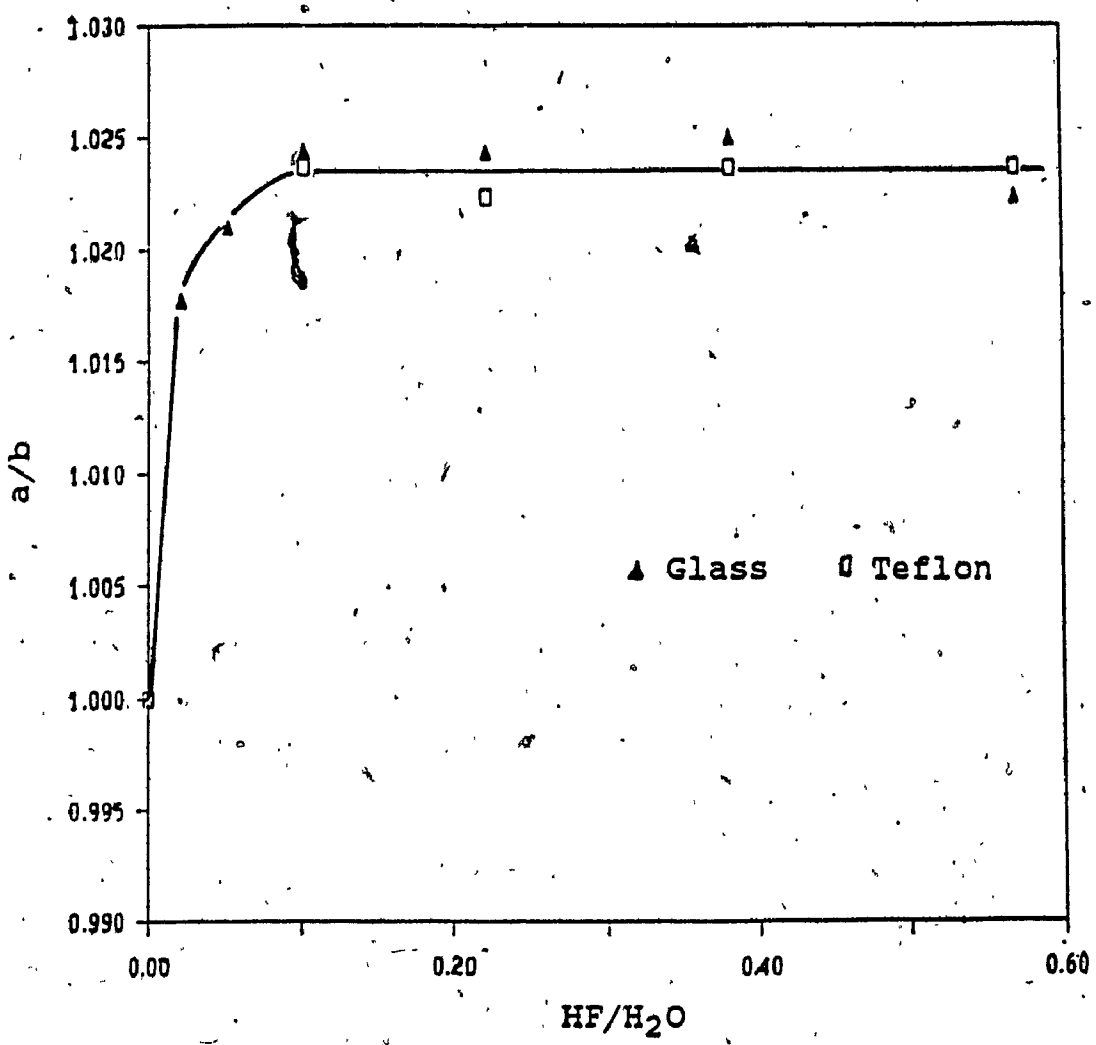

Fig. 12. Orthorhombic distortion of $PbSnF_4$ versus HF/H_2 and the nature of the beaker, X = 0.20, $t(SnF_2) = 0$ and $t(PbSnF_4) = 0$.

For HF/H_2O > 0 o-$PbSnF_4$ is obtained and the distortion is seen to increase until HF/H_2O = c.a. 0.10 where a maximum is reached and maintained at higher ratios. For 0 < HF/H_2O < 0.10, the size of the orthorhombic distortion is strongly dependant on the amount of HF present.

Fig. 13 shows that no significant variation of the c parameter occurs, within experimental error. It is important to note that the accuracy of determining θ is ± 0.01 degree which corresponds to ± 0.01Å.

However, the cell volume does fall slightly to compensate for the slightly larger decrease in b than increase in a from ca. 203.5$Å^3$ to ca. 202.0$Å^3$ as shown in fig. 14.

Also, fig. 15 shows the tetragonal distortion is seen to increase upon the addition of HF to the SnF_2 solution from ca. 1.353 to ca. 1.357.

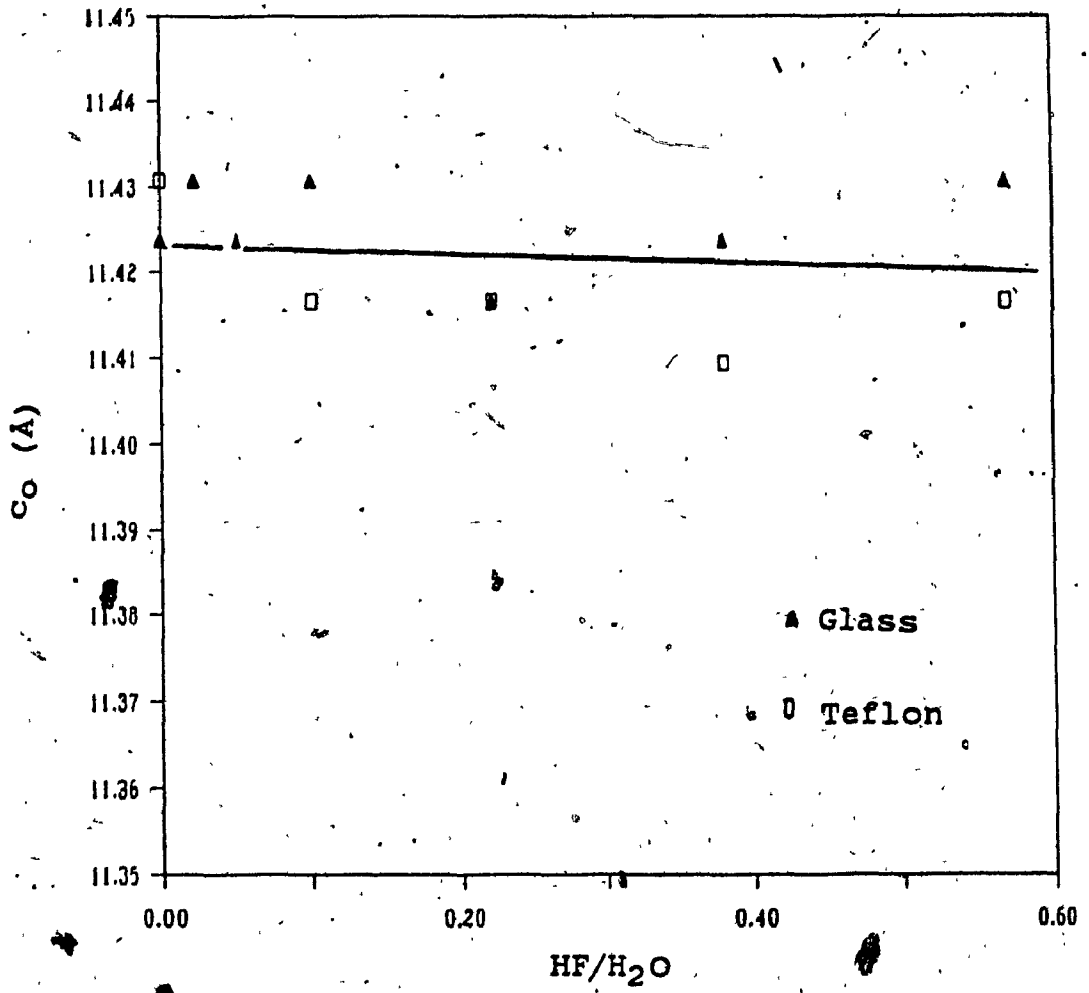

Fig. 13. Evolution of the c parameter with HF/H_2O and the nature of the beaker, X = 0.20, $t(SnF_2)$ = 0 and $t(PbSnF_4)$ = 0.

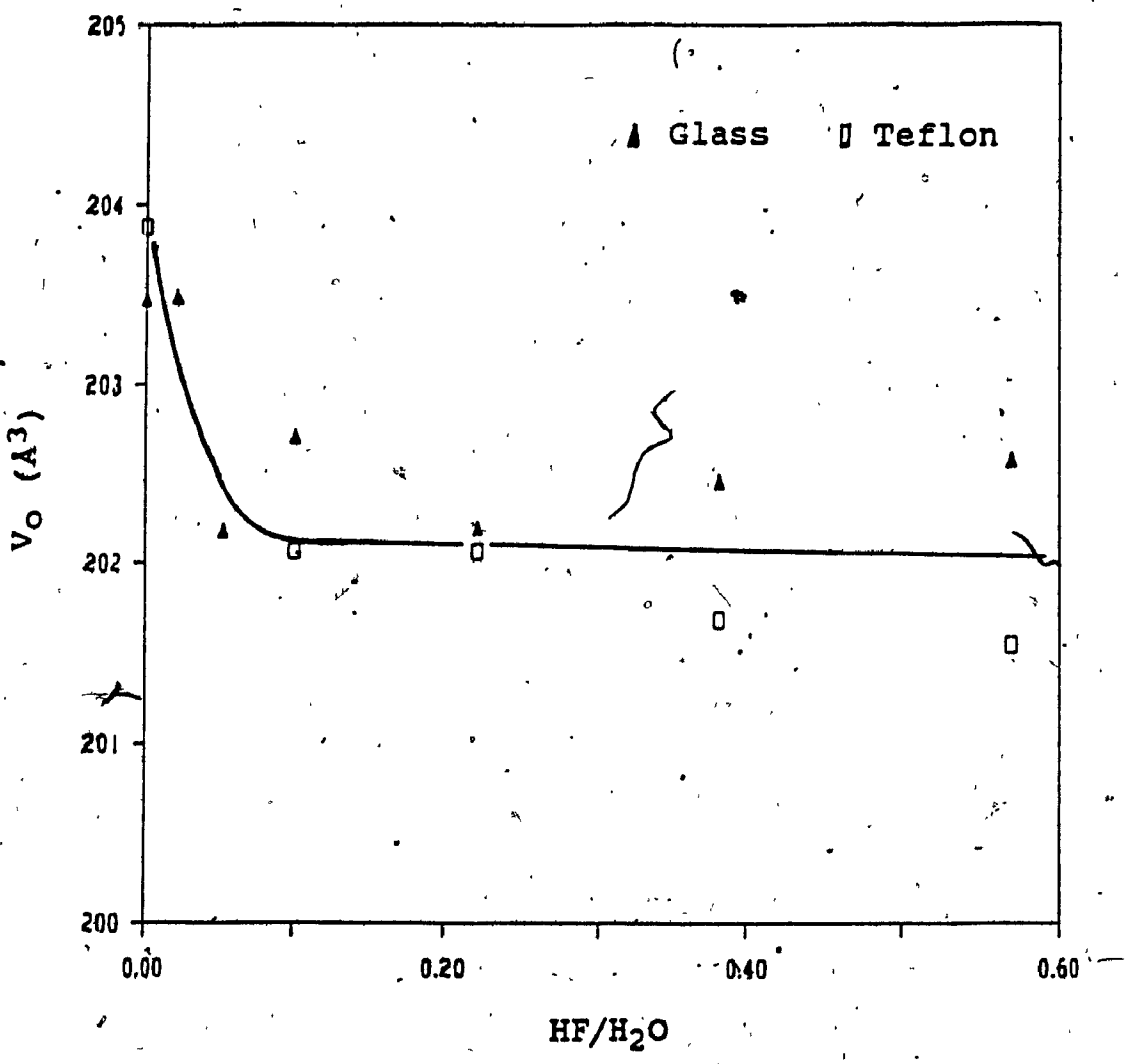

Fig. 14. Evolution of the cell volume with HF/H_2O and the nature of the beaker, X = 0, $t(SnF_2)$ and $t(PbSnF_4)$.

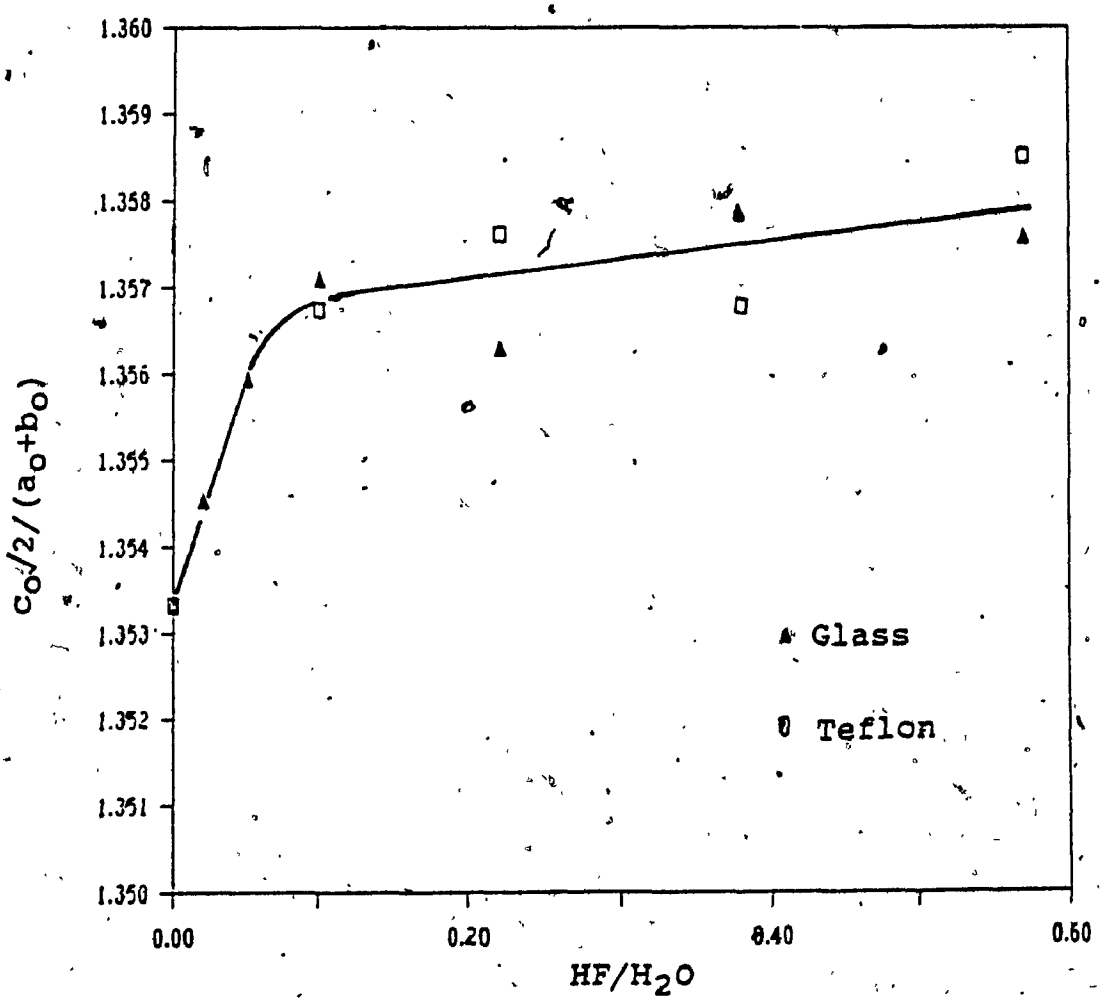

Fig. 15. Evolution of tetragonal distortion with HF/H_2O and nature of the beaker, X = 0.20, $t(SnF_2)$ = 0 and $t(PbSnF_4)$ = 0.

It is clear from these results that the orthorhombic distortion is purely a bidimensional phenomenon occurring in the (a,b) plane, with no change in the order along c. SnF_2 is known to hydrolyze slowly, spontaneously, in aqueous solutions (9) and this hydrolysis can be reversed upon addition of an excess of HF (Equation II).

Equation II

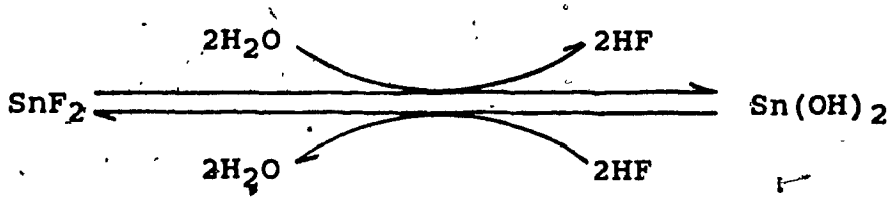

Therefore, when no HF is added, there is lack of fluoride ions because hydrolysis leads to loss of HF by evaporation. One can therefore postulate that the tetragonal form of $PbSnF_4$ is formed when there are not enough fluoride ions present. As a result, some fluoride ions may be substituted by OH^- or O^{2-} ions. Substitution with oxide would also create vacancies on the anion sublattice as $2F^-$ would be replaced by one oxygen atom. When HF is added, more fluoride ions are available and less substitution with OH^- and/or O^{2-} occurs, and for $HF/H_2O > 0.10$, stoichiometric $PbSnF_4$ with no substitution of fluoride is obtained.

Hydrolysis, giving free HF, also leads to etching of the reaction vessel when pyrex is used. Therefore, one could suspect interference from elements etched from the glass, mainly sodium and silicon. However, the results shown on fig. 11-15 clearly establish that identical results are obtained in both cases. As a consequence, because of the large number of beakers necessary and as glass etching by HF does not affect the results, pyrex beakers were used in the rest of this study.

3.2.3 INFLUENCE OF $t(SnF_2)$

In this investigation, the same conditions were used as in the above study except that only two values of HF/H_2O (0 and 0.10) were used and $t(SnF_2)$ was varied. The results are shown in fig. 16-22.

As can be seen on fig. 16, a and b are equal and constant for all values of $t(SnF_2)$ when $HF/H_2O = 0$ (data points not shown), i.e. α-$PbSnF_4$ phase is always obtained. On the other hand, for $HF/H_2O = 0.10$, a and b are unequal for $t(SnF_2) > 0$ as o-$PbSnF_4$ is obtained. However, for $t(SnF_2) > 0$, a decreases regularly while b is constant, up to $t(SnF_2) = 40$. Then b is seen to increase suddenly and becomes equal to a at around $t(SnF_2) = 60$ min.

Fig. 17 shows that α-$PbSnF_4$ is always obtained when no HF is used.

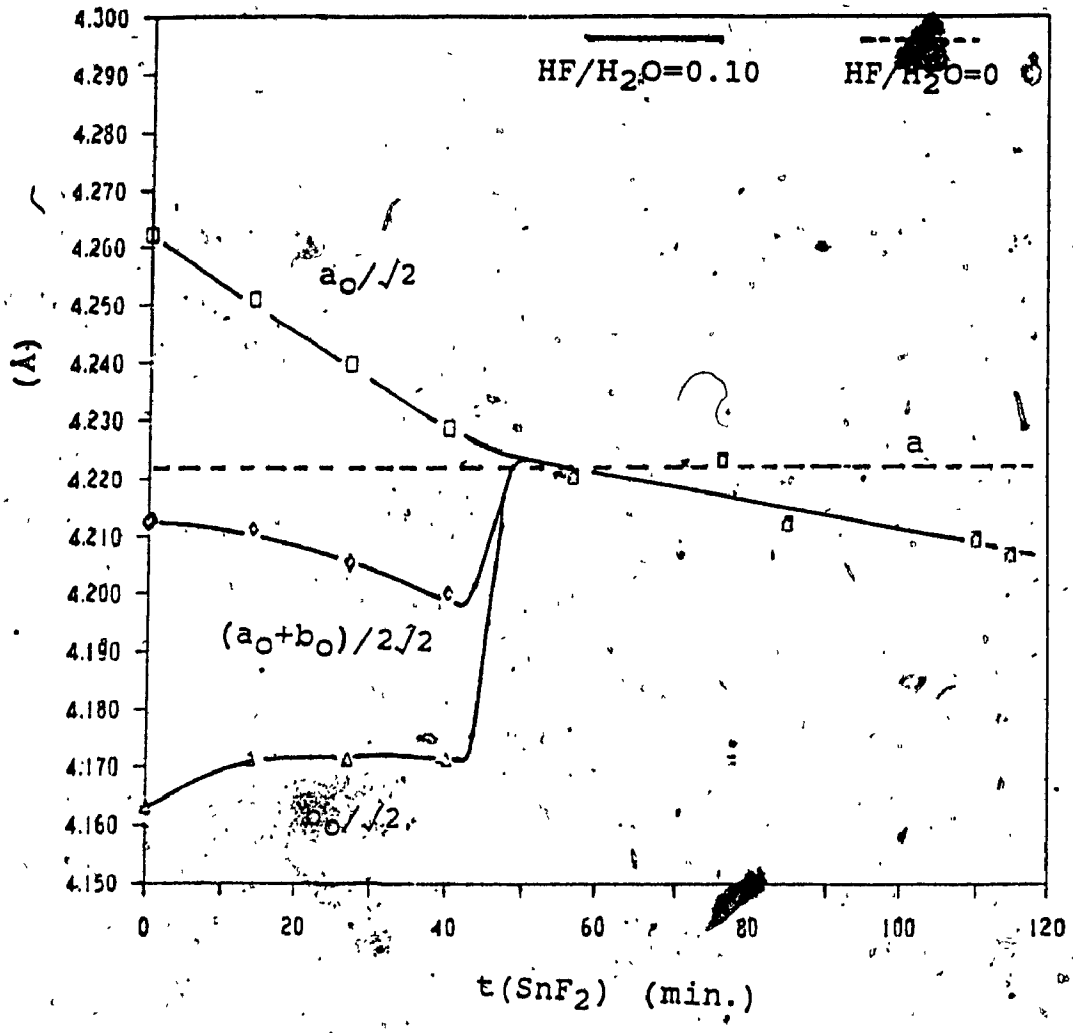

Fig. 16. Evolution of the a and b parameters of $PbSnF_4$ versus (SnF_2) for HF/H_2O = 0 and 0.10, with t($PbSnF_4$) = 0, X = 0.20.

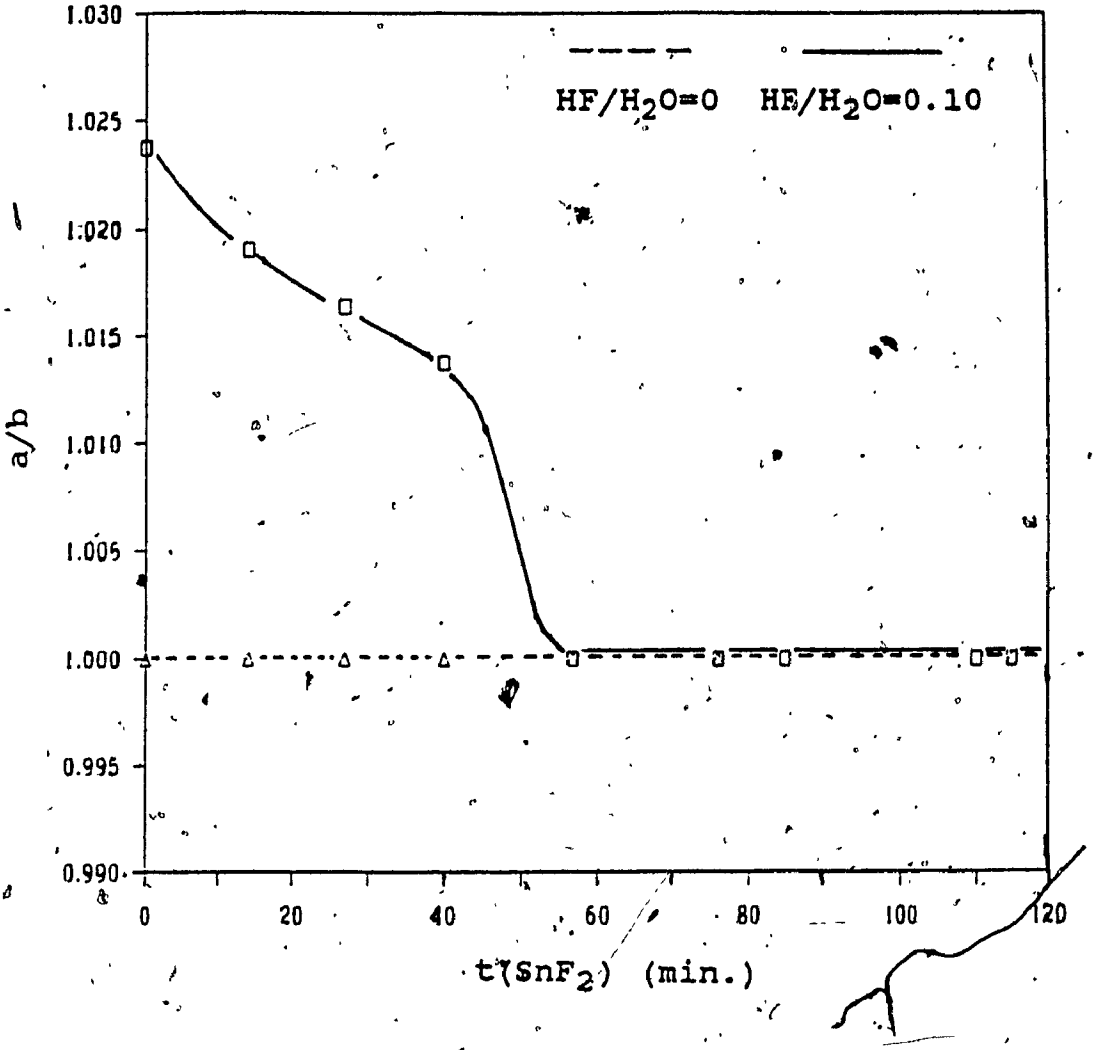

Fig. 17. Orthorhombic distortion of $PbSnF_4$ versus $t(SnF_2)$ for HF/H_2O = 0 and 0.10 with $t(PbSnF_4)$ = 0, X = 0.20.

Where HF/H_2O = 0.10, orthorhombic distortion is observed and decreases until $t(SnF_2)$ > 60 min., at which point α-$PbSnF_4$ is obtained and behaves as if no HF was used. We find that varying $t(SnF_2)$ affects the $\vec{c}$ direction in addition to the $(\vec{a},\vec{b})$ plane. This is shown in fig. 18 where, for HF/H_2O = 0.10 we see the c parameter fall steadily with increasing $t(SnF_2)$.

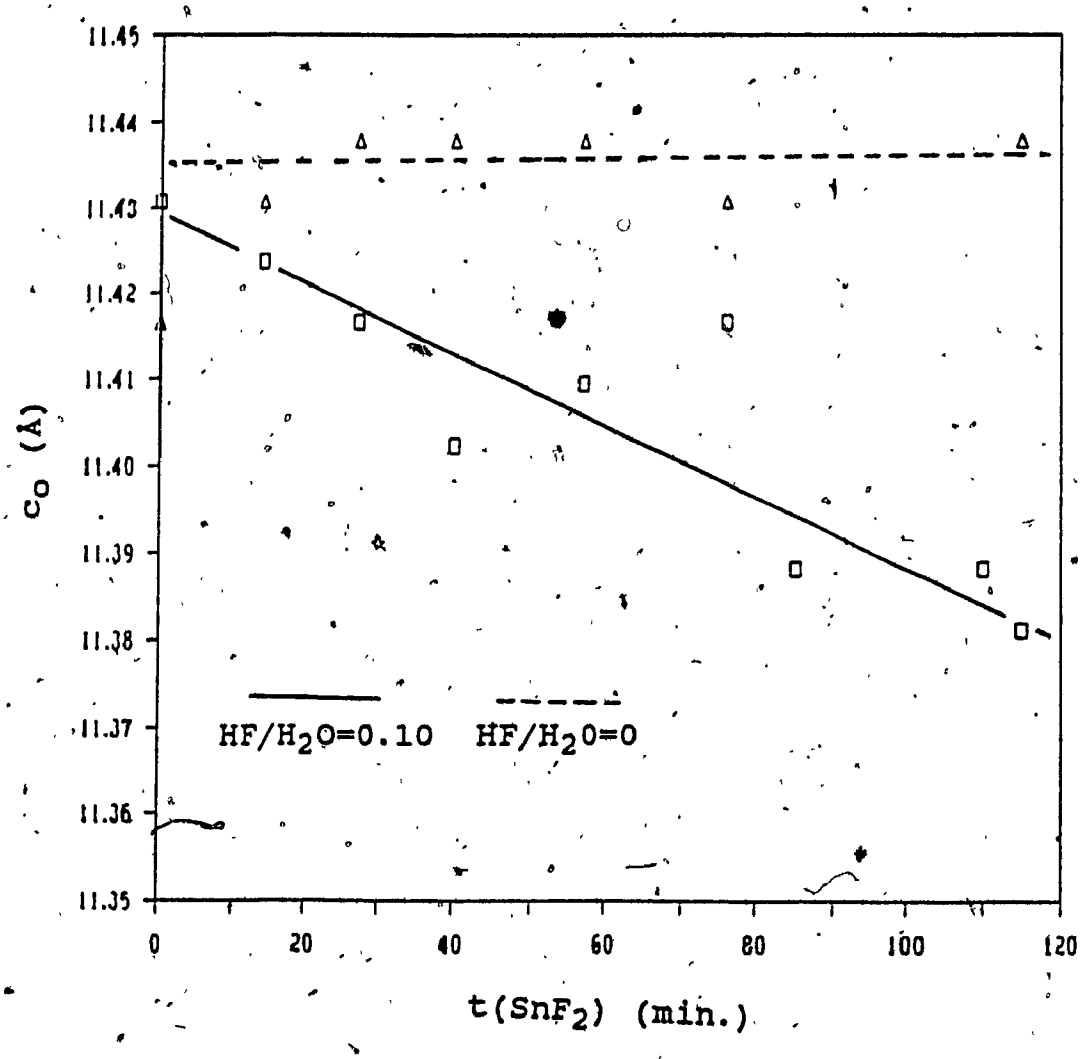

Fig. 18. Evolution of the c parameter with $t(SnF_2)$; for HF/H_2O = 0 and 0.10 with $t(PbSnF_4)$ = 0, X = 0.20.

These changes in a, b and c for HF/H_2O = 0 and 0.10 are further illustrated in fig. 19 and 20 where, for those preparations where HF/H_2O = 0, no change in the cell volume and just a slight change in the tetragonal distortion is observed. In the case where HF/H_2O= 0.10, significant changes occur to both the cell volume and tetragonal distortion, with discontinuity occurring at $t(SnF_2)$ = 50 min. From the cell volume we can see that both o-$PbSnF_4$ and α-$PbSnF_4$, prepared with HF/H_2O = 0.10 and $t(SnF_2)$ > 60 min., show a decrease in cell volume with $t(SnF_2)$. This is particularly interesting in that α-$PbSnF_4$ prepared with no HF shows no variation in any of the unit cell parameters. The effect of increasing $t(SnF_2)$, at constant HF/H_2O, on the orthorhombic distortion, seems opposite to the effect of increasing HF/H_2O at constant $t(SnF_2)$ in that as $t(SnF_2)$ is increased, α-$PbSnF_4$ is obtained. It is doubtful, however, whether this α-$PbSnF_4$ is the same as the α-$PbSnF_4$ prepared for HF/H_2O = 0 due to the behavior of the unit cell parameters, which are not similar.

As shown on fig. 21, the yield of product drastically decreases from c.a. 80% to 15% for $t(SnF_2)$ increasing from 0 to 20 hours.

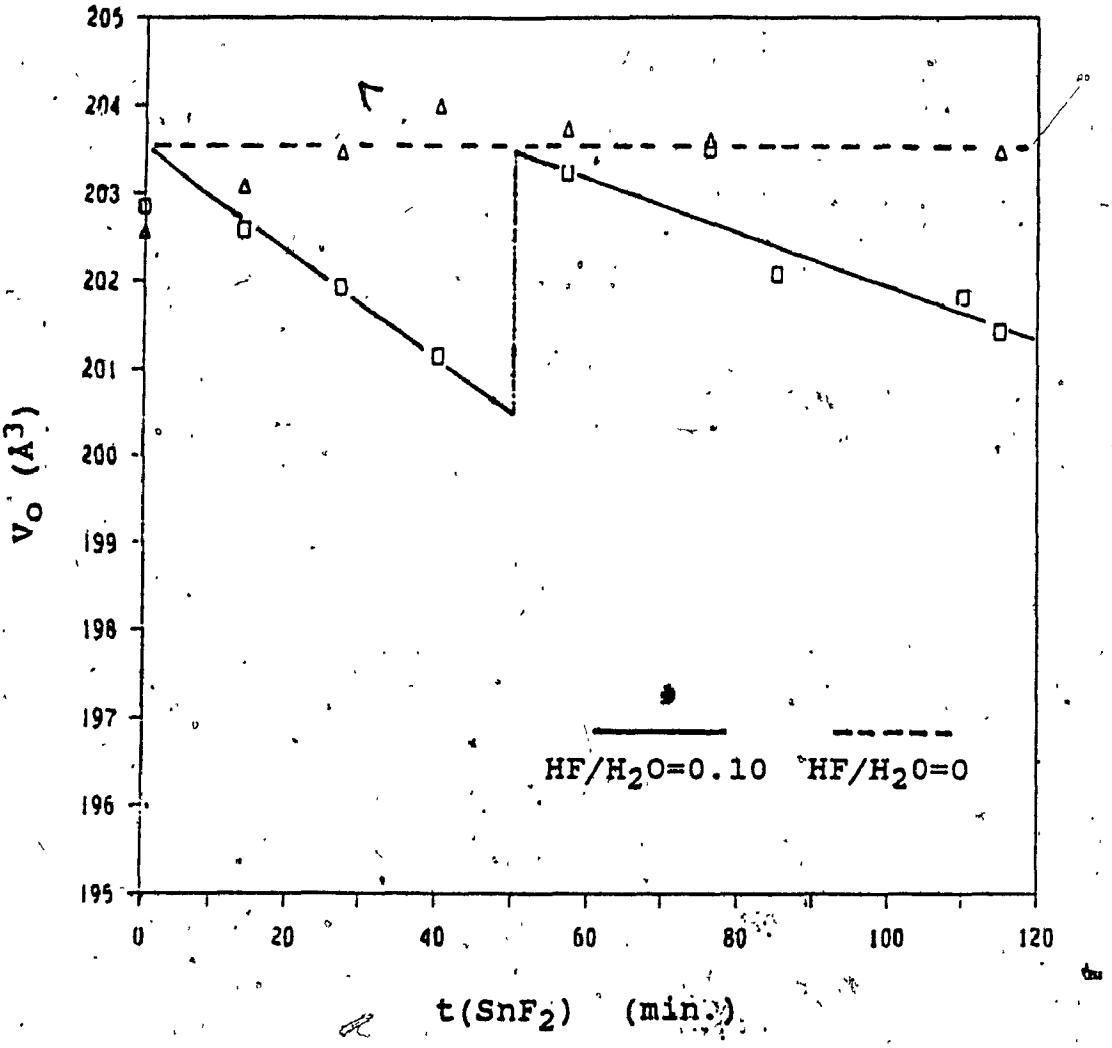

Fig. 19. Evolution of the cell volume of $PbSnF_4$ with t(SnF_2) for HF/H_2O = 0 and 0.10 with t($PbSnF_4$) = 0, X = 0.20.

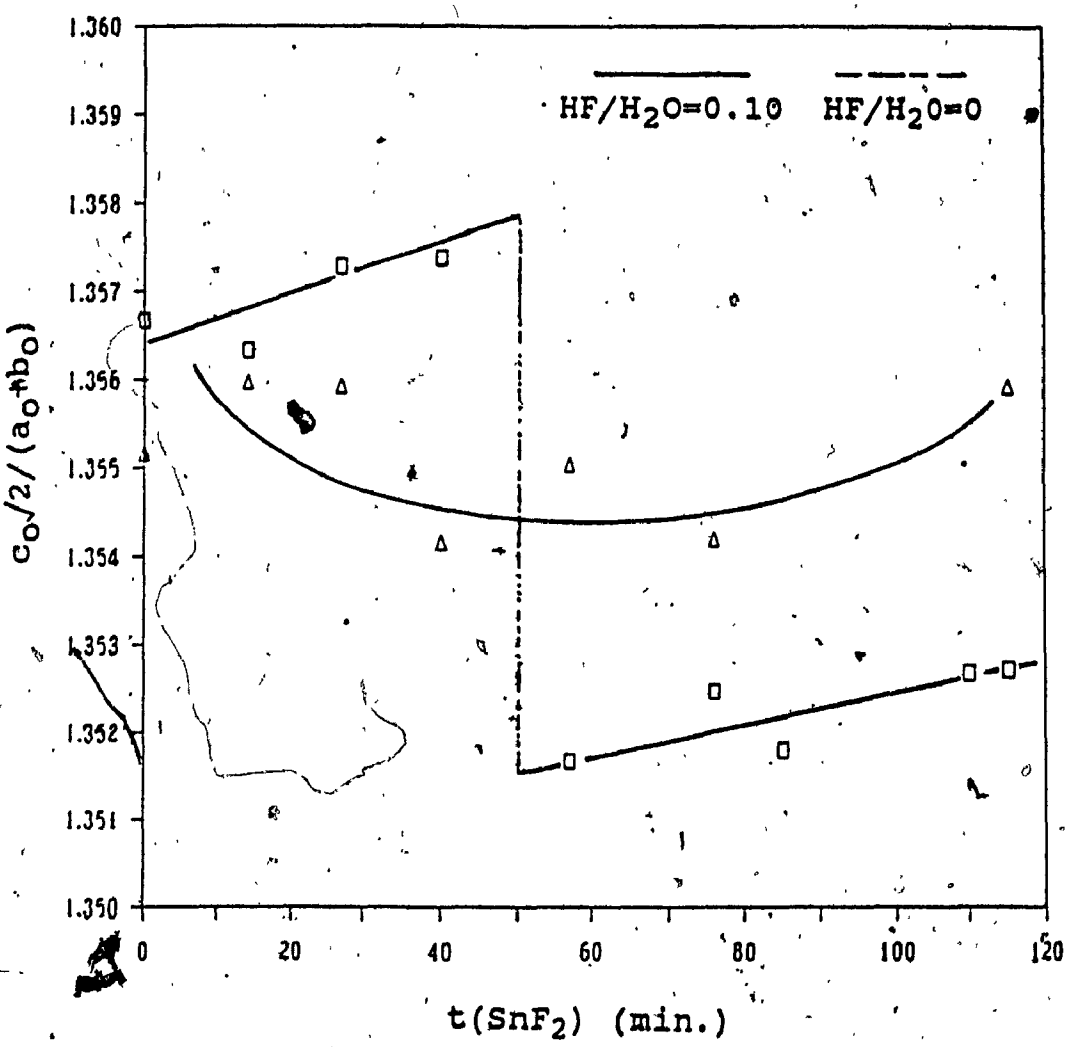

Fig. 20. Evolution of the tetragonal distortion of $PbSnF_4$ with $t(SnF_2)$ for HF/H_2O = 0 and 0.10 with $t(PbSnF_4)$ = 0 and X = 0.20

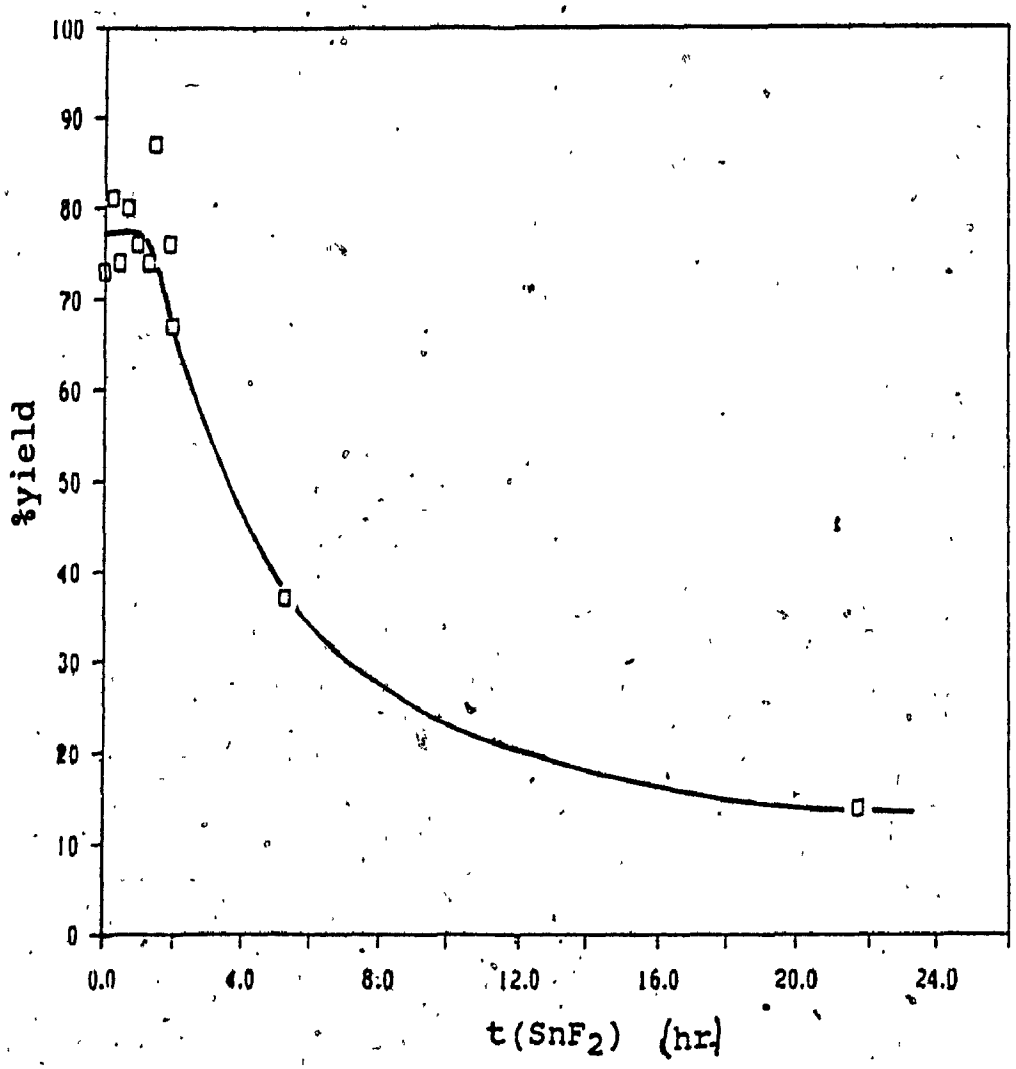

Fig. 21. %Yield of $PbSnF_4$ versus $t(SnF_2)$ for $HF/H_2O = 0$ with $t(PbSnF_4) = 0$, X = 0.20.

The decrease in yield can be explained by the loss of HF by evapotation and etching as $t(SnF_2)$ increases, which results in less fluoride ions available. Therefore, increasing $t(SnF_2)$ results in cancelling the effect of addition of HF and makes the reaction of hydrolysis shift to the right hand side. The decrease of yield can also be explained, at least in part, based on loss of fluorine. Indeed, loss of fluorine upon hydrolysis of SnF_2 results in less SnF_2 available and as a result, the yield of Equation II will be lower. In addition, it has been established that hydrolysis of SnF_2 is slowly followed by oxidation of tin (II) to tin (IV) (Equation III) and, as a result, there is also deficiency of divalent tin in the reaction mixture which results in a lower yield.

Equation III

$$Sn^{2+}(aq) + H_2O + 1/2O_2 \xrightarrow{H_2O/O_2} Sn^{4+}(aq) + 2OH^-$$

$$Sn^{4+}(aq) \xrightarrow{H_2O} SnO_2.nH_2O$$

A last possibility for the drastic decrease of yield could be loss of tin by the SnF_2 as high losses of tin from aqueous solutions have been reported even though these experiments were carried out on much more dilute solutions. (10)

Atomic absorption spectroscopy was performed on the samples in the above mentioned study and the results are given in fig. 22. When $HF/H_2O = 0$, corresponding to α-$PbSnF_4$, the results show that when $t(SnF_2) = 0$, the ratio Pb/Sn is close to one indicating that α-$PbSnF_4$, stoichiometric, is obtained, which is in agreement with previous reports. As $t(SnF_2)$ approaches 60 min., this ratio is seen to fall slightly to Pb/Sn = c.a. 0.95 which corresponds to more Sn being incorporated into the lattice of α-$PbSnF_4$. At $t(SnF_2) > 60$ min, the Pb/Sn ratio falls drastically and then seems to level out at Pb/Sn = c.a. 0.85. The fact that more tin is found in $PbSnF_4$ is not surprising as the reaction mixture is rich in Sn (i.e. X = 0.20), however, the higher tin content for $t(SnF_2) > 0$ shows that there is probably no tin loss by the solutions and oxidation of tin (II) to tin (IV) is negligible.

When $HF/H_2O = 0.10$, corresponding to o-$PbSnF_4$ at $t(SnF_2) < 60$ min., Pb/Sn = c.a. 0.91 and as $t(SnF_2)$ increases to 60 min. a steady increase to Pb/Sn = c.a. 1.0 occurs. At $t(SnF_2) > 60$ min. (α-$PbSnF_4$), the Pb/Sn ratio again begins to fall slowly and shows no tendency to level off at $t(SnF_2) = 120$ min. Here, it can be said that both forms of α-$PbSnF_4$ (prepared with $HF/H_2O = 0$ and 0.10) behave the same way, however, they are not the same material as their Pb/Sn ratios are different.

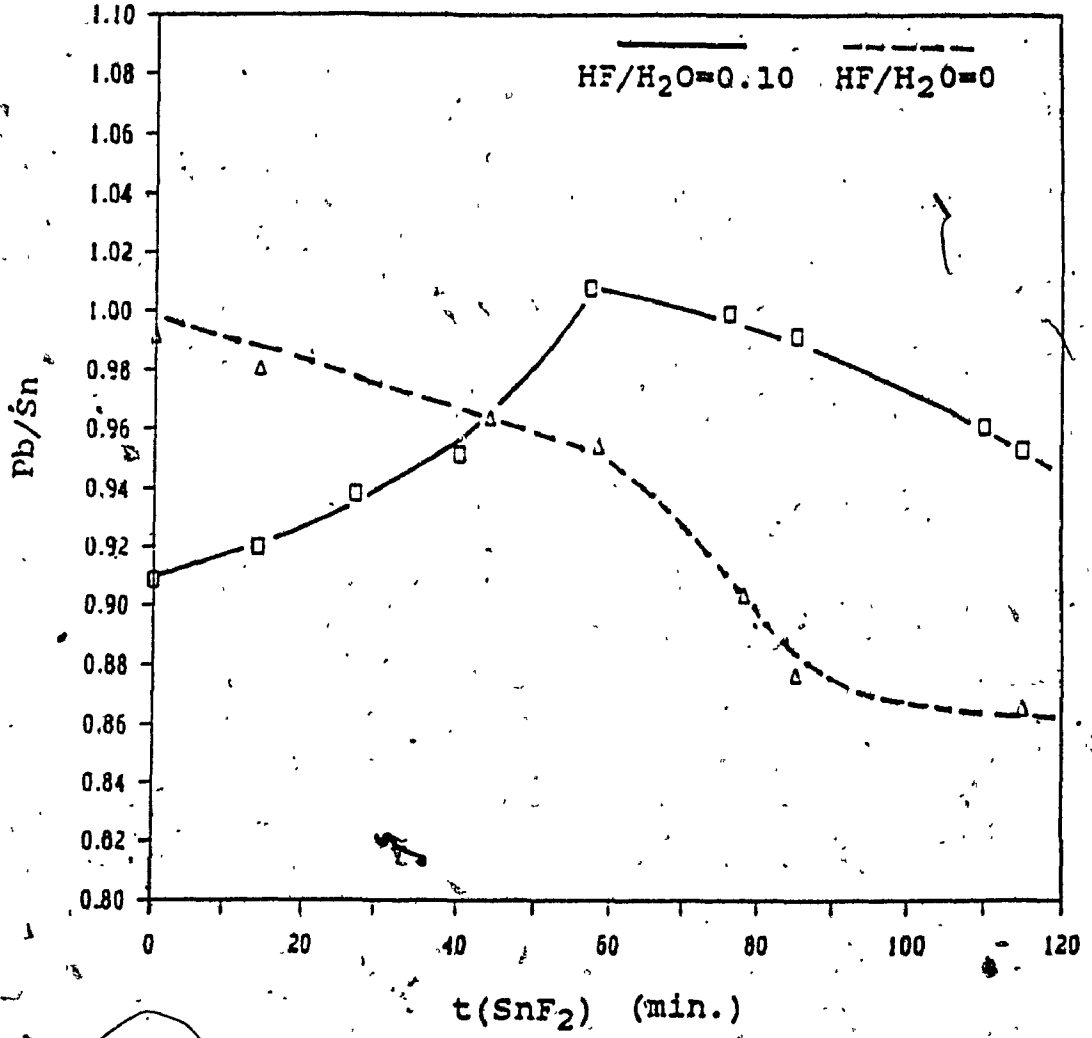

Fig. 22. Influence on Pb/Sn of $t(SnF_2)$ for HF/H_2O = 0 and 0.10, $t(PbSnF_4)$ = 0 and X = 0.20.

From the above results, there are two conditions which give stoichiometric α-$PbSnF_4$ and they are:

1) when $t(SnF_2)$ = 0 and HF/H_2O = 0

2) when $t(SnF_2)$ = c.a. 60 min. and HF/H_2O = 0.10

Stoichiometric o-$PbSnF_4$ is never obtained when X = 0.20, with an excess of Sn being incorporated into the o-$PbSnF_4$ lattice.

3.2.4 INFLUENCE OF $Pb(NO_3)_2/SnF_2$ MOLAR RATIO AND $t(SnF_2)$

In this study, $PbSnF_4$ was prepared by varying X from 0.05 to 0.95, for $t(SnF_2)$ = 0 , 20 and 30 min., HF/H_2O = 0 and 0.10, and $t(PbSnF_4)$ = 0. The results are shown in fig. 23-29. For HF/H_2O = 0 (data points not shown), α-$PbSnF_4$ ($a_\alpha = b_\alpha$) is obtained for all values of X.

For HF/H_2O= 0.10, o-$PbSnF_4$, with a_o and b_o being very weakly dependent on X is obtained. For $t(SnF_2)$ = 20 and 30 min., a strange dependence on X is observed with, in both cases, a larger difference between a_o and b_o in the middle of the diagram, i.e. for molar ratio close to 0.5. However, for $t(SnF_2)$ = 20 min., o-$PbSnF_4$ is obtained for all values of X, when for $t(SnF_2)$ = 30 min., a α=$PbSnF_4$ is obtained for X < 0.25 and X > 0.65, and o-$PbSnF_4$ between these values.

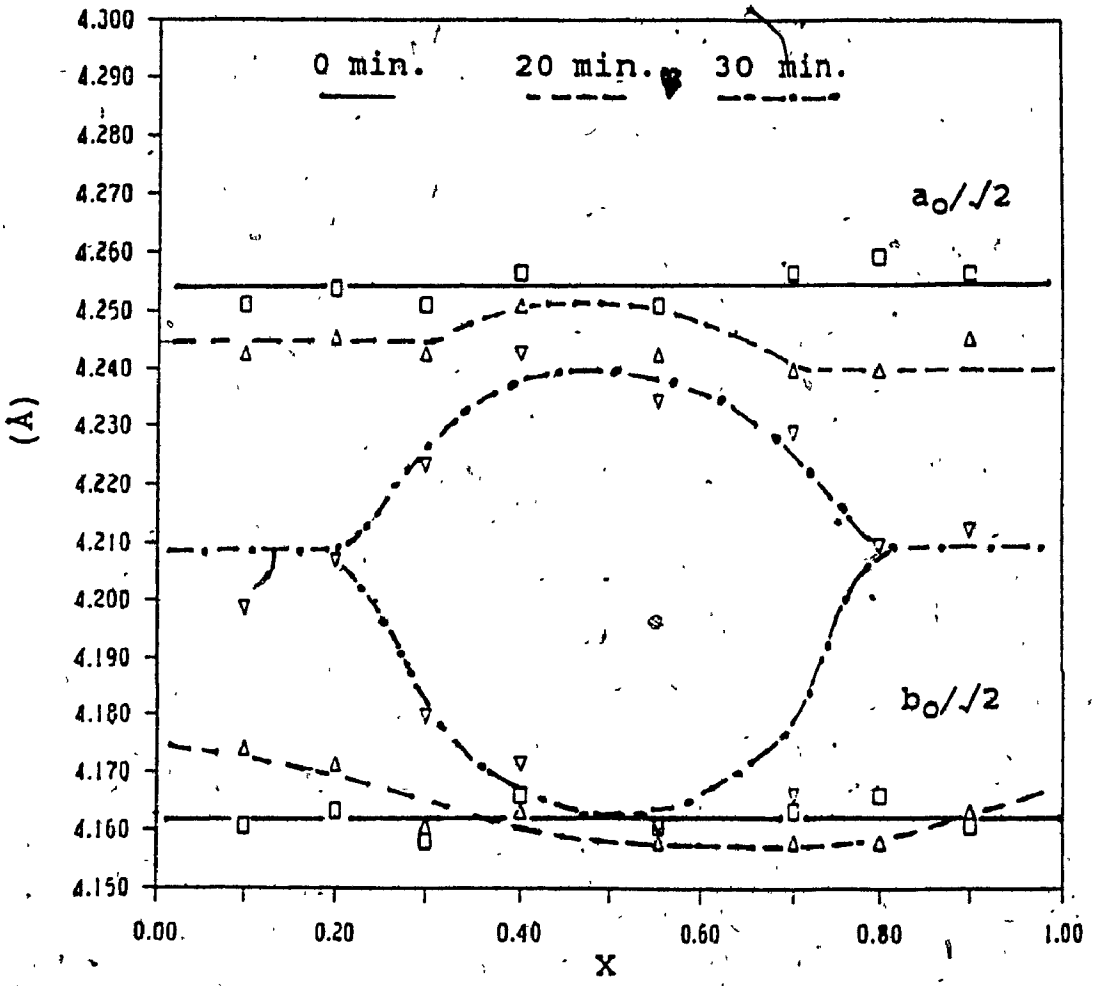

Fig. 23. Evolution of a and b parameters of $PbSnF_4$ versus X, for $t(SnF_2)$ = 0, 20 and 30 min., $t(PbSnF_4)$ = 0 and HF/H_2O = 0.10.

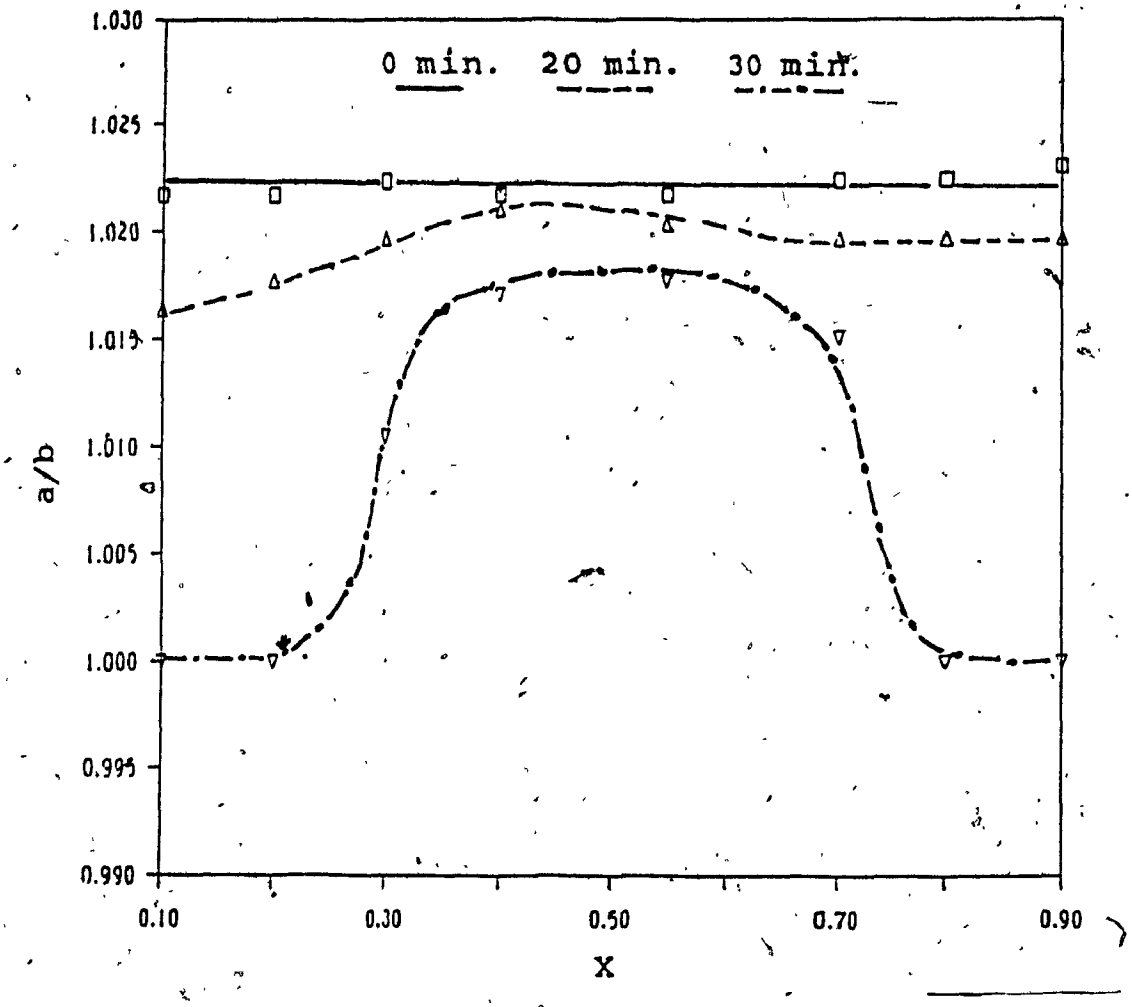

Fig. 24. Orthorhombic distortion of $PbSnF_4$ versus X, $t(SnF_2)$ = 0, 20 and 30 min., $t(PbSnF_4)$ = 0 and HF/H_2O = 0.10.

Fig. 24 shows the orthorhombic distortion versus X. o-$PbSnF_4$ with constant orthorhombic distortions equal to 1.022Å are obtained for $t(SnF_2) = 0$. At $t(SnF_2) = 20$ and 30 min., the orthorhombic distortion is seen to fall as $t(SnF_2)$ increases from 20 to 30 minutes, with α-$PbSnF_4$ being obtained for $X < 0.25$ and $X > 0.65$. The meaning of the results presented in fig. 23 and 24 is not fully understood at this point. However, it is probably not a coincidence that the maximum orthorhombic distortion occurs for a molar ratio close to 0.5, i.e. for the exact stoichiometry for equation (I). In addition, close examination of fig. 24 shows that this maximum shifts slowly towards smaller molar ratios as $t(SnF_2)$ increases. This is not surprising as maximum distortions are observed for higher fluoride concentrations. As $t(SnF_2)$ increases, loss of HF upon hydrolysis of SnF_2 results in constant values of $Pb(NO_3)_2/[SnF_2]_{actual}$ obtained for lower values of $Pb(NO_3)_2/(SnF_2)_{initial}$, $(SnF_2)_{initial}$ being the initial amount of SnF_2 in the solution (i.e. at $t(SnF_2) = 0$), and $(SnF_2)_{actual}$ being the actual amount of SnF_2 in the solution for $t(SnF_2) > 0$, respectively.

Fig. 25 shows an increase in the c parameter for $t(SnF_2) = 0$, 20 and 30 min. as X increases. Also, as $t(SnF_2)$ increases from 0 to 30 minutes, the c parameter decreases for a given value of X. The same behavior is observed for the cell volume (fig. 26) except that more scatter is

observed for $t(SnF_2)$ = 20 min. The tetragonal distortion, shown in fig. 27, reveals little difference observed for $t(SnF_2)$ = 0 and 20 min. At $t(SnF_2)$ = 30 min., the tetragonal distortion is seen to go through a maximum at X = 0.50.

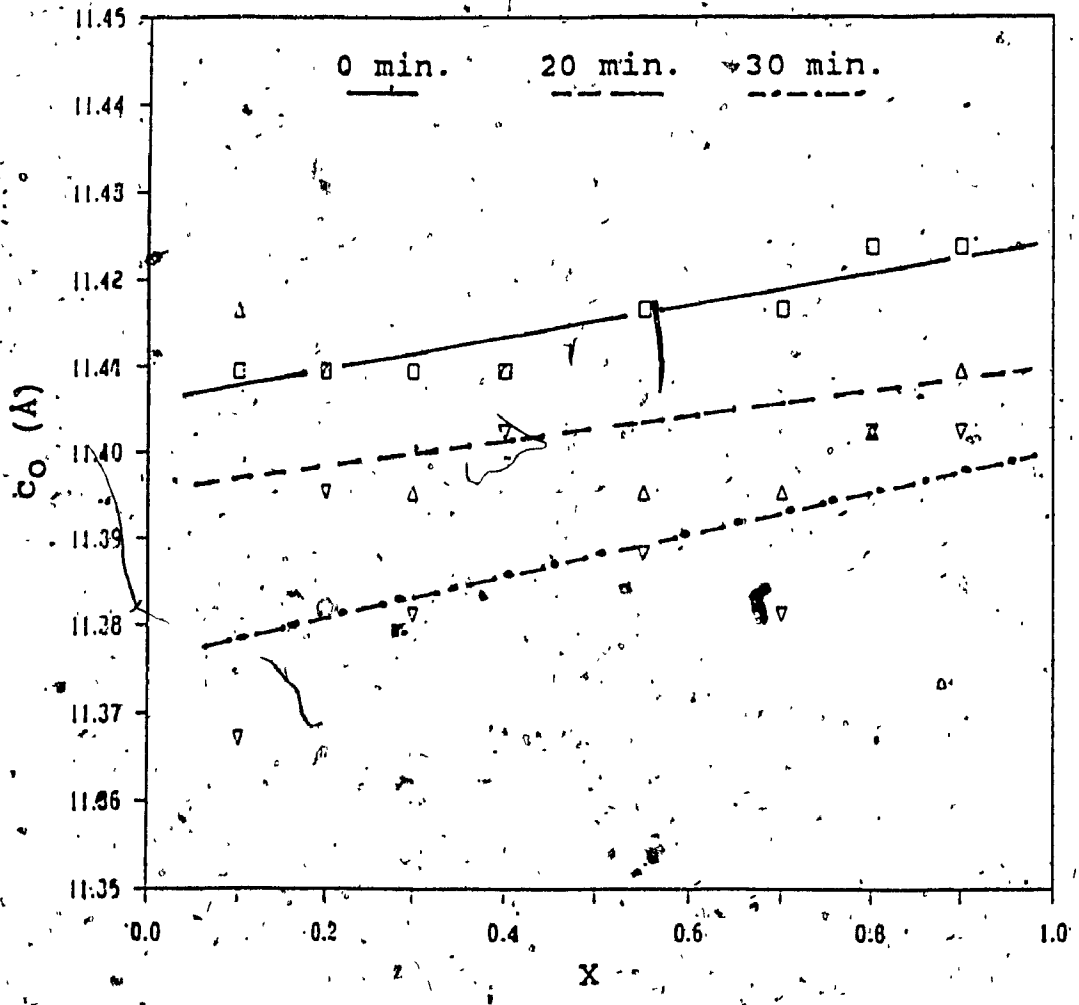

Fig. 25. Evolution of the c-parameter of $PbSnF_4$ versus X, $t(SnF_2)$ = 0, 20 and 30 min, $t(PbSnF_4)$ = 0 and HF/H_2O = 0.10.

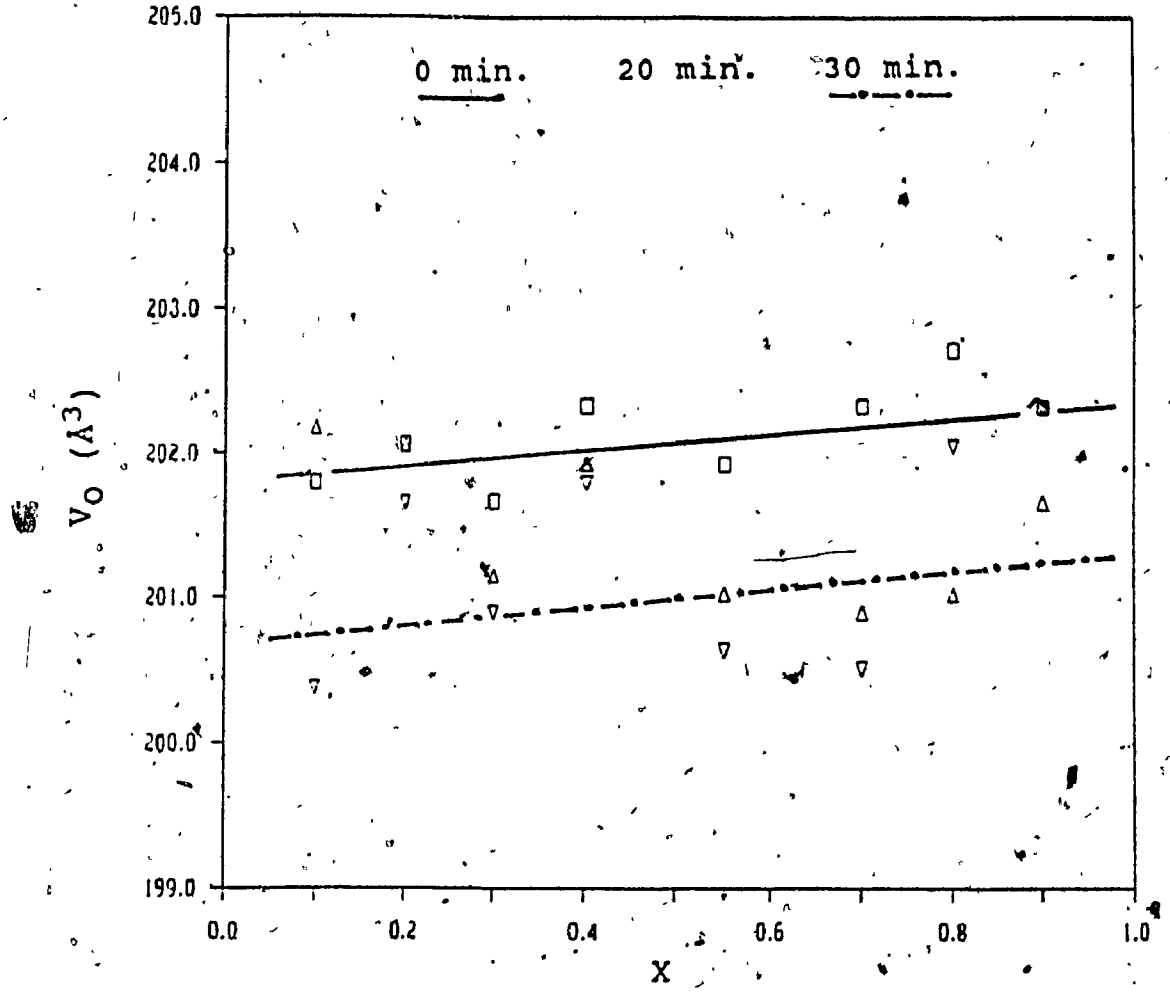

Fig. 26. Evolution of the cell volume versus X, $t(SnF_2)$ = 0, 20 and 30 min. with $t(PbSnF_4)$ = 0 and HF/H_2O = 0.10.

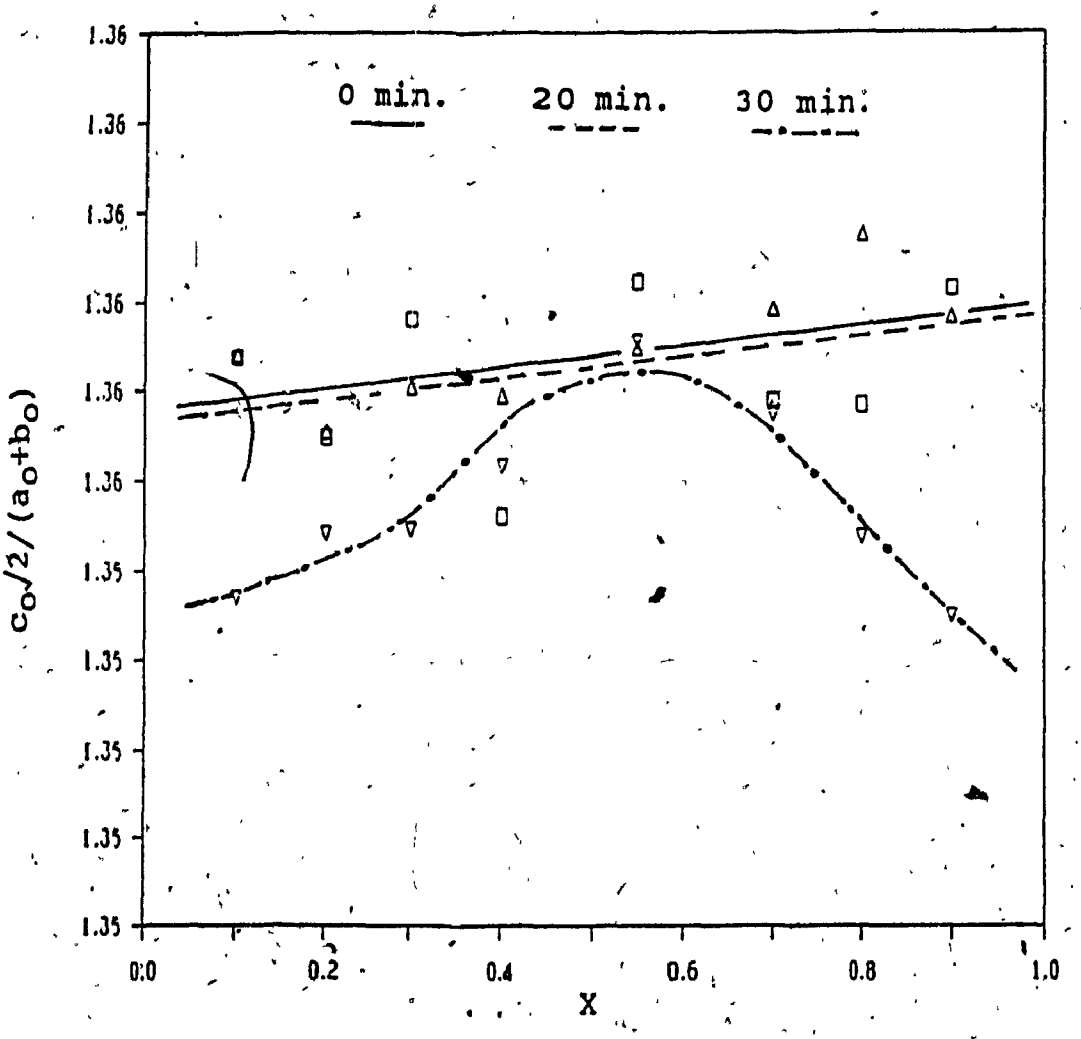

Fig. 27. Evolution of the tetragonal distortion versus X, $t(SnF_2)$ = 0, 20, and 30 min, with $t(PbSnF_4)$ = 0 and HF/H_2O = 0.10.

A plot of the yield of the above study for t(SnF_2) = 0 and 30 min is shown in fig. 28. Higher yield are obtained for t(SnF_2) = 0 than for 30 min. An interesting thing occurs at X = c.a. 0.75 for t(SnF_2) = 30 min.; the yield is seen to jump from about 55% to 70%. This corresponds to the presence of $Pb_2SnNO_3F_5.2H_2O$ which coprecipitates with $PbSnF_4$ from these reaction mixtures very rich in lead.

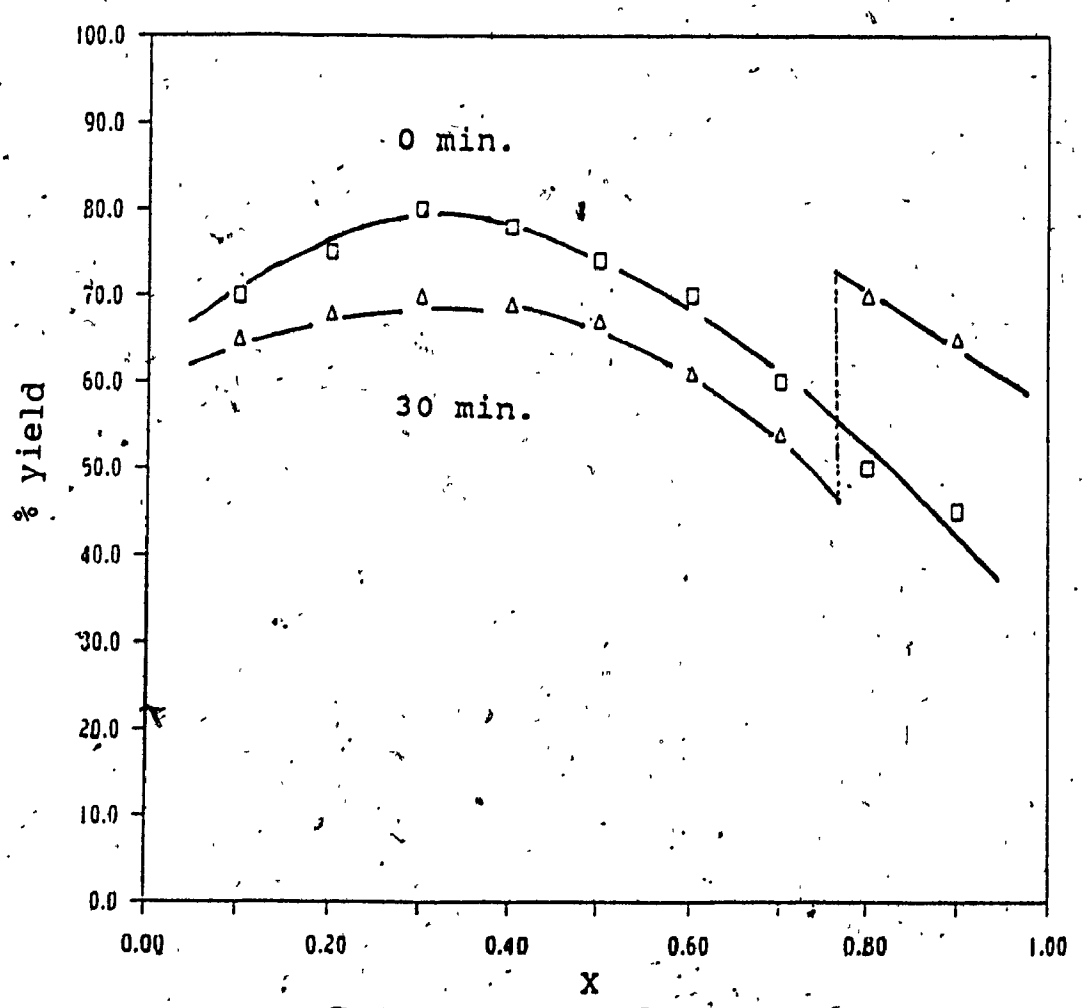

Fig. 28. % Yield versus X for t(SnF_2) = 0 and 30 min. with t($PbSnF_4$) = and HF/H_2O = 0.10.

Fig. 29 shows the typical X-ray powder pattern obtained for $t(SnF_2)$ = 30 min., X = 0.80 and HF/H_2O = 0.10. Those extra peaks that could not be indexed as belonging to α-$PbSnF_4$ are indexed as $Pb_2SnNO_3F_5.2H_2O$. For simplicity, those peaks due to $Pb_2SnNO_3F_5.2H_2O$ are shown in broken lines.

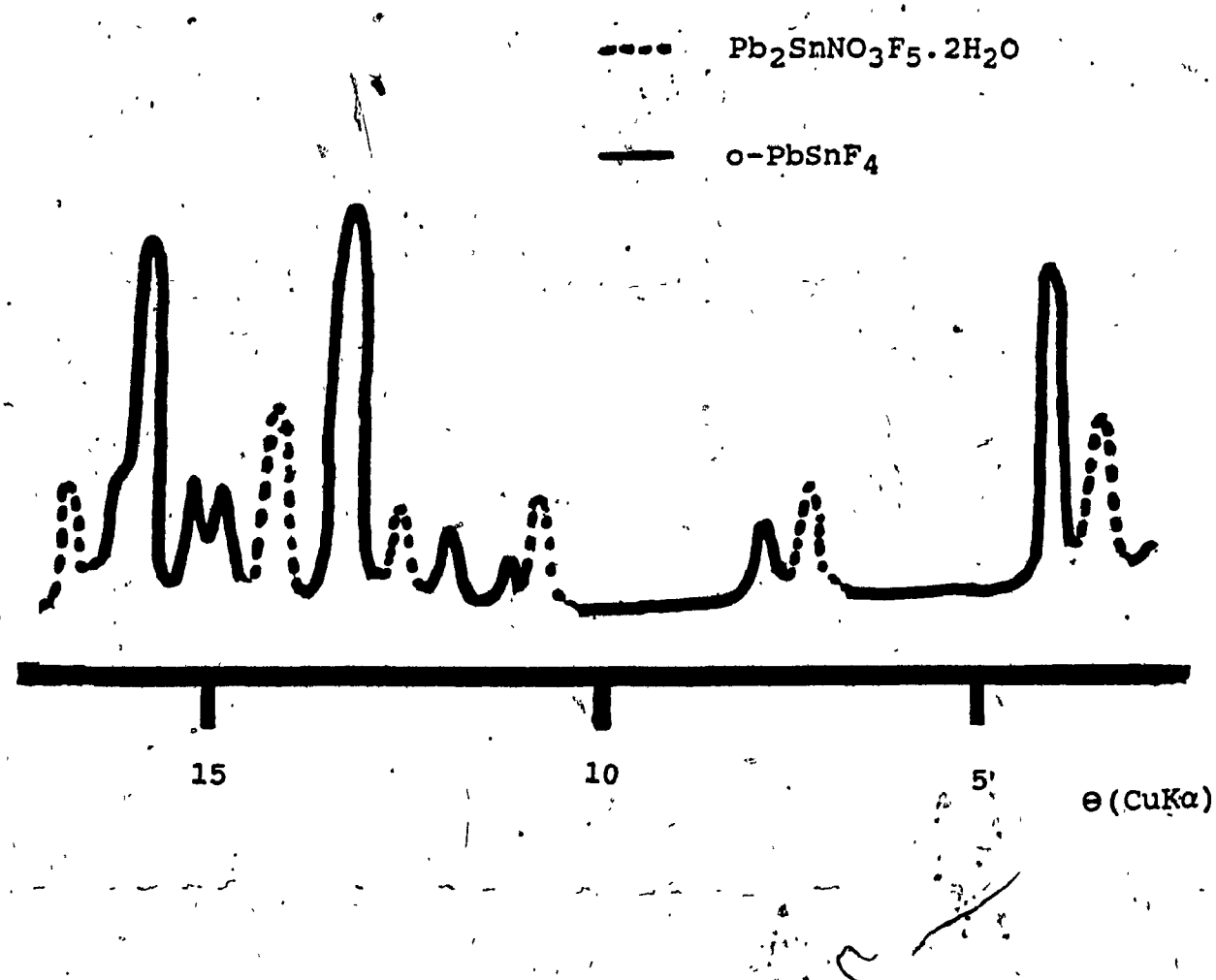

Fig. 29. Powder X-ray pattern obtained when $t(SnF_2)$ = 30 min., $t(PbSnF_4)$ = 0, HF/H_2O = 0.10 and X = 0.80.

3.2.5 INFLUENCE OF $t(PbSnF_4)$

In this study, $PbSnF_4$ was prepared for X fixed at 0.20, 0.50 and 0.70. In all cases $t(SnF_2) = 0$ and reactions were done with $HF/H_2O = 0$ and 0.10. Time intervals for $t(PbSnF_4)$ were 0, 2, 4 and 6 hours. The influence of $t(PbSnF_4)$ for $HF/H_2O = 0.10$, as shown on fig. 30, reveals that two separate effects are observed. No change in the a and b parameters occurs for all values of $t(PbSnF_4)$. However, at $t(PbSnF_4) = 2$, 4, and 6 hours the a and b parameters are lower in all cases in comparison with $t(PbSnF_4) = 0$. A possible explanation for this is most likely due to some solid/liquid interaction between o-$PbSnF_4$ and the reaction matrix resulting in an expansion of the unit cell in the (a,b) plane, for $t(PbSnF_4) = 0$.

The evolution of the a and b parameters for $HF/H_2O = 0$ is given in fig. 31. For $t(PbSnF_4) = 0$, α-$PbSnF_4$ is obtained and the a and b parameters are the same and constant. At $t(PbSnF_4) = 2$ hours and X = 0,20, a = c.a. 4.24Å and b = c.a. 4.20Å. These values become equal to 4.22Å at X values above 0.50. For $t(PbSnF_4) > 2$ hours the a parameter decreases for $t(PbSnF_4) = 4$ and 6 hours, while the b parameter seems to be constant. Some preparative condition, not yet specified, seems to influence the product for $HF/H_2O = 0$.

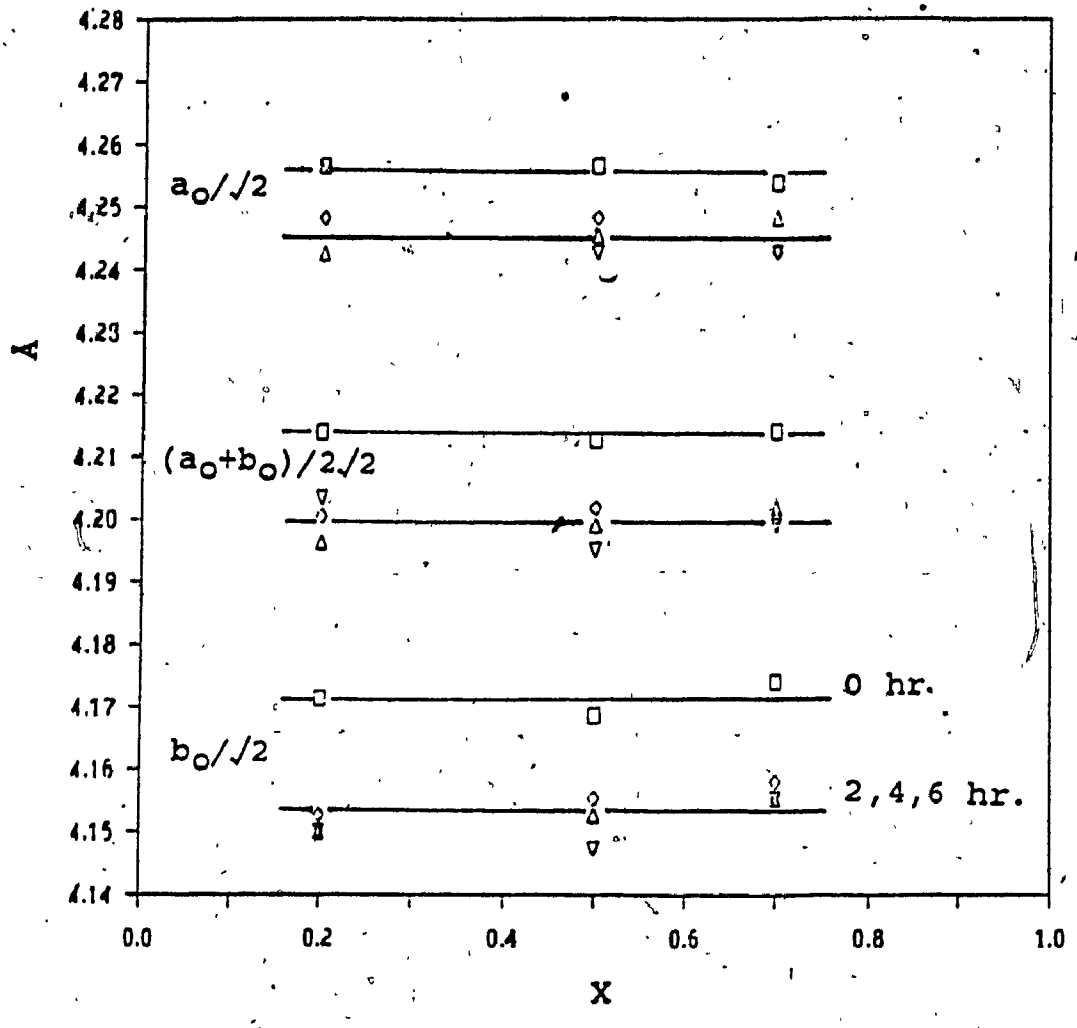

Fig. 30. Evolution of the a and b parameters of $PbSnF_4$ versus X and $t(PbSnF_4)$ for HF/H_2O = 0.10, $t(SnF_2)$ = 0.

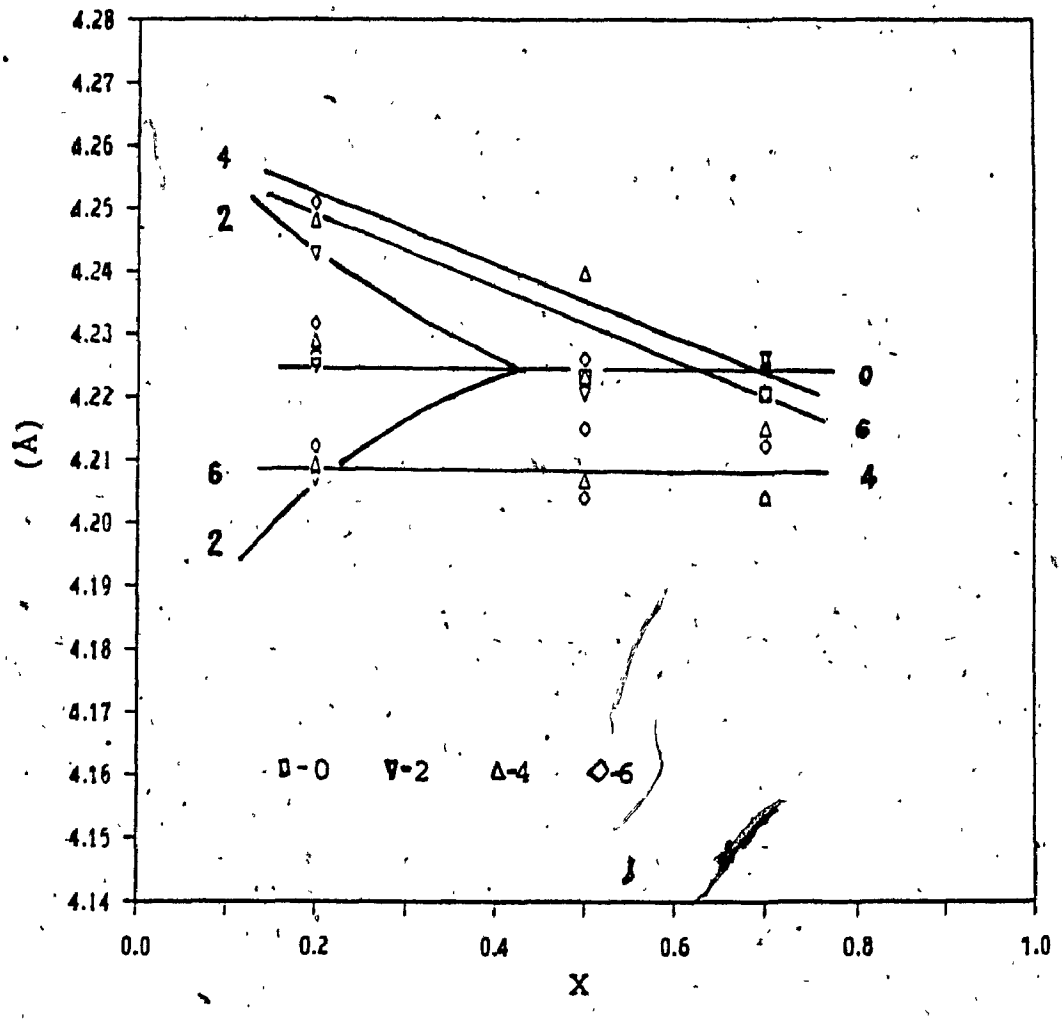

Fig. 31. Evolution of the a and b parameters of $PbSnF_4$ versus X for $t(PbSnF_4)$ = 0, 2, 4, and 6 hrs. with HF/H_2O = 0 and $t(SnF_2)$ = 0.

Fig. 32 shows the behavior of the orthorhombic distortion for HF/H_2O = 0 and 0.10 with t($PbSnF_4$) and X. When HF/H_2O = 0.10 the orthorhombic distortion is almost the same irrespective of t($PbSnF_4$) and o-$PbSnF_4$ is always obtained. The distortion is seen to fall slightly from X = 0.20 to X = 0.70, with more scatter occurring at X = 0.20. When HF/H_2O = 0, α-$PbSnF_4$ is obtained for t($PbSnF_4$) = 0, all values of X and t($PbSnF_4$) = 2 hours, X = 0.50 and 0.70. All other preparations yield o-$PbSnF_4$, whose orthorhombic distortion is considerably smaller than when HF/H_2O = 0.10. The distortion is seen to fall slightly as X increases when o-$PbSnF_4$ is obtained.

The evolution of the c parameter is given in fig. 33 for HF/H_2O = 0 and fig. 34 for HF/H_2O = 0.10. When t($PbSnF_4$) = 0 and HF/H_2O = 0 the c parameter goes through a maximum at X = 0.50 (fig. 33). At t($PbSnF_4$) = 2 hours, c is much smaller and goes through a minimum at X = 0.50. At t($PbSnF_4$) = 4 hours, c goes through a maximum, similar to that observed for t($PbSnF_4$) = 0 but with lower values. At t($PbSnF_4$) = 6 hours no change occurs in the c parameter. Very little scatter occurs which leads us to believe that the difference in results, although small, may be real. No explanation can be given at this time as to why the c parameter behaves in this manner.

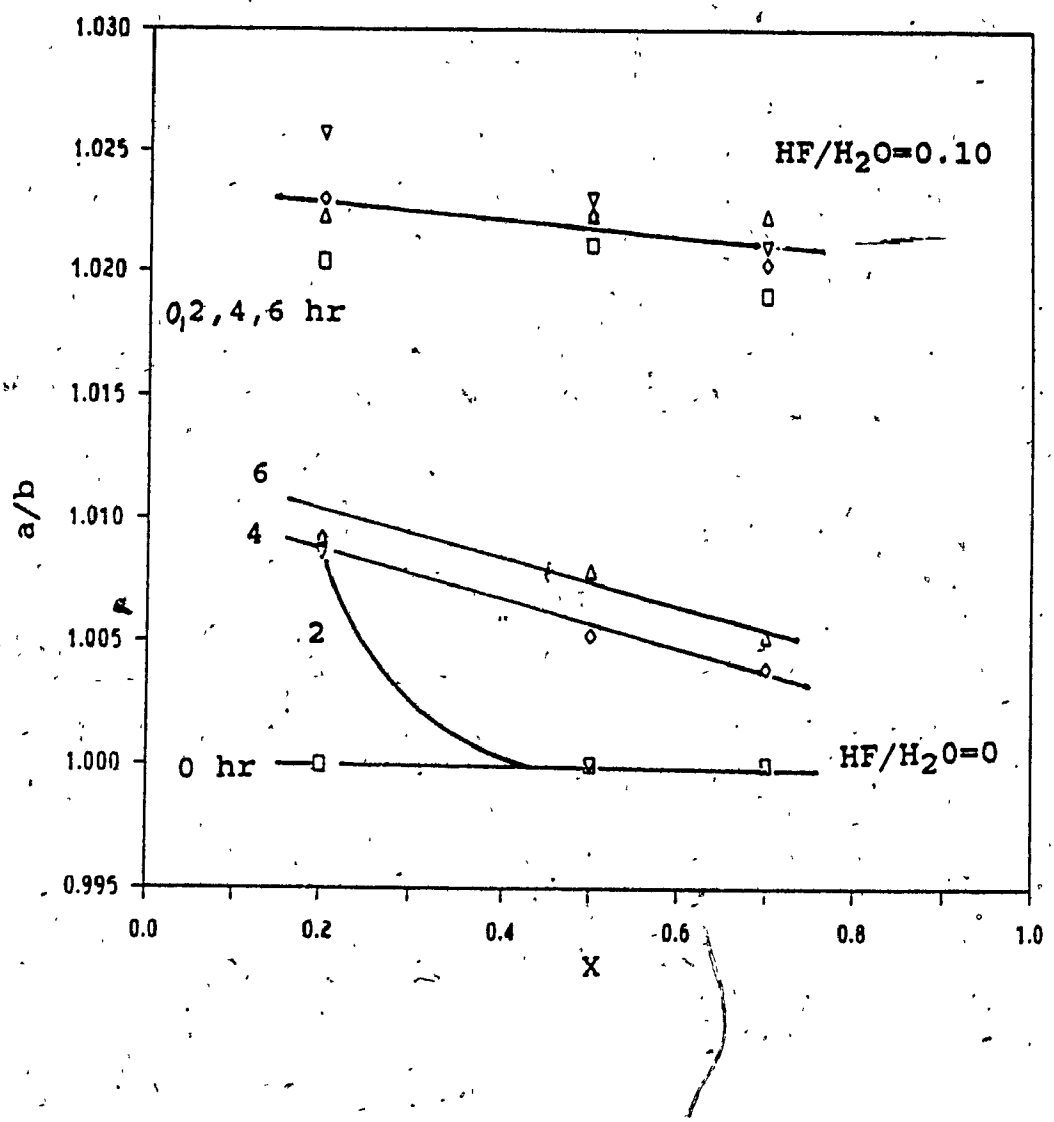

Fig. 32. Orthorhombic distortion of $PbSnF_4$ versus X and $t(PbSnF_4)$ for HF/H_2O =0 and 0.10 and $t(SnF_2)$ = 0.

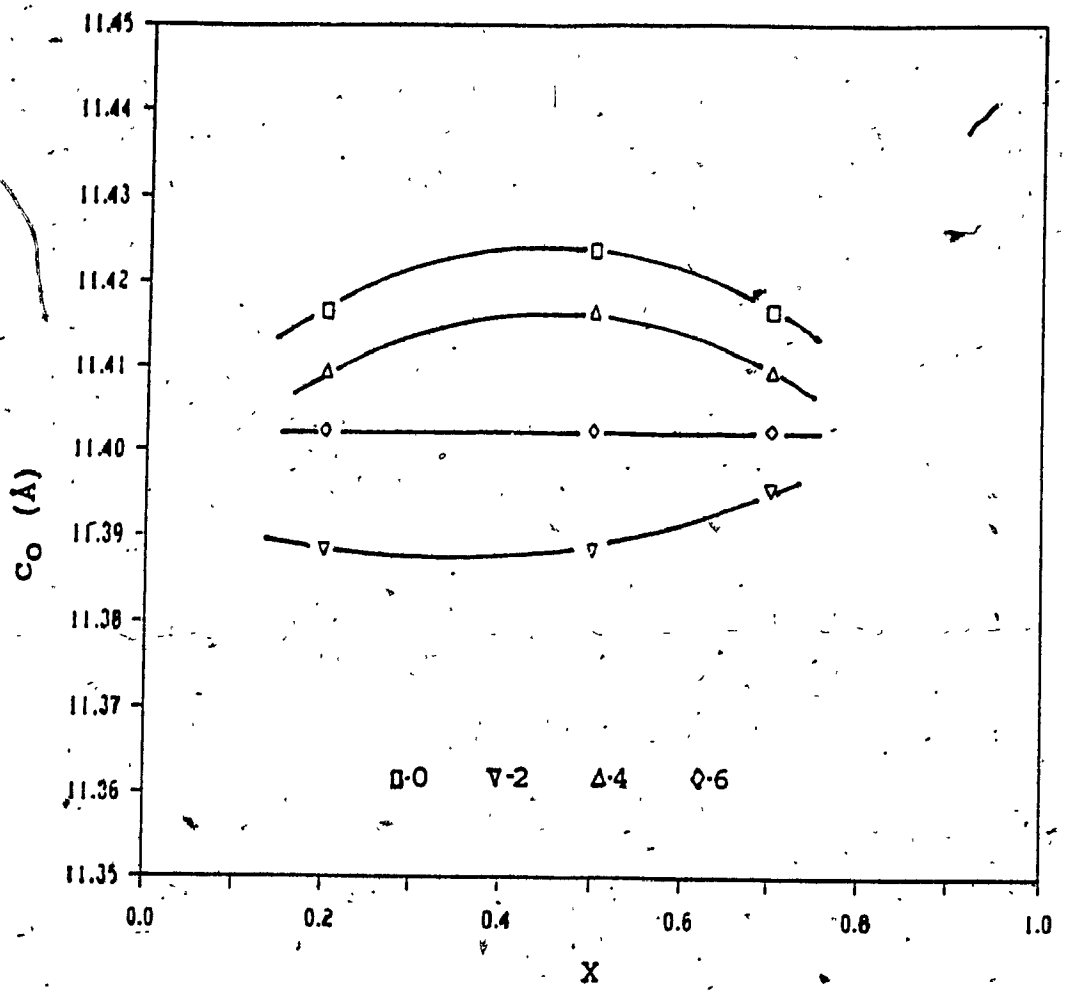

Fig. 33 - Evolution of the c parameter with X and $t(PbSnF_4)$ for HF/H_2O = 0 and $t(SnF_2)$ = 0.

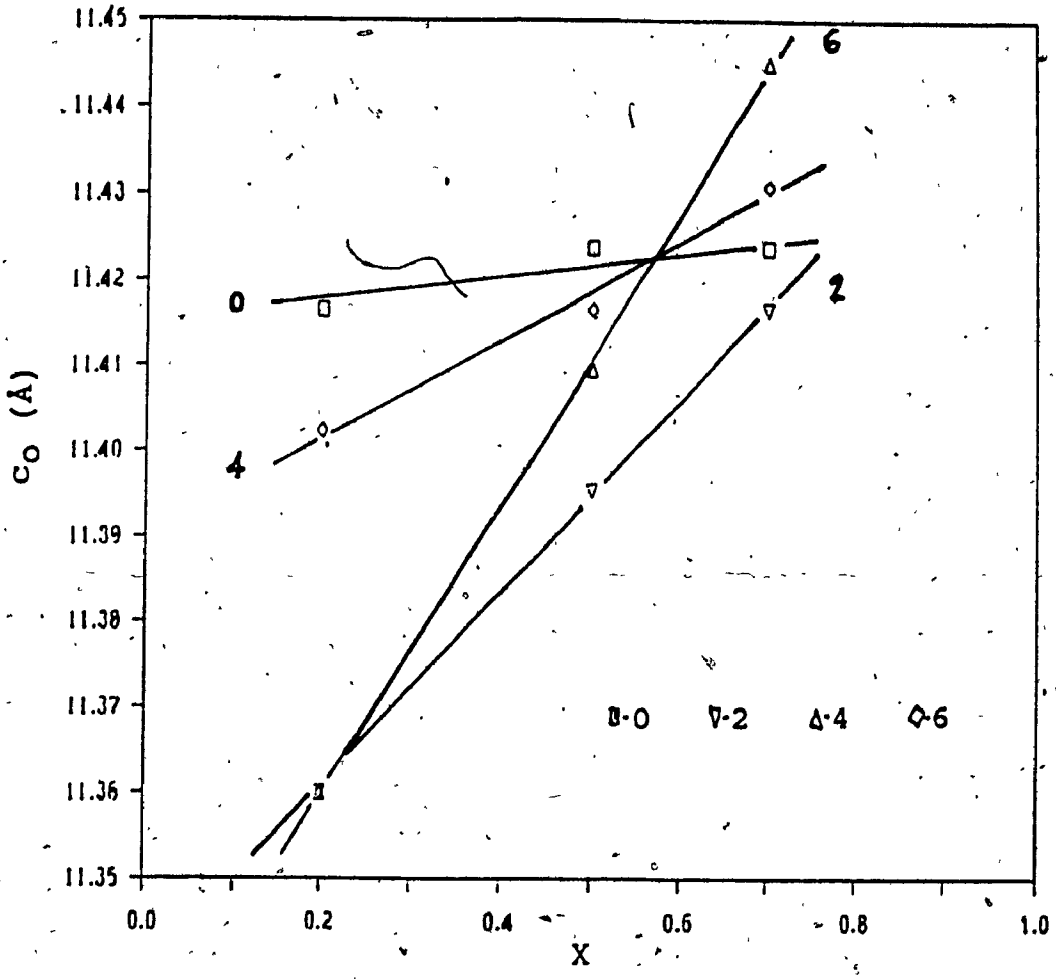

Fig. 34. Evolution of the c parameter with X and t($PbSnF_4$) for HF/H_2O = 0.10 and t(SnF_2) = 0.

The evolution of the c parameter when HF/H_2O = 0.10, shown in fig. 34 reveals even more erratic results. Although straight lines can be drawn through points, their interpretation is impossible. In all cases the c parameter increases with increasing X, but on the one hand it is very small, i.e. $t(PbSnF_4)$ = 0 and on the other hand it is extreme, i.e. $t(PbSnF_4)$ = 6 hours. Again, the absence of scatter of experimental points for a given $t(PbSnF_4)$ suggest they are real.

The cell volume, shown in fig. 35, reveals that when HF/H_2O = 0, little change is observed and cell volumes between 203.0Å and 204.0Å are obtained. At HF/H_2O = 0.10 and for $t(PbSnF_4)$ = 0, the cell volumes are slightly smaller than when no HF is used. For $t(PbSnF_4)$ > 0, much lower cell volumes are obtained and little change occurs irrespective of $t(PbSnF_4)$ and X.

A study of the X-ray powder patterns reveals new, unidentifiable peaks that could not be indexed as either phase of $PbSnF_4$ or $Pb_2SnNO_3F_5.2H_2O$. Fig 36 shows the two different X-ray powder patterns were obtained.

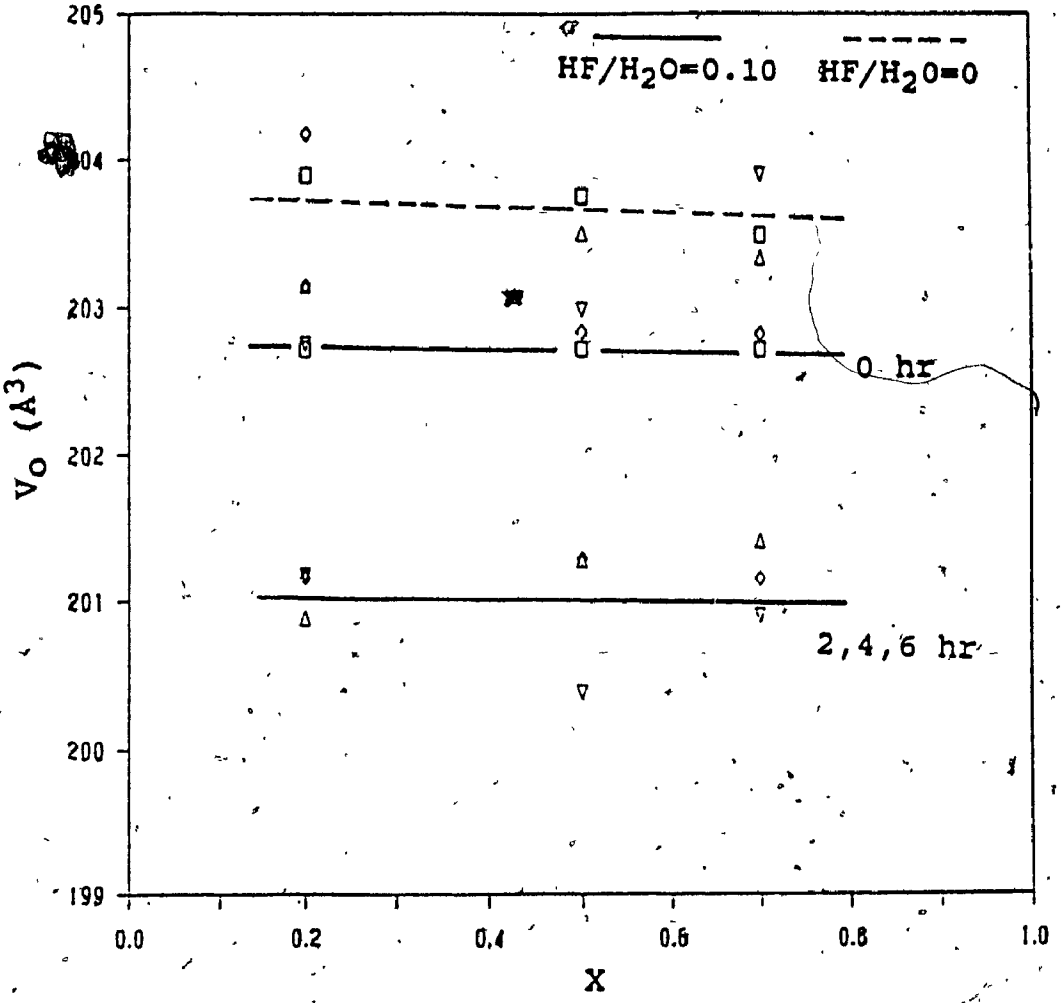

Fig. 35. Evolution of the cell volume of $PbSnF_4$ with X, $t(PbSnF_4)$ and HF/H_2O = 0 and 0.10 for $t(SnF_2)$ = 0

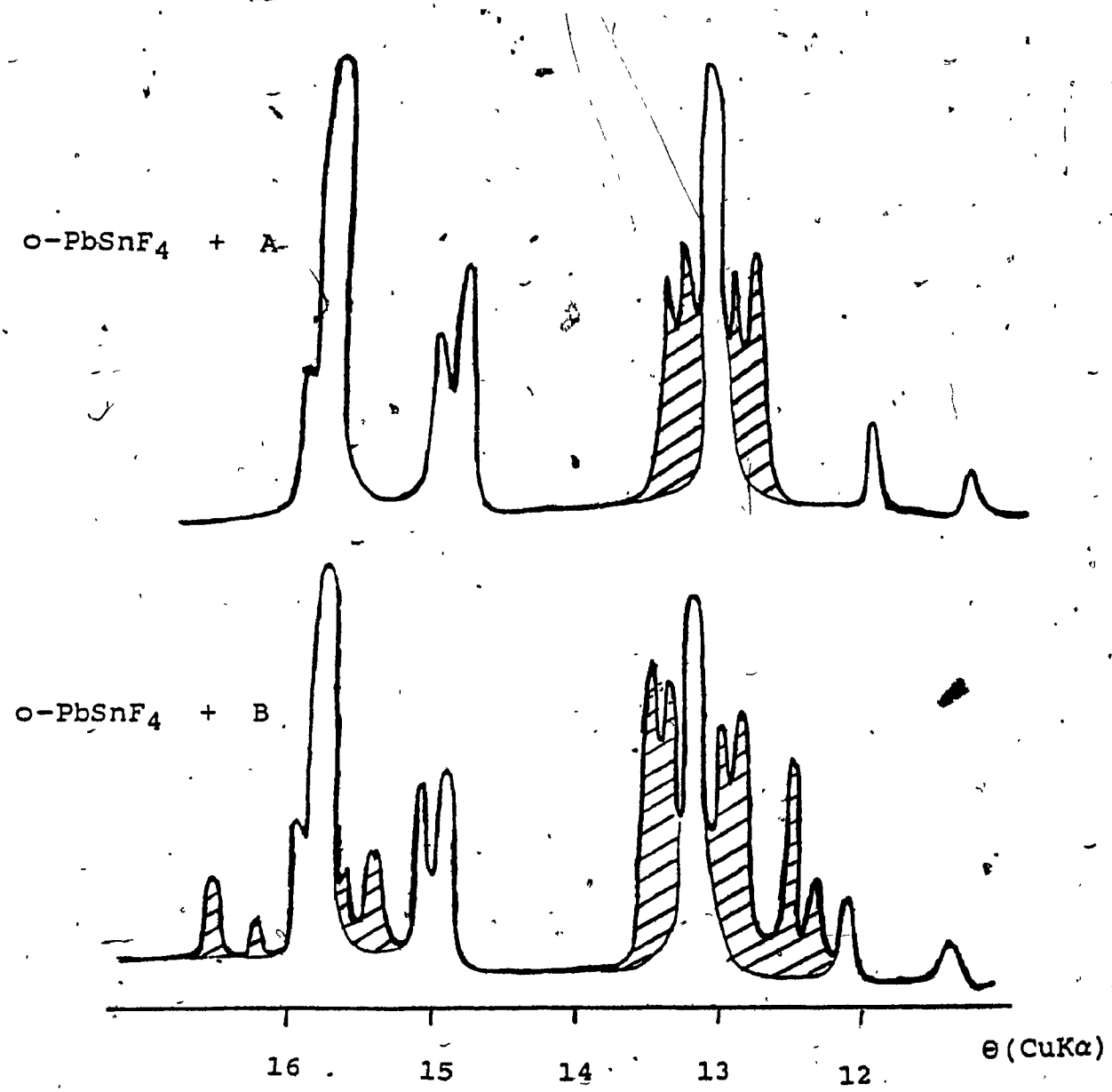

Fig. 36. X-ray powder patterns obtained when (a) $t(PbSnF_4)$ = 2 hours and (b) $t(PbSnF_4)$ = 6 hours for HF/H_2O = 0 and 0.10, $t(SnF_2)$ = 0.

$Pb_2SnNO_3F_5.2H_2O$ was only obtained for $t(PbSnF_4)$ = 4 and 6 hours and for HF/H_2O = 0.10. It was never obtained for HF/H_2O = 0. HF seems not to influence the formation of this 'new' phase and seems to be dependant on $t(PbSnF_4)$ as it is

observed for t($PbSnF_4$) > 0 and when HF/H_2O = 0 or 0.10. A summary of the products identified by X-ray powder diffraction when t($PbSnF_4$) is varied is given in Table IV. The results refer to X = 0.20, 0.50 and 0.70 as no influence due to X was observed.

Table IV

Products Identified by X-ray Powder Diffraction

t($PbSnF_4$) hours	$\frac{HF}{H_2O}$	α-$PbSnF_4$	o-$PbSnF_4$	$Pb_2SnNO_3F_5 \cdot 2H_2O$	A	B
0	0	X				
0	0.10	X	X			
2	0		X		X	
2	0.10		X		X	
4	0		X			X
4	0.10		X	X		X
6	0		X		X	X
6	0.10		X	X	X	X

A corresponds to those extra peaks shown in fig. 36(a) occurring between 12.80 and 13.25°θ whereas B includes A and those occurring between 15.25 and 16.75°θ as shown in fig.

36(b). As the peaks of A (12.80 - 13.25 °(θ)) are observed in fig. 36(a), without the extra peaks of B (15.25-16.75°(θ)), it seem that A and B are two different phases. The X-ray powder diffraction file was checked for compounds of Pb and/or Sn and their mixed oxides, hydroxides, fluorides and nitrates. No compounds, with Bragg peaks corresponding to A or B, could be found.

3.2.6 ^{119}Sn MÖSSBAUER SPECTROSCOPY

^{119}Sn Mössbauer spectroscopy was used at room temperature on several tetragonal and orthorhombic samples, the latter with various values of the orthorhombic distortion. All samples gave identical results within experimental error. A typical spectrum is shown in fig. 37, For all samples, the isomer shift, relative to $CaSnO_3$ at room temperature, is 3.25 (1) mm/s and the quadrupole splitting 1.55 mm/s. A small Sn(IV) impurity is clearly visible at ≈0mm/s, which is also present in the SnF_2 used in the preparation. These values are characteristic of divalent tin with a stereoactive lone pair of electrons, in agreement with structural results (9). These results agree perfectly with a model of a non-mobile electron pair, which is localized on a non-bonding orbital of tin (II). Therefore, such an electron pair is not on a conduction band, and cannot participate in the conduction mechanism.

This agrees with transport number measurements done on isotropic $BaSnF_4$ (3) which gave $T_i > 0.99$.

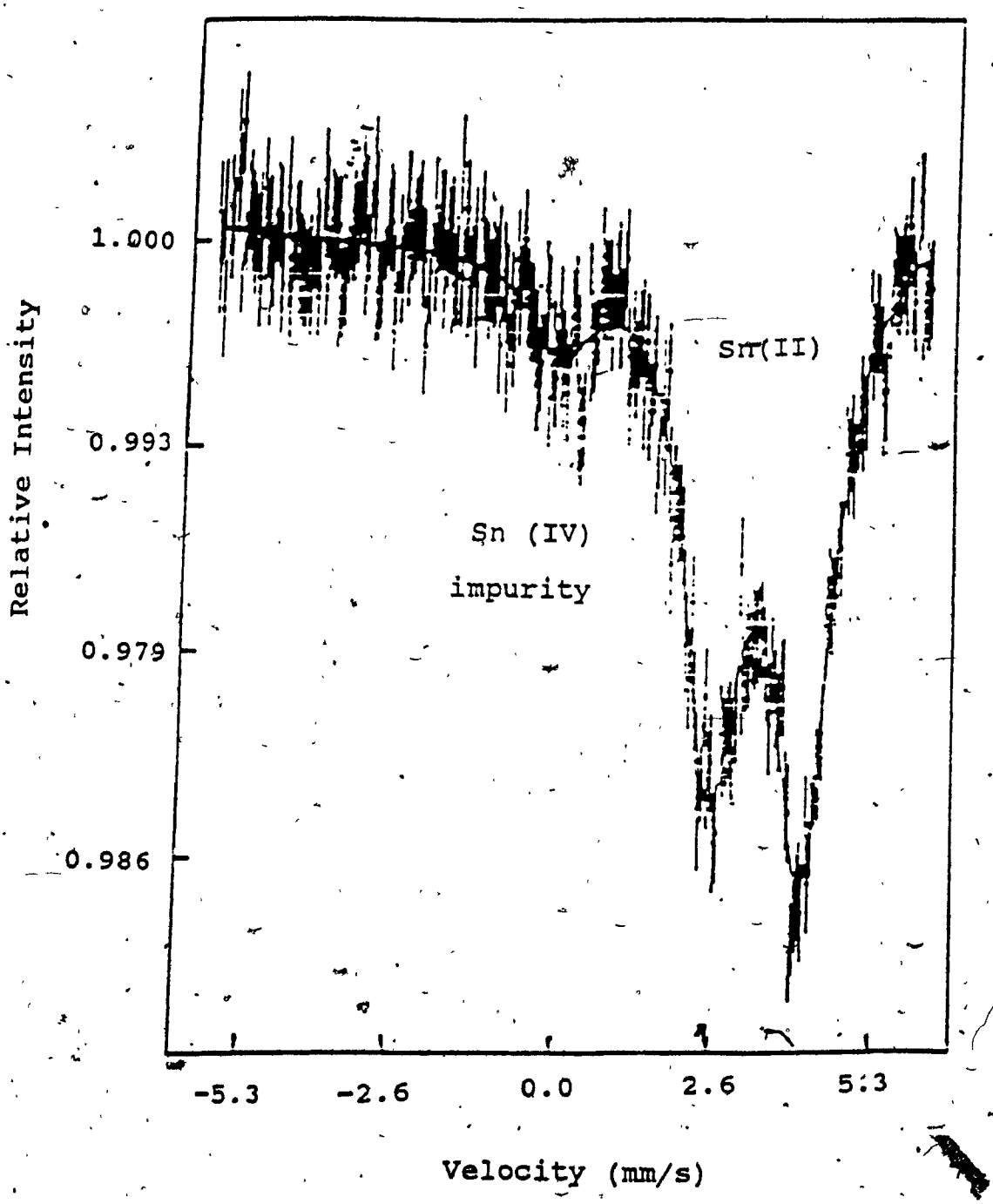

Fig. 37. ^{119}Sn Mössbauer spectrum of α-$PbSnF_4$ at room temperature.

As the Mössbauer parameters are identical for tetragonal and orthorhombic $PbSnF_4$ and no change is observed with the orthorhombic distortion, the first coordination sphere of Sn(II) does not change. One can conclude that the bonding to tin and its coordination are basically unchanged upon symmetry change. It is very likely that there are only minor structural changes between the tetragonal and orthorhombic forms, for example the M - F - M (where M = Pb and Sn) angles may change, which occurs in the $(\vec{a},\vec{b})$ plane. Such changes in some Sn - F - Sn angles were shown to be responsible for the β to γ transition of SnF_2 (16) and these resulted in no measurable change in Mössbauer parameters (17) because the tin environment was not significantly affected by the transition. This is particularly true in the amount of p_z contribution to the lone pair, which is the major factor responsible for the large quadrupole splitting. However, as the structure of o-$PbSnF_4$ is not presently known, no further interpretation is possible.

3.3 NON-AMBIENT TEMPERATURE REACTIONS

3.3.1 INFLUENCE OF T = 0°C

In this study, reactions between $Pb(NO_3)_2$ and SnF_2 were carried out in aqueous solutions at 0°C. Both $t(PbSnF_4)$ and $t(SnF_2)$ were equal to zero and X was varied between 0.10 and 0.90. The results are given in fig. 38-43. In fig. 38, we see that the a and b parameters for HF/H_2O = 0.10 are constant with a = c.a. 4.25Å and b = c.a. 4.15Å. When HF/H_2O = 0, the a parameter is constant, but with lower values than when HF/H_2O= 0.10. The b parameter shows a discontinuity, with constant values at around 4.20Å for X between 0.10 and 0.50 then a sharp drop to about 4.14Å at X above 0.60.

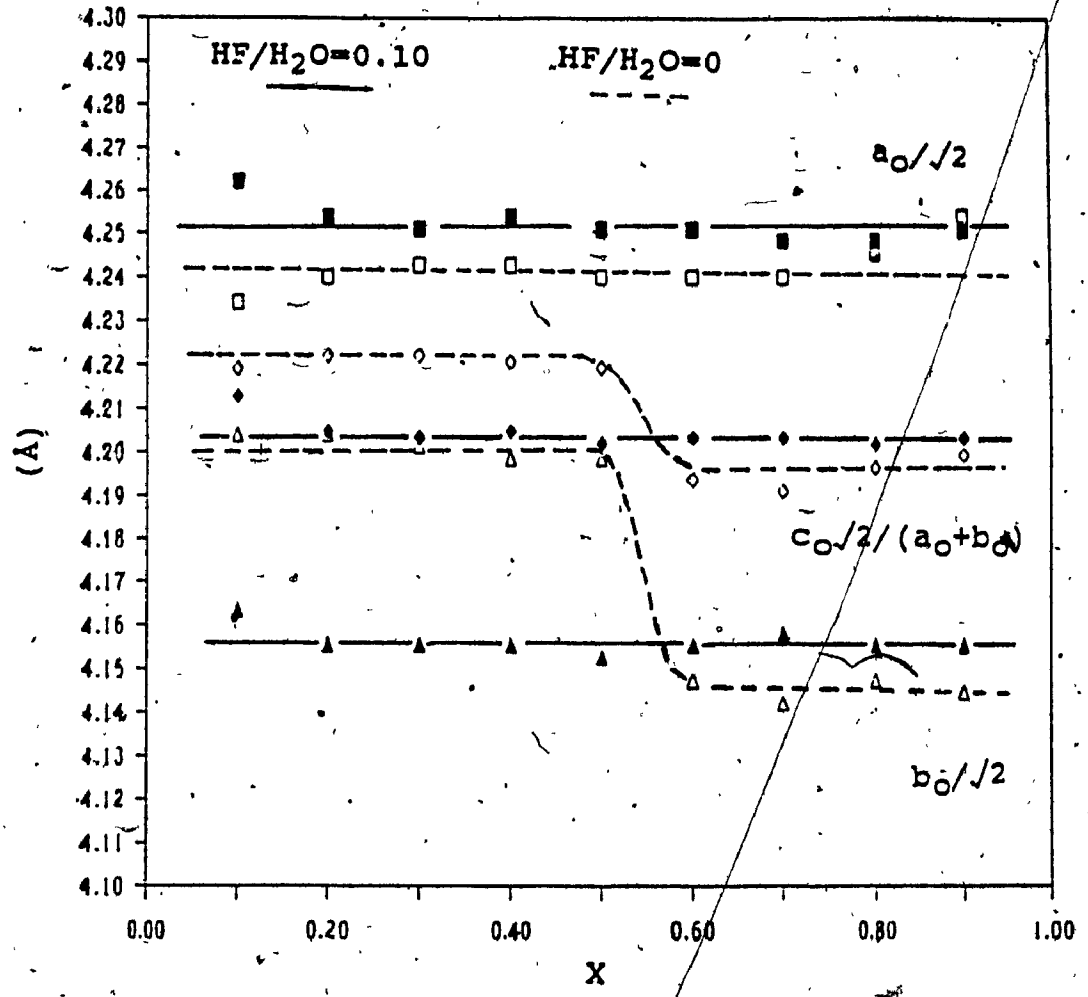

Fig. 38. Evolution of the a and b parameters versus X for T = 0°C and HF/H_2O = 0 and 0.10 for t(SnF_2) and t($PbSnF_4$) = 0.

Fig. 39 shows the orthorhombic distortion of $PbSnF_4$ as

a function of X for HF/H_2O = 0 and 0.10. When HF/H_2O = 0.10, o-$PbSnF_4$ is obtained with a fairly constant orthorhombic distortion. The average value obtained is equal to 1.024Å. When HF/H_2O = 0, orthorhombic distortions with much smaller values than those for HF/H_2O = 0.10 are obtained, and they are seen to increase slightly as X approaches 0.50. Between X = 0.50 and X = 0.60, a dramatic increase by 0.020Å in the orthorhombic distortion is observed.

The evolution of the c parameter, cell volume and tetragonal distortion of $PbSnF_4$ are given in fig. 40-42. In fig. 40, for HF/H_2O = 0.10, the c parameter decreases constantly as X increases until X = 0.50. Beyond X = 0.50, little change occurs and constant values are obtained. When HF/H_2O = 0, the c parameter remains unchanged, at c.a. 11.365Å, up to X = 0.50. Then a sharp increase occurs between X = 0.50 and 0.60, and from X = 0.60 to X = 0.90, c is seen to increase linearly from 11.390Å to 11.410Å.

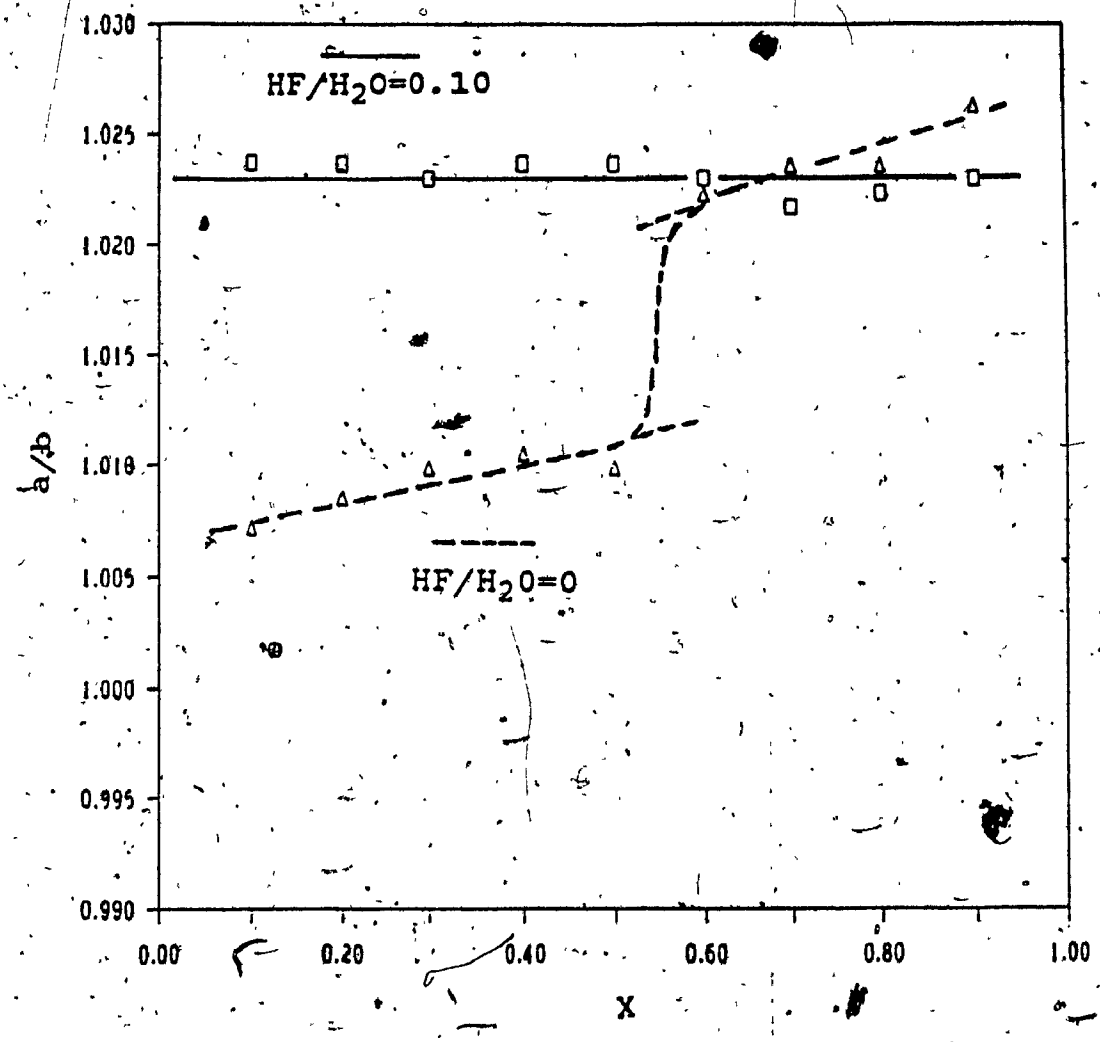

Fig. 39. Evolution of the orthorhombic distortion of $PbSnF_4$ versus X for T = 0°C and HF/H_2O = 0 and 0.10 with $t(SnF_2)$ and $t(PbSnF_4)$ = 0.

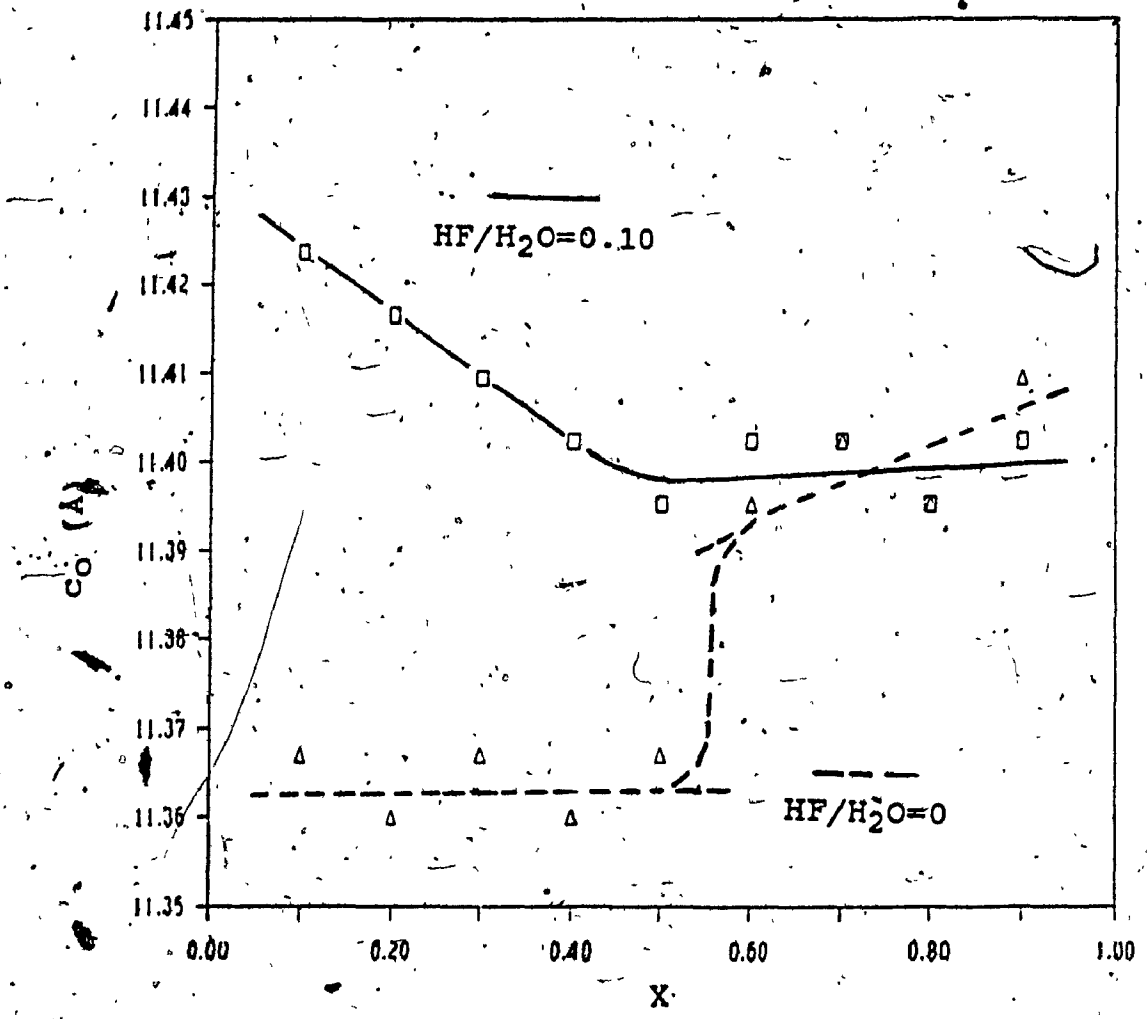

Fig. 40. Evolution of the c parameter of $PbSnF_4$ versus X for T = 0°C and HF/H_2O = 0 and 0.10 with $t(SnF_2)$ and $t(PbSnF_4)$ = 0.

The cell volume, for HF/H_2O = 0.10, shown in fig. 41 reveals similar behavior as above with the cell volume falling linearly as X increases to X = 0.50 and then no change is observed beyond X = 0.60. Also, for HF/H_2O = 0, discontinuity occurs in the cell volume at X = 0.50. In the case where HF/H_2O = 0.10, the change in volume is due to the change in c parameter whereas for HF/H_2O = 0 it is due to a combination of changes in the b and c parameters.

The tetragonal distortion of $PbSnF_4$ is given in fig. 42. No change is observed for HF/H_2O = 0.10 and for HF/H_2O = 0 a discontinuity at X = 0.50 occurs. No explanation can be given for these results, however it is very apparent from the data presented that something interesting is occurring at X = 0.50. Also, the presence or absence of HF seems to cause a different effect on the cell parameters of o-$PbSnF_4$ than in studies carried out at room temperature. This may be due to the rate of hydrolysis of SnF_2 (equation II) which is temperature dependant and is much slower at low temperature.

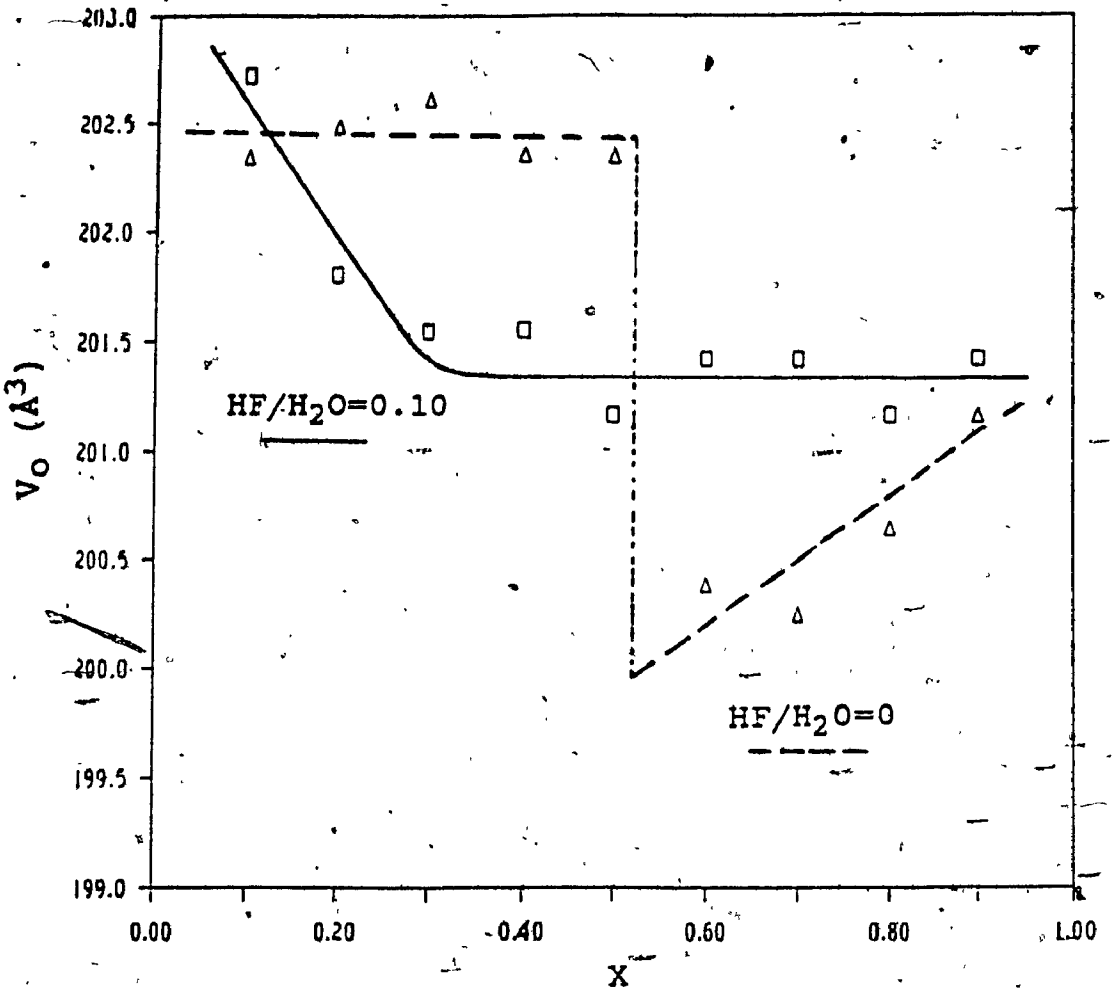

Fig. 41. Evolution of the cell volume of $PbSnF_4$ versus X for T = 0°C and HF/H_2O = 0 and 0.10 with $t(SnF_2)$ and $t(PbSnF_4)$ = 0.

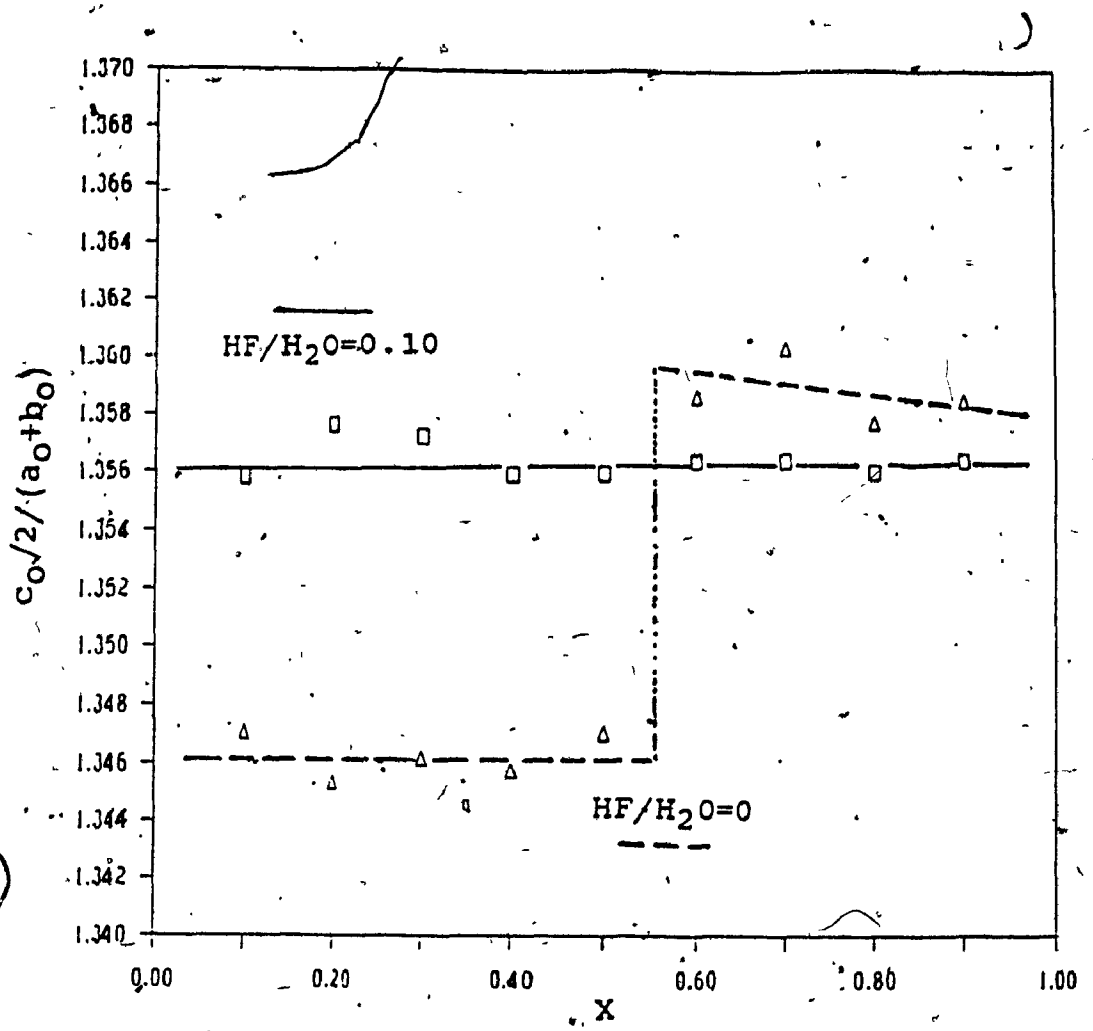

Fig. 42. Evolution of the tetragonal distortion of $PbSnF_4$ versus X for T = 0°C with $t(SnF_2)$ and $t(PbSnF_4)$ = 0.

The yield versus X and for HF/H_2O = 0 and 0.10 at T = 0°C is shown in fig. 43. As in previous studies, higher

yields are obtained when HF is present. Also, the presence of HF seems to retard the formation of $Pb_2SnNO_3F_5.2H_2O$ which, for HF/H_2O = 0.10, does not appear until X > 0.70. When HF/H_2O = 0, $Pb_2SnNO_3F_5.2H_2O$ appears at X > 0.50. It is interesting to note that for HF/H_2O = 0, the yield is seen to go through a maximum around X = 0.50, whereas for HF/H_2O = 0 the yield decreases constantly for all values of X.

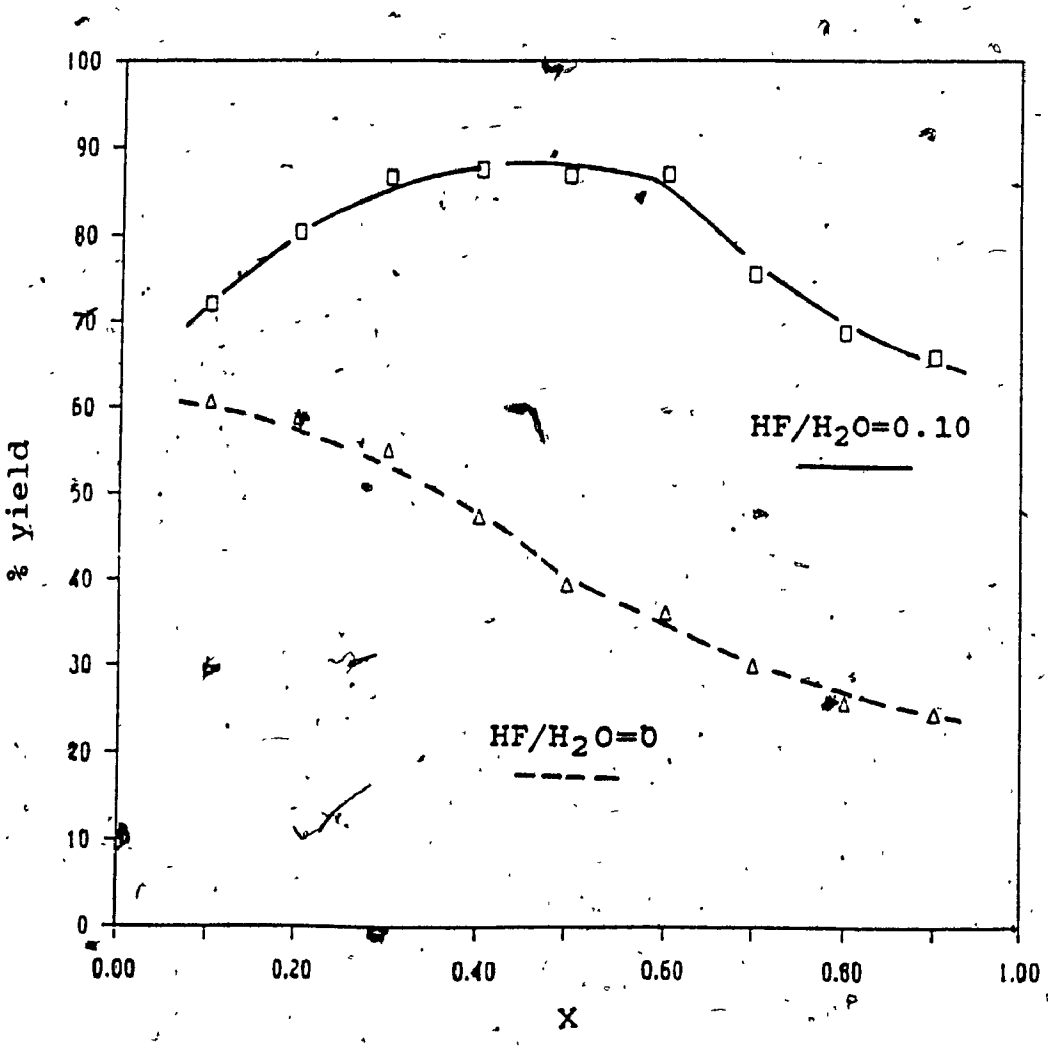

Fig. 43. % Yield versus X for T =0°C with HF/H_2O = 0 and 0.10 for t(SnF_2) and t($PbSnF_4$)) = 0.

3.3.2 INFLUENCE OF T = 75°C

Results obtained when T = 75°C are given in fig. 44-49. In fig. 44, when HF/H_2O = 0, no difference is observed in the a and b parameters. For HF/H_2O = 0.10, the a parameter gives constant results whereas the b parameter is seen to fall at X > 0.50 by c.a. 0.15A and then level of.

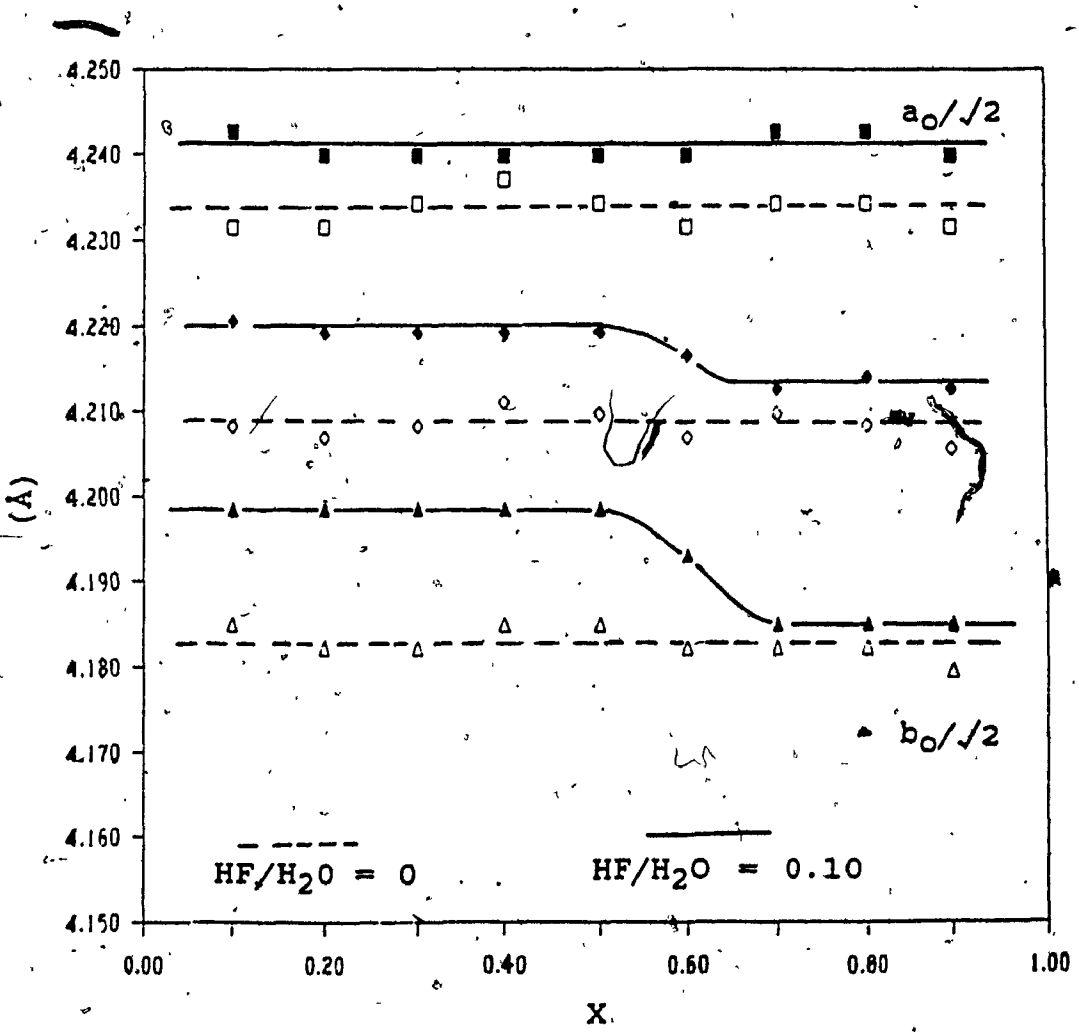

Fig. 44. Evolution of the a and b parameters of $PbSnF_4$ versus X for T = 75°C and HF/H_2O = 0 and 0.10 with $t(SnF_2)$ and $t(PbSnF_4)$ = 0

The orthorhombic distortion is given in fig. 45. No differences are observed for $HF/H_2O = 0$. When $HF/H_2O = 0.10$ slightly lower values are obtained for $X < 0.60$, however at $X > 0.60$, the orthorhombic distortion increases slightly to values above those for $HF/H_2O = 0$.

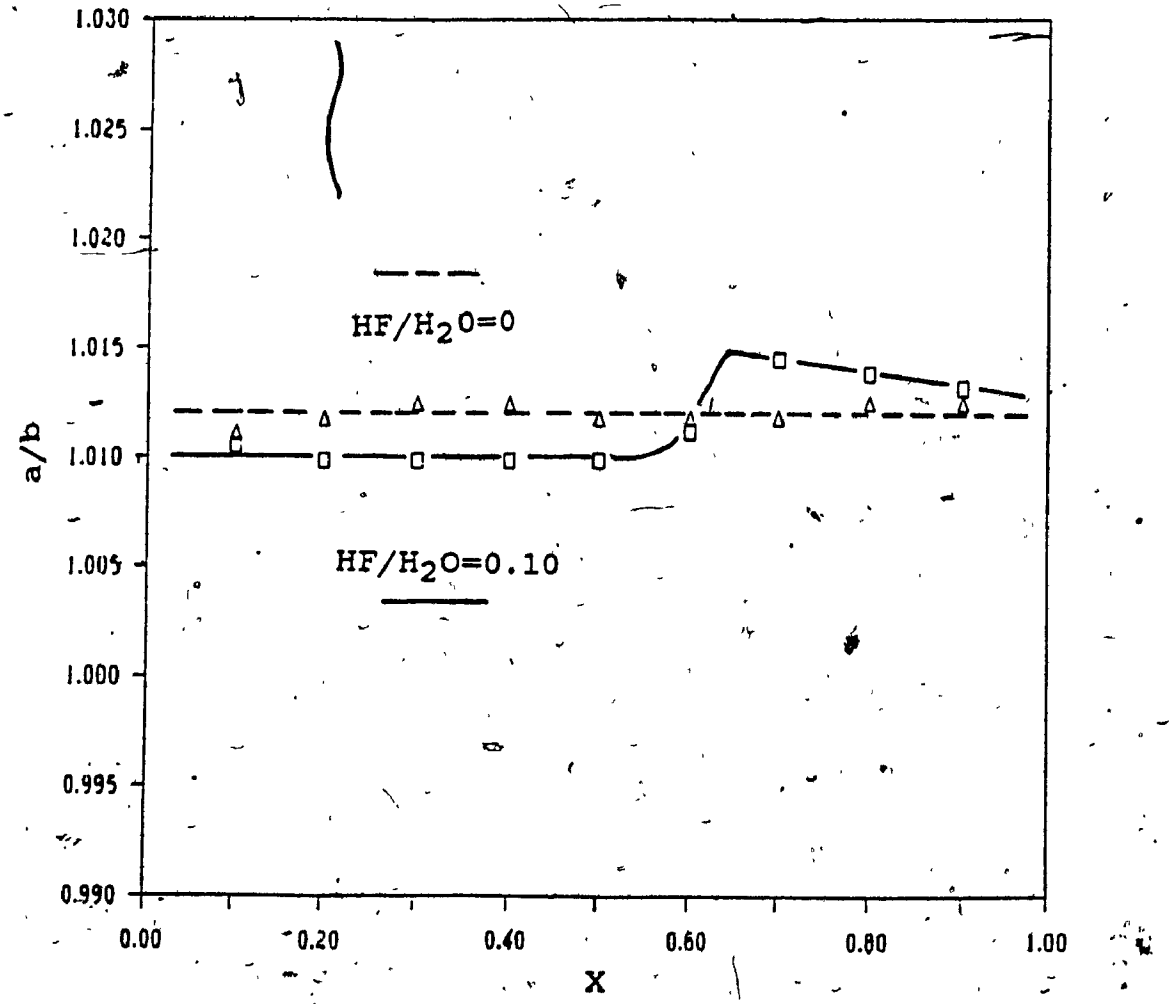

Fig. 45 Orthorhombic distortion of $PbSnF_4$ at 75°C with X for $HF/H_2O = 0$ and 0.10 with $t(SnF_2)$ and $t(PbSnF_4) = 0$.

No change in the c parameter occurs for $HF/H_2O = 0.10$ as shown in fig. 46. However, for $HF/H_2O = 0$, c is higher for X less than 0.70, in comparison with when HF is present, and then falls as X is further increased.

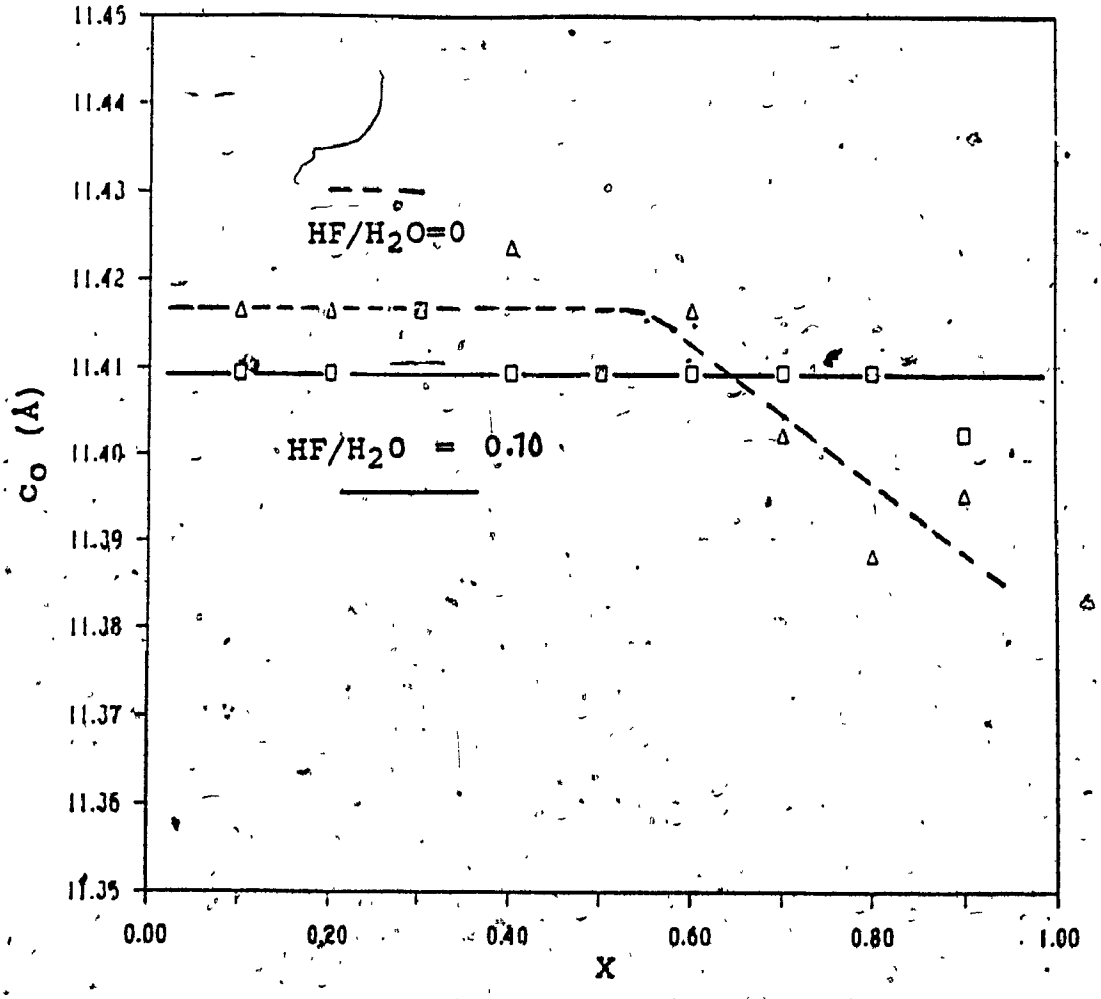

Fig. 46. Evolution of the c parameter of $PbSnF_4$ at T = 75°C with X for $HF/H_2O = 0$ and 0.10 with $t(SnF_2)$ and $t(PbSnF_4) = 0$.

Fig. 47 shows the evolution of the cell volume. For HF/H_2O = 0 and 0.10, the cell volumes are fairly constant below X = 0.50 however superior values are obtained for HF/H_2O = 0.10. Beyond X = 0.50, the cell volumes fall as X is increased. For HF/H_2O = 0, any changes in the cell volume are due to changes in the c parameter and for HF/H_2O = 0.10 the changes are due to changes in the b parameter. No explanation can be given as to why this behavior is observed.

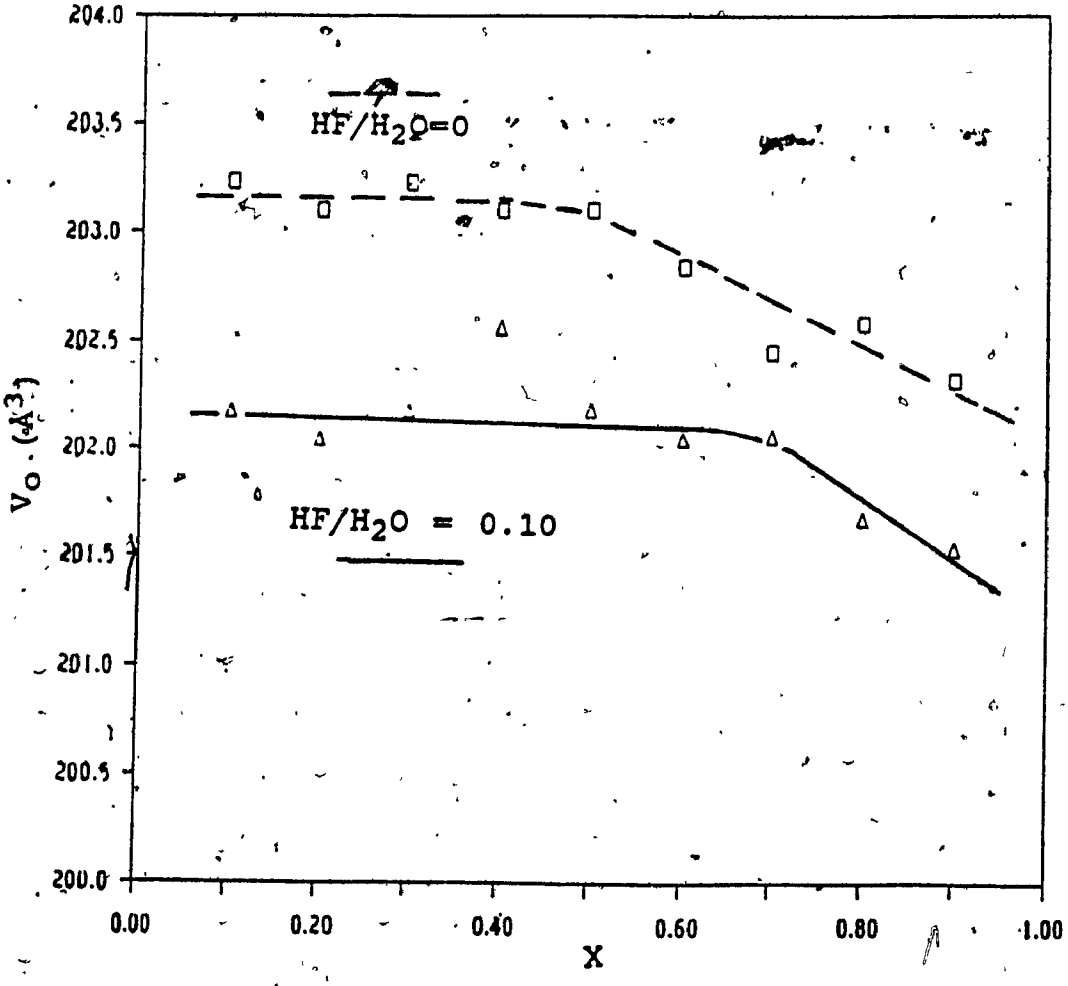

Fig. 47. Evolution of the cell volume of $PbSnF_4$ at 75°C for HF/H_2O = 0 and 0.10 with $t(SnF_2)$ and $t(PbSnF_4)$ = 0.

The tetragonal distortion at 75°C is shown in fig. 48 and reveals that for HF/H_2O = 0, higher results are obtained than for HF/H_2O = 0.10 when X is less than 0.70. However, at X = 0.70 and greater, the tetragonal distortion becomes comparable and equal irrespective of whether HF was present.

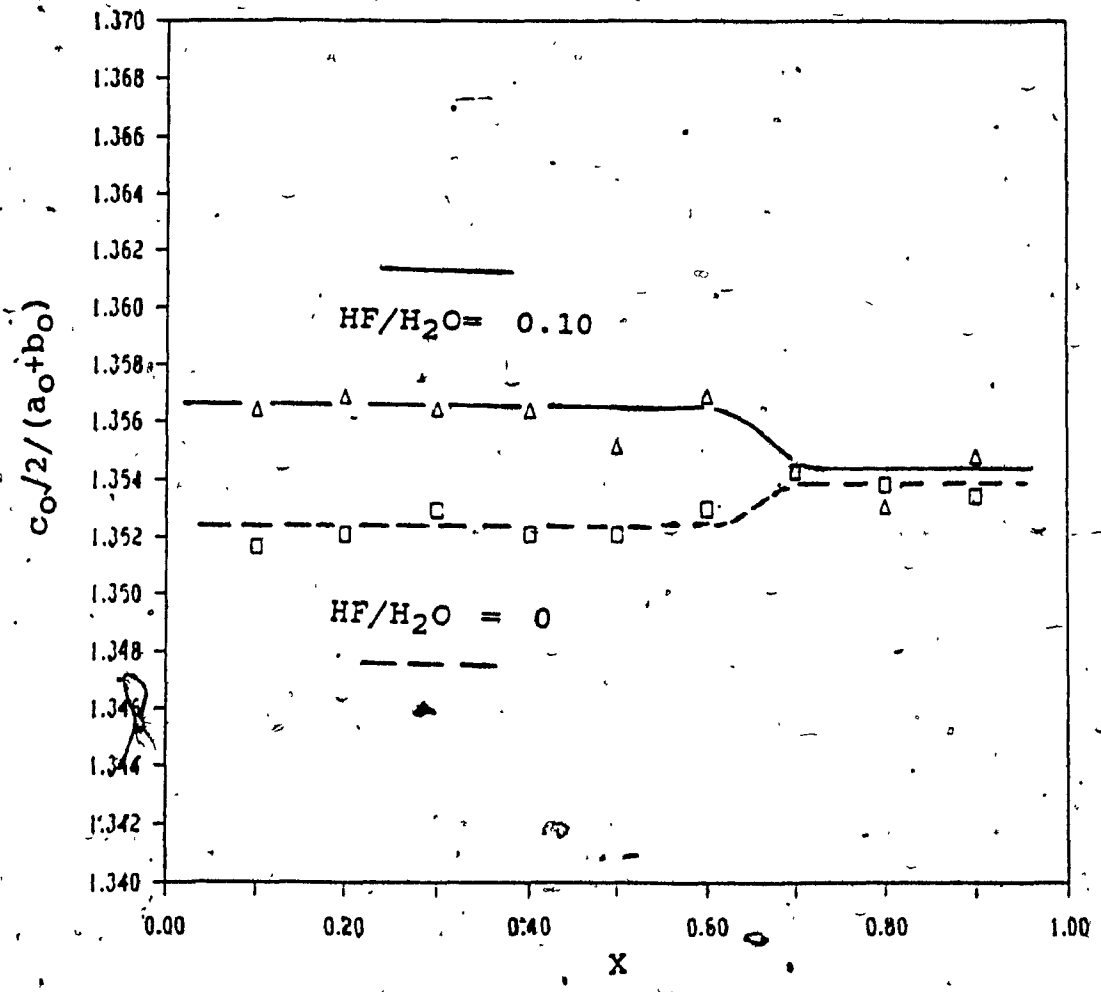

Fig. 48. Evolution of the tetragonal distortion of $PbSnF_4$ at 75°C for HF/H_2O = 0 and 0.10 with $t(SnF_2)$ and $t(PbSnF_4)$ = 0.

The yield versus X at 75°C and HF/H_2O = 0 and 0.10 is given in fig. 49. Superior yields are obtained for HF/H_2O = 0.10 and $Pb_2SnNO_3F_5.2H_2O$ is observed, when HF is present, for X > 0.70. $Pb_2SnNO_3F_5.2H_2O$ was never obtained at this temperature when no HF was present. The yield decreases as X increases except for X = 0.10. For X = 0.10 more error is associated with both the measuring of the $Pb(NO_3)_2$ and the subsequent weighing of the product due to smaller samples sizes.

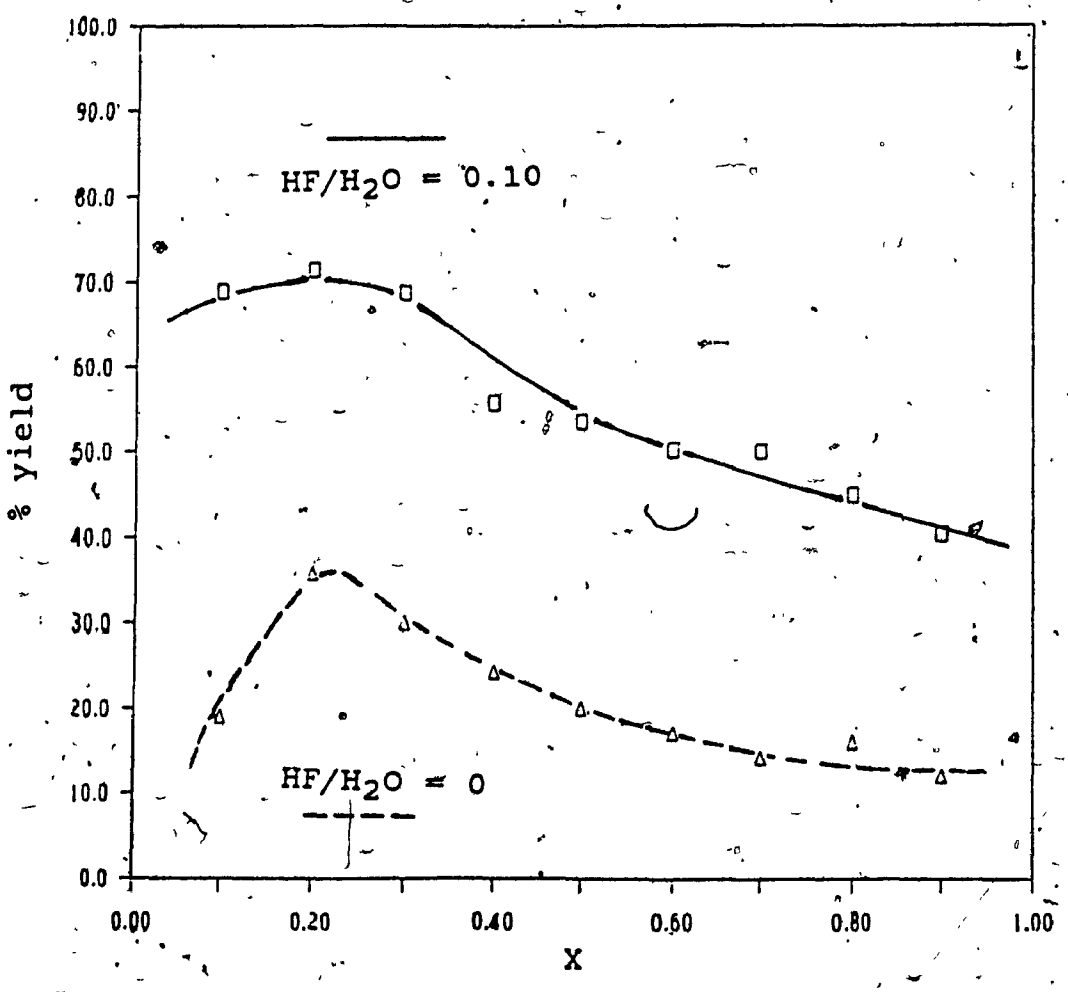

Fig. 49. % Yield versus X at 75°C with HF/H_2O = 0 and 0.10 for $t(SnF_2)$ and $t(PbSnF_4)$ = 0.

3.3.4 INFLUENCE OF T = 90°C

In this final investigation, the temperature of the reaction was 90°C. The results are shown in fig. 50-55. As can be seen in fig. 50 a and b are equal and constant for all values of X when $HF/H_2O = 0$. For $HF/H_2O = 0.10$, a and b are equal and constant for X below 0.30 and above 0.70. For X between 0.30 and 0.70, o-$PbSnF_4$ is obtained with a values comparable to α-$PbSnF_4$ and b values of c.a. 4.17Å.

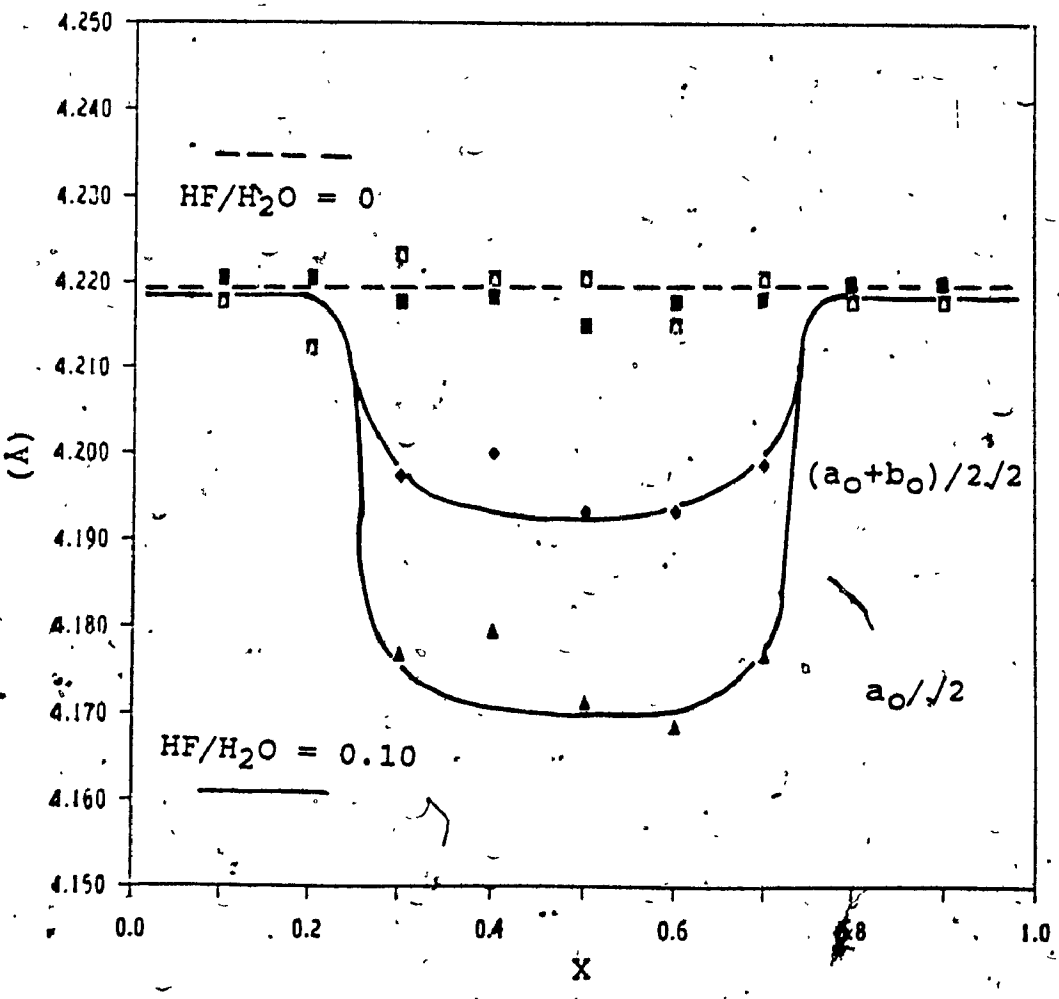

Fig. 50. Evolution of the a and b parameter of $PbSnF_4$ at 90°C for $HF/H_2O = 0$ and 0.10 with $t(SnF_2)$ and $t(PbSnF_4) = 0$.

Fig. 51 shows that α-$PbSnF_4$ is obtained for all values of X when no HF is used and for X < 0.30 and X > 0.70 when HF is used. o-$PbSnF_4$, with orthorhombic distortions equal to c.a. 1.01Å is obtained between X = 0.30 and 0.70.

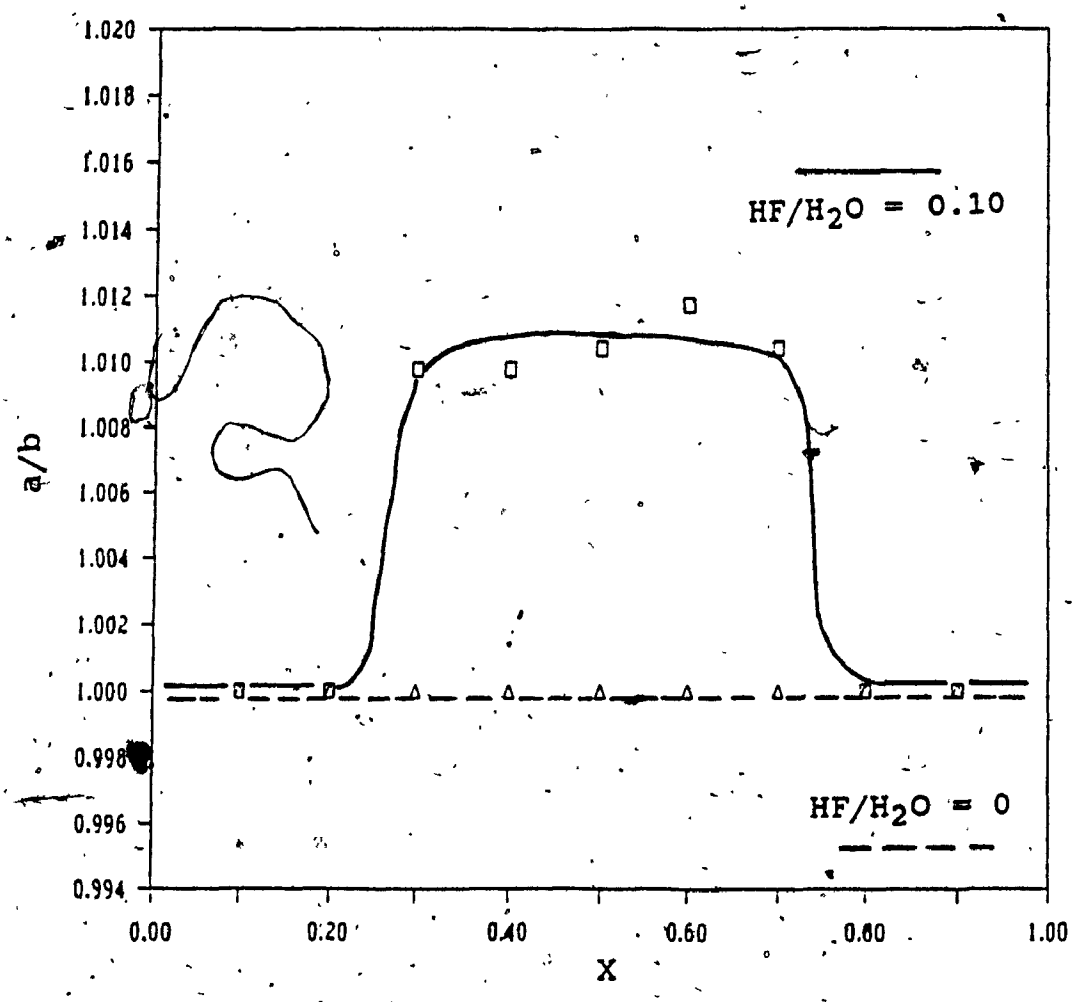

Fig. 51. Orthorhombic distortion of $PbSnF_4$ at 90°C for HF/H_2O = 0 and 0.10 with t(SnF_2) and t($PbSnF_4$) = 0.

The c parameter is shown in fig. 52 and reveals that higher values are obtained for $HF/H_2O = 0$, however, there is much scatter in these results and further interpretation is impossible.

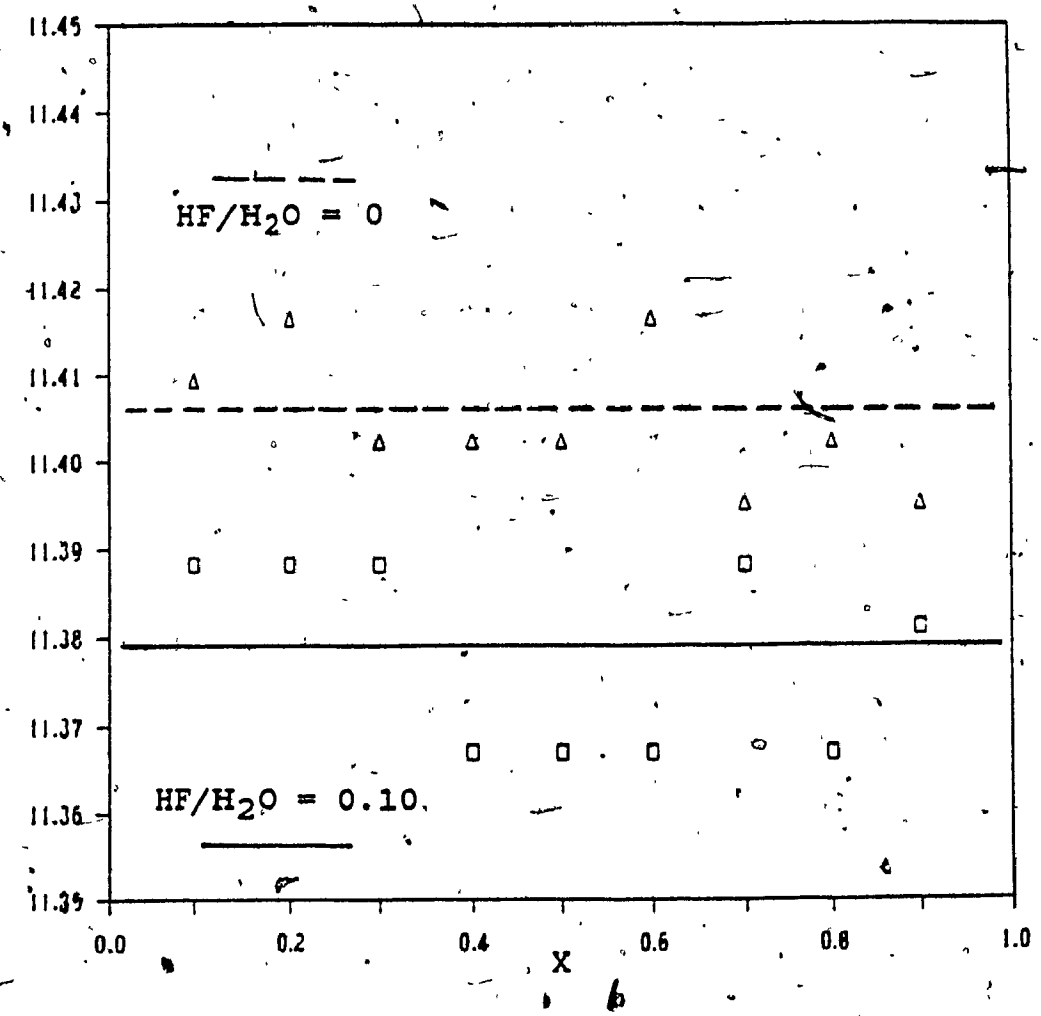

Fig. 52. Evolution of the c parameter of $PbSnF_4$ at 90°C for $HF/H_2O = 0$ and 0.10 with $t(SnF_2)$ and $t(PbSnF_4) = 0$.

The evolution of the cell volume is shown in fig. 53. For $HF/H_2O = 0$ the cell volume falls slightly as X increases and for $HF/H_2O = 0.10$ it is seen to go through a large minimum centered at X = 0.50. This change is due to the large decrease of the b parameter.

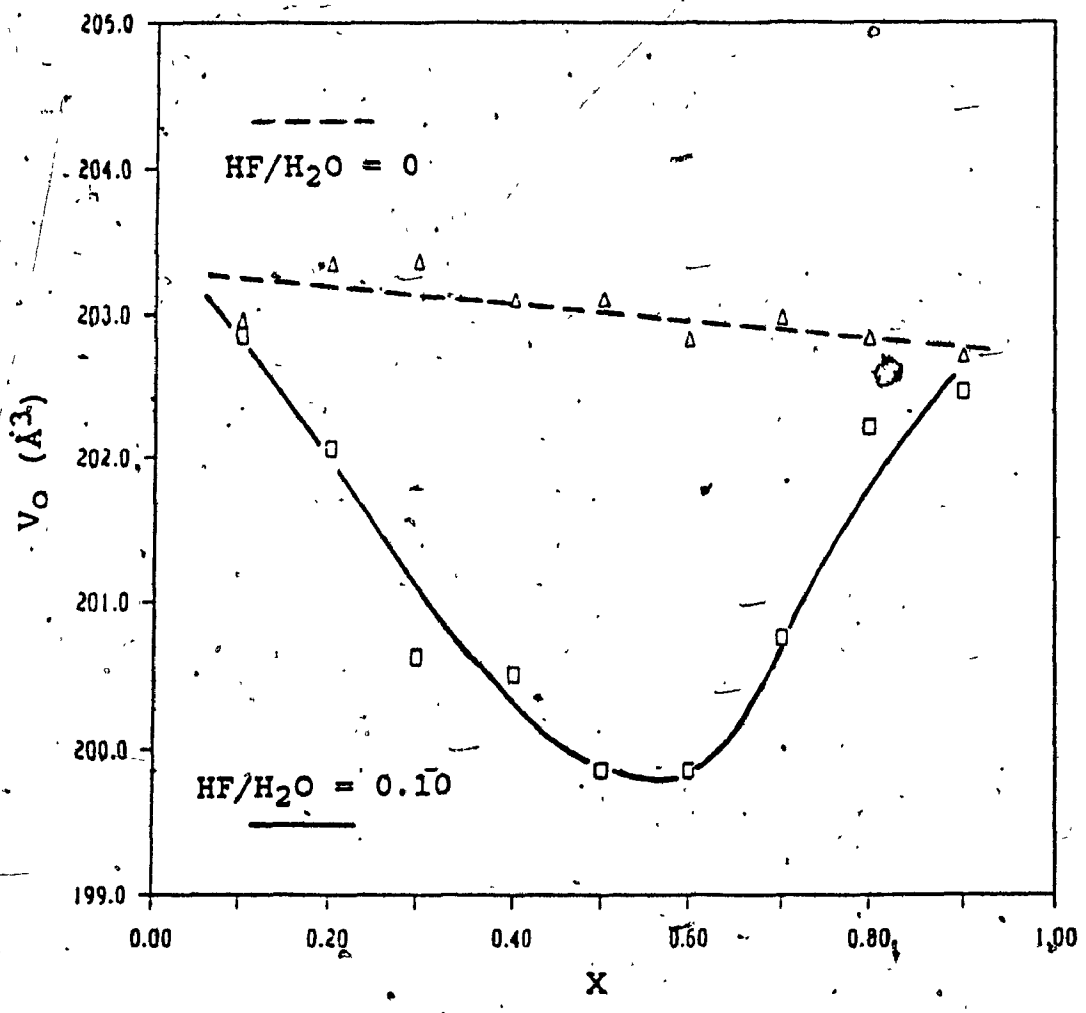

Fig. 53. Evolution of the cell volume of $PbSnF_4$ at 90°C for $HF/H_2O = 0$ and 0.10 with $t(SnF_2)$ and $t(PbSnF_4) = 0$.

The tetragonal distortion shows erratic results for both HF/H_2O = 0 and 0.10 in fig. 54. When HF/H_2O = 0.10 it could be argued that the cell volume goes through a maximum at X = c.a. 0.50 and that for HF/H_2O = 0 no change is observed, however, interpretation would be tentative at best.

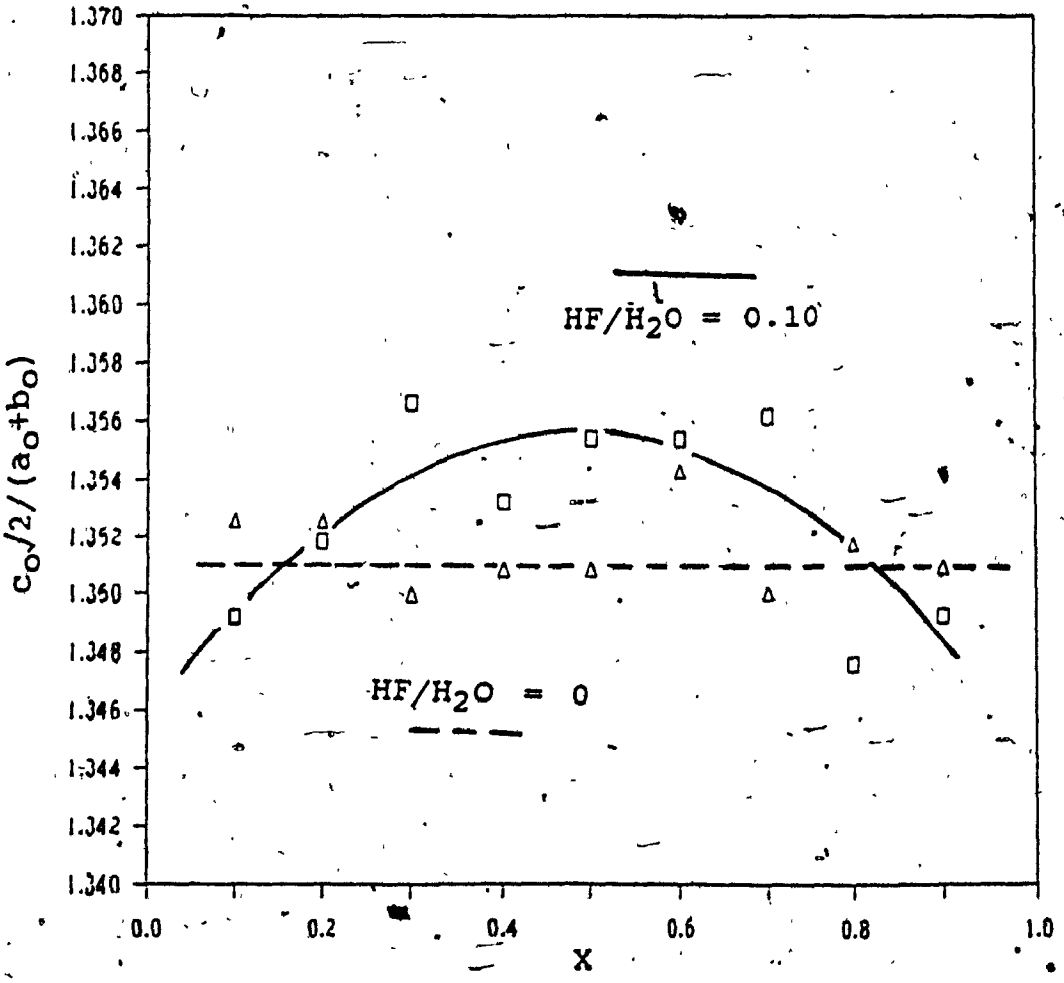

Fig. 54. Evolution of the tetragonal distortion cell volume at 90°C for HF/H_2O = 0 and 0.10 for $t(SnF_2)$ and $t(PbSnF_4)$=0.

As shown in fig. 55 the yield obtained when HF is present is superior than when HF is absent. Overall, much lower yields are obtained when compared to preparations carried out at lower temperatures. $Pb_2SnNO_3F_5.2H_2O$ is observed only when $HF/H_2O = 0.10$ and for values of X greater than 0.20.

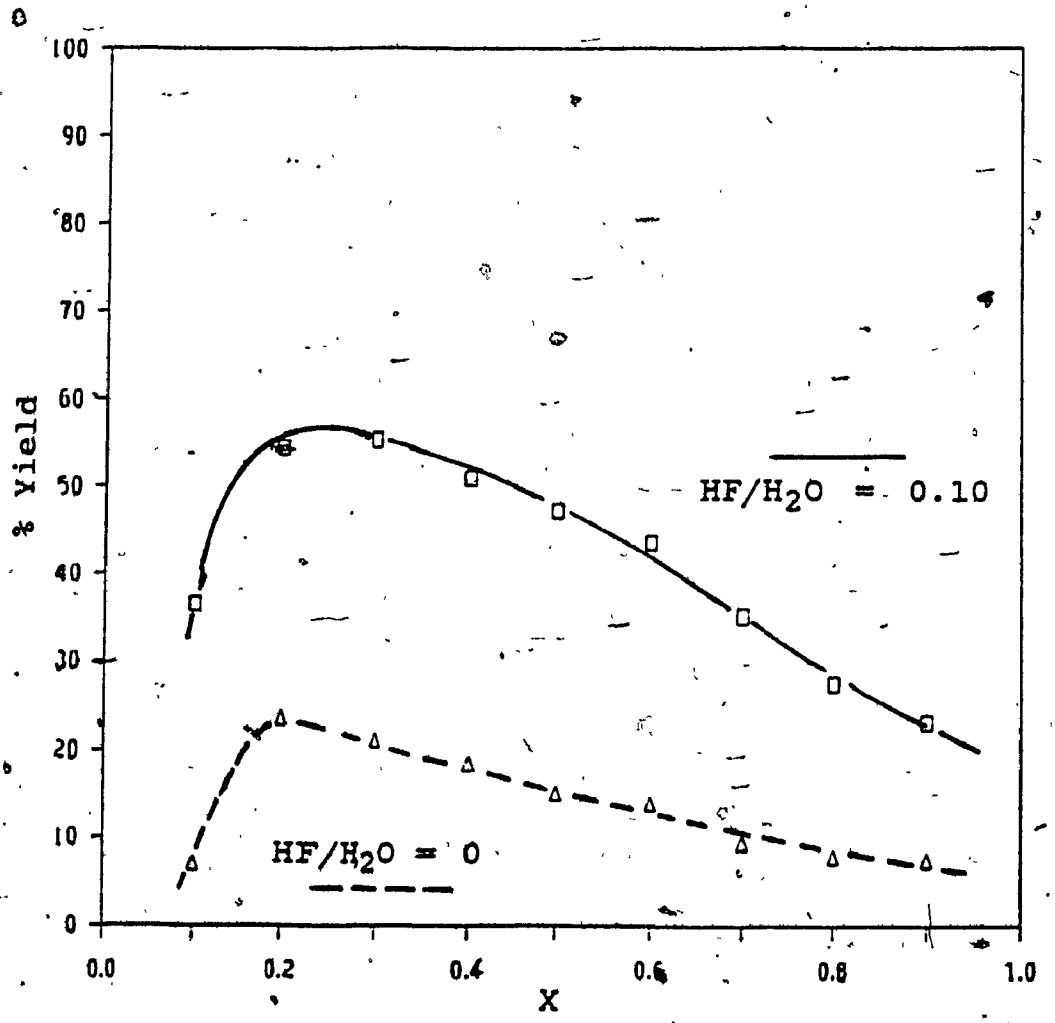

Fig. 55. % Yield versus X at 90°C for $HF/H_2O = 0$ and 0.10 with $t(SnF_2)$ and $t(PbSnF_4) = 0$.

4.0 CONCLUSION

The results presented here clarify the conflicts reported in the literature regarding the symmetry of the $PbSnF_4$ phase obtained upon reaction of lead (II) nitrate with stannous fluoride in aqueous solutions while showing the reactions to be complex in nature. Two groups (3,4 and 6) reported obtaining tetragonal α-$PbSnF_4$ while two others (5 and 8) claimed orthorhombic or monoclinic $PbSnF_4$ was obtained. No evidence of the monoclinic phase has been found in this work.

We find that the symmetry of $PbSnF_4$ prepared at room temperature to depend on two factors: excess fluoride ions present in solution and possible solid/solution reactions between $PbSnF_4$ and the reaction mixture. The fluoride ionic concentration was controlled in two ways: by the addition of aqueous HF or, with HF present, allowing the stannous fluoride solution to sit, and therefore hydrolyse, prior to the addition of the lead (II) nitrate.

Tetragonal $PbSnF_4$ was obtained in the reactions where no HF was added to the SnF_2 solution and no delay for the SnF_2 solution prior to the addition of $Pb(NO_3)_2$ or the precipitated $PbSnF_4$ prior to filtration were taken. Tetragonal $PbSnF_4$ was obtained when HF was present after 60 minutes had elapsed for the SnF_2 and when two hours had elapsed before filtration. In these preparations, it was

on the molar ratio $Pb(NO_3)_2/SnF_2$ in the reaction mixture.

At room temperature, orthorhombic $PbSnF_4$ was obtained when HF was present as long as the SnF_2 was reacted immediately with $Pb(NO_3)_2$. This prevented loss of HF from solution. A dependance on the molar ratio $Pb(NO_3)_2/SnF_2$ in the reaction mixture was also observed and centered around ratios of 0.50. The magnitude of the orthorhombic distortion was found to be variable.

Atomic absorption results show that stoichiometric o-$PbSnF_4$ was never obtained for reactions carried out in solutions that were rich in Sn. Pb/Sn < 1.0 indicates that Sn was incorporated into the lattice and it is possible that this would affect the lattice parameters. Stoichiometric α-$PbSnF_4$ was obtained but it was found that the ratio Pb/Sn to be dependant on the time the SnF_2 sat prior to addition of $Pb(NO_3)_2$. For α-$PbSnF_4$, Sn was also found to be incorporated into the lattice.

In reactions carried out at 0, 75 and 90°C, α-$PbSnF_4$ was only obtained at 90°C when no HF was present. o-$PbSnF_4$ was obtained in all other cases with significant changes occurring to the b and c parameter.

For all temperature, the presence of HF in the SnF_2 solutions gave superior yields than when HF was absent. Also, at room temperature and higher, the presence of HF encouraged the formation of $Pb_2SnNO_3F_5.2H_2O$, whereas its absence at 0°C retarded it.

absence at 0°C retarded it.

This study is by no means complete. The present parameters must be completed. Unidentified interactions must be found and isolated, particularly in the case where t($PbSnF_4$) and high temperatures are concerned. The influence of atmosphere, order of mixing and concentration of solutions should also be studied. Bulk density measurements of the pure product and elemental analyses for Pb, Sn and F are also very important.

The ultimate task is to ba able to see if the presence of HF, which is seen to influence the unit cell parameters of both phases of $PbSnF_4$, has any affect on the conductivity.

5.0 REFERENCES

1. Subbarao, E.C., ed. Solid State Electrolytes and Their Applications. Plenum Press, New York, 1980.
2. West, Anthony R. Solid State Chemistry and its Applications. John Wiley & Sons, New York, 1984.
3. G. Dénès, T. Birchall, M. Sayer and M.F. Bell, Solid State Ionics, 13, 213 (1984).
4. T. Birchall, G. Dénès, K. Ruebenbauer and J. Pannetier, J. Chem. Soc., Dalton Tr., 2296 (1981).
5. J.D. Donaldson and B.J. Senior, J. Chem Soc. (A), 1821 (1967).
6. G. Dénès, J. Pannetier and J. Lucas, C.R. Acad. Sc. Paris, 280C, 831 (1975).
7. J.M. Réau, C. Lucat, J. Portier and P. Hagenmuller, Mat. Res. Bull, 13, 877 (1979).
8. J. Pannetier, G. Dénès and J. Lucas, Mat. Res. Bull, 14, 627 (1979).
9. T. Birchall, G. Dénès, K. Ruebenbauer and J. Pannetier, submitted.
10. G. Pérez, S. Vilminot, W. Granier, L. Cot, C. Lucat, J.M. Réau, J. Portier and P. Hagnemuller, Mat. Res. Bull., 15, 587 (1980).
11. Mckie, D. and C. Mckie. Crystalline Solids. Thomas Nelson & SOns Ltd., Great Britain, 1974.
12. Willard, R.H., L.L. Merritt and J.A. Dean. Instrumental

Methods of Analyses. Litton Educational Publishing Co. Inc., New York, 1974.

13. E.S. Gladney and W.E. Goode, Anal. Chem Acta., 91, 411 (1977).
14. Gibb, T.C. Principles of Mössbauer Spectroscopy. Chapman and Hall Ltd., London, 1976.
15. T. Birchall and G. Dénès, Can. J. Chem. 62, 591 (1984).
16. J. Pannetier, G. Dénès, M. Durand and J.L. Buevos, J. Physique 41, 1015 (1980).
17. T. Birchall, G. Dénès, K. Ruebenbauer and J. Pannetier, J. Chem Soc., Dalton Tr., 1831 (1981).

APPENDIX I

Relationship Between Unit Cell Parameters and Crystal Symmetry

Cubic

$$d_{hkl} = \frac{a}{(h^2 + k^2 + l^2)^{1/2}}$$

$$a = b = c$$

$$\alpha = \beta = \gamma = 90°$$

$$V = a^3$$

Tetragonal

$$d_{hkl} = \frac{a}{(h^2 + k^2 + l^2(a^2/c^2))^{1/2}}$$

$$a = b \neq c$$

$$\alpha = \beta = \gamma = 90°$$

$$V = a^2c$$

Orthorhombic

$$d_{hkl} = \frac{1}{(a^2/h^2 + k^2/l^2 + c^2/l^2)^{1/2}}$$

$$a \neq b \neq c$$

$$\alpha = \beta = \gamma = 90°$$

$$V = abc$$

All data was reduced to the tetragonal unit cell in order for comparisons to be made.

APPENDIX II

Typical Mössbauer Data for Different Environments and Oxidation States of Sn

Isomer Shifts Referenced to $CaSnO_3$ = 0.

Dependance on oxidation state

Sn^{o} = 1.5 to 2.5mm/s

Sn^{2+} = 2.5 to 4.0mm/s

Sn^{4+} = -0.6 to 1.5mm/s

Quadrupole Splitting Due to unequal occupancy of the 5p orbitals resulting from covalent bonding.

Sn^{o} and inorganic Sn^{4+} = < 1.0mm/s

Organotin (IV) = 0 to 2.0mm/s

Organotin (IV) halides = 3.0 to 4.0mm/s

(due to electron withdrawing power between organic ligands and halides).

Sn^{2+} dominated by non-bonding electrons

Stereoactive: large (>1.5mm/s)

Not stereoactive: small (0 to 0.5mm/s)

Magnetic Splitting

All oxidation states of tin are diamagnetic, therefore there is no spontaneous internal field. Magnetic splitting is observed only if an external magnetic field is applied or if a transferred field from a magnetically ordered sublattice is present.